5-2013

Automated CNC Tool Path Planning and Machining Simulation on Highly Parallel Computing Architectures

Dmytro Konobrytskyi
Clemson University

AUTOMATED CNC TOOL PATH PLANNING AND MACHINING SIMULATION ON HIGHLY PARALLEL COMPUTING ARCHITECTURES

A Dissertation
Presented to
the Graduate School of
Clemson University

In Partial Fulfillment
of the Requirements for the Degree
Doctor of Philosophy
Automotive Engineering

---

by
Dmytro Konobrytskyi
May 2013

Accepted by:
Dr. Laine Mears, Committee Chair
Dr. Thomas R. Kurfess
Dr. Tommy Tucker
Dr. Stan Birchfield

ABSTRACT

This work has created a completely new geometry representation for the CAD/CAM area that was initially designed for highly parallel scalable environment. A methodology was also created for designing highly parallel and scalable algorithms that can use the developed geometry representation. The approach used in this work is to move parallel algorithm design complexity from an algorithm level to a data representation level. As a result the developed methodology allows an easy algorithm design without worrying too much about the underlying hardware. However, the developed algorithms are still highly parallel because the underlying geometry model is highly parallel.

For validation purposes, the developed methodology and geometry representation were used for designing CNC machine simulation and tool path planning algorithms. Then these algorithms were implemented and tested on a multi-GPU system. Performance evaluation of developed algorithms has shown great parallelizability and scalability; and that main algorithm properties are required for modern highly parallel environment. It was also proved that GPUs are capable of performing work an order of magnitude faster than traditional central processors.

The last part of the work demonstrates how high performance that comes with highly parallel hardware can be used for development of a next level of automated CNC tool path planning systems. As a proof of concept, a fully automated tool path planning system capable of generating valid G-code programs for 5-axis CNC milling machines

was developed. For validation purposes, the developed system was used for generating tool paths for some parts and results were used for machining simulation and experimental machining. Experimental results have proved from one side that the developed system works. And from another side, that highly parallel hardware brings computational resources for algorithms that were not even considered before due to computational requirements, but can provide the next level of automation for modern manufacturing systems.

TABLE OF CONTENTS

Page

Table of Contents (Continued)

Page

Table of Contents (Continued)

Page

Table of Contents (Continued)

Page

LIST OF TABLES

LIST OF FIGURES

List of Figures (Continued)

Figure Page

List of Figures (Continued)

Figure Page

List of Figures (Continued)

Figure Page

List of Figures (Continued)

Figure Page

List of Figures (Continued)

Figure Page

List of Figures (Continued)

Figure Page

LIST OF ALGORITHMS

List of Algorithms (Continued)

Algorithm Page

I. INTRODUCTION

During the last century the manufacturing industry has moved from pure manual or simple mechanically automated production of goods to a new level where almost everything is controlled by electronic control systems and computers. Although areas like assembling or repairing are still done mostly by people, it is almost impossible to see large scale manual mechanical processing today mainly due to the requirements of precision, repeatability and speed. In order to meet the increasing requirements of produced components, the way of controlling machine tools evolved from manual operation to mechanical control systems during 19th century, then to Numerical Control (NC) systems in the middle of 20th century and finally to Computer Numerical Control (CNC) systems (Figure I-1).

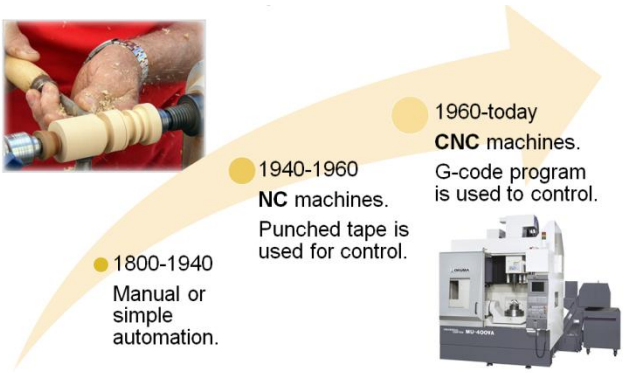

Figure I-1: History of milling machines

Modern CNC machines are extremely versatile in their ability to make parts with complex geometry and good surface quality. However, efficient usage of all machine capabilities requires highly experienced personnel and a relatively long time to program.

The main reason it requires tremendous time investments is a lack of efficient and flexible automatic path planning algorithms and, as a result, a lack of reliable, fast and fully automatic software for CNC programming. Existing algorithms are usually limited to specific problem solutions due to the geometric and computational complexity of path planning. In addition, existing algorithms cannot be run efficiently on modern, highly parallel hardware for utilization of modern computing capacity and as a result are limited to performance of traditional serial processors.

Importance of automated tool path planning

It is hard to underestimate the importance of the further automation of the milling process and especially of automated tool path planning. Although modern Computer Aided Manufacturing (CAM) systems have significantly simplified the process of machine programming, creating a program for an average part still takes several hours. As a result, the cost of low volume production when only few parts are required may consist mainly of a programming cost. For example, in an extreme case of one part milling, which is a popular mold and die manufacturing scenario, programming cost may be 90% of the entire manufacturing cost. This extremely high cost of low-volume production with CNC milling is also one of the main reasons that subtractive manufacturing is not used in Rapid Prototyping (RP) industry. The RP industry is almost monopolized by a variety of additive manufacturing techniques today which usually do not require such complicated programming process. As a result, development of highly automated path planning systems could create a completely new market for RP by CNC

milling, which would provide a unique combination of cost, speed, precision and ability to use production materials. It is obvious that decreasing prototyping cost is extremely important for an entire manufacturing industry, due to shorter product development life cycle and much cheaper testing.

It may look like the high programming cost is important only for low volume production and not for high volumes where a programming cost is shared between millions of parts. This is partially true and actual milling time is much more important in this case, but usually designing of an optimal trajectory, which does take as little time as possible, is not a trivial problem and requires multiple iterations. In this case automated tool path planning may significantly improve a tool path planning iteration time and allow a significantly higher number of iterations with a much shorter resulting tool path. In an extreme case of fully automated tool path planning and simulation, these tool path planning iterations can be performed without human assistance in a cloud by thousands of servers with a much more efficient result than a human can ever achieve.

The importance of automated path planning is also proved by a survey [1] that was conducted online in March and April of 2010 among 188 machine tool professionals by Centrifuge Brand Marketing Inc. and sponsored by Siemens Industry, Inc. The survey showed that 81% of job shops and 72% of manufacturers are looking for faster programming and setup; and 74% of job shops and 70% of manufacturers are looking for easiness of use for reduced training time, which is one of the benefits of automated tool path planning.

Importance of parallel processing

Automatic tool path planning is obviously an important research area for modern manufacturing industry and there many research projects have been conducted on this subject in the past few decades. The “Background” chapter will provide more detailed information about past research projects, but it is important to notice that all tool paths planning today is done by computers and that path planning algorithms are becoming more and more complicated and require more computational resources. It is also important to notice that until a very recent time, tool path planning and simulation algorithms could be designed quite independently from knowledge about the hardware that actually performs them, and all algorithms were serial. This approach was good enough for the early stage of the computer industry when new processors were always faster than old processors and algorithm developers could expect seeing better performances of their algorithms every year. This state of continuous performance improvement was possible mainly because of the increasing of Central Processing Unit (CPU) and memory clock frequencies. But increasing clock frequency also means higher heat production and further increasing of a clock frequency creates physical limitations that become more and more complicated for processor manufacturing.

At the beginning of 2000’s further increasing of a clock frequency had become too expensive from the heat production point of view and the decision made by processor manufacturers was to use multiple CPU cores and single-instruction, multiple-data (SIMD) processors with a lower frequency in order to increase the available computational performance for the next generations of their processors. The power

efficiency requirements for making “greener” products actually forced manufacturers to reduce clock frequency even more. The “Trend tracking for ISSCC 2012” [2] paper for IEEE International Solid-State Circuits Conference says: “As power reduction becomes mandatory in every application, the trend toward lower clock frequencies also continues, as shown in the frequency trends chart in Figure I-2. This is driven by decreased supply voltages, with processors operating in the nearthreshold or even the subthreshold voltage domain. The performance loss resulting from reduced voltages and clock frequencies is compensated for by further increased parallelism.”

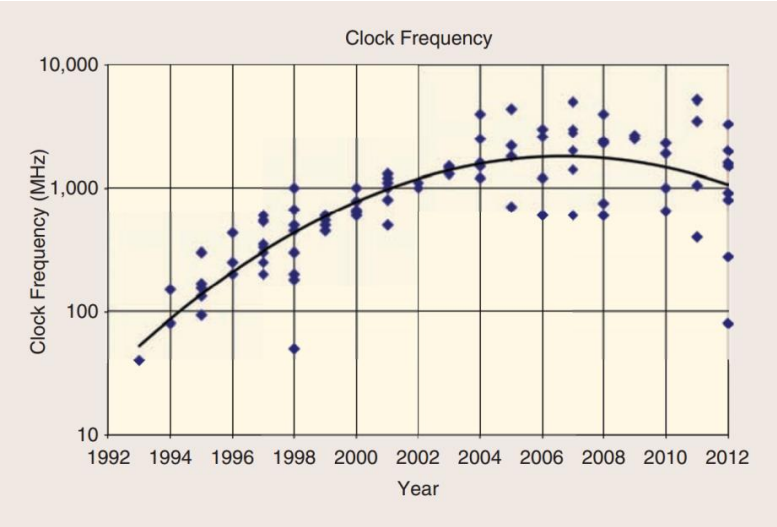

Figure I-2: Processor clock frequency over time [2]

It can be seen that the significant increasing of CPU clock frequency is not possible without a fundamental breakthrough in physics and processor manufacturing and that the processor manufacturing industry has selected the way of multiple cores and higher parallelism. Although the selected way means further increasing of available performance, it also means that the performance of traditional serial algorithms will not

increase significantly anymore. As a result, algorithm developers cannot expect seeing continuous computational time improvement for traditional algorithms anymore and will be required to develop new parallel algorithms using modern hardware.

The proposed approach for solving automated milling problem

Previous parts have shown the importance of automatic tool path planning for the manufacturing industry and also the importance of parallel processing as a critical component for any high performance algorithms. This work proposes a high level approach for solving both problems in terms of automated CNC tool path planning and provides a foundation for further research and development of this solution.

The global problem of the manufacturing industry (and many other industries as well) today is an absence of a centralized knowledge base with information about milling processes, materials, path planning strategies and good practices. Although the industry has already found solutions for many problems, there is still no way for automated selection, applying and evaluation of these solutions. Traditionally the knowledge about milling processes and path planning strategies is shared between independent CNC programmers and cannot be reused without actual interaction with people, implemented though CAM systems User Interface (UI). At the same time CAM packages already have multiple tool path planning strategies implemented and there are existing tool and material properties databases, which can be used for covering most of everyday milling needs.

It is also obvious that there is no way to put all of the available knowledge of all CNC engineers, CAM developers and tool and material properties databases into one place immediately. The proposed solution is to develop a centralized system, which can be continuously improved in an iterative way by adding new knowledge about path planning strategies, tools, materials and machines on each iteration. Although it may look like the proposed approach is just to create a knowledge data base, the key component of the proposed solution is to develop a software system that can actually use this knowledge for solving tool path planning problems automatically. The proposed system would perform 5 main steps as shown on Figure I-3:

1) Feature detection
2) Tool path planning strategy selection
3) Tool path planning with selected strategy strategies
4) Simulation
5) Performance evaluation

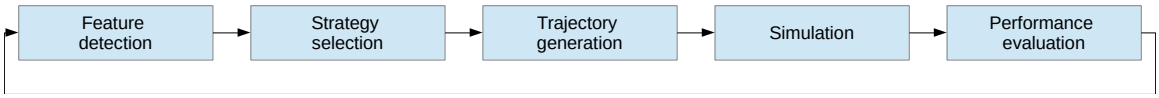

Figure I-3: Tool path planning iteration

There are multiple ways to use the proposed approach. One way is to apply these steps iteratively with optimization of path planning parameters on each step as is usually done in tradition optimization problems. Another way is to actually make a tree of all (or all of the most probable) decisions made at the second step for each detected feature and

process a tree by generating a tool path and simulation of each decisions sequence as shown on

Figure I-4.

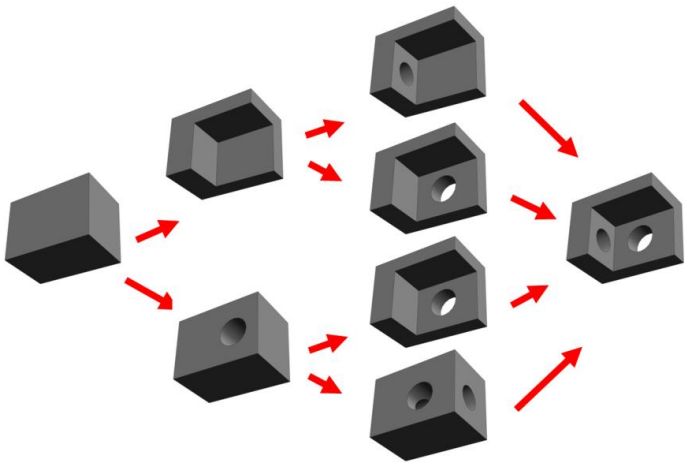

Figure I-4: Tree of possible path planning decisions

Evaluation of every generated tool path for a tree can be done by simulation of milling process and collecting some measurements like path length, milling time, tool load, material removing rate and even tool and workpiece temperatures. The results of this evaluation can be processed for selection of the best tool path, based on user defined criteria like the fastest milling time or the most efficient tool wear or the maximum scallop height. As with path planning strategies, tool path evaluation would have a modular structure and could be extended by adding new evaluation algorithms.

The proposed solution is significantly different from any modern CAM system in the way that it is initially fully automated and becomes better over time by continuously accumulating knowledge about path planning strategies, simulation and tool path evaluation techniques.

The role of this work in the proposed automated milling framework

Although an implementation of the proposed solution is obviously not simple, and it is more of a computer engineering and organizational problem than a research problem, there are some fundamental scientific problems that have to be solved in order to actually develop the proposed system.

One of the main problems is the need of a very robust algorithm which can be applied to any possible geometry and produce a valid tool path. One of the reasons for this need is an ability to generate a tool path at the beginning of system development when there are no tool path planning algorithms. Another more general reason is a requirement for robustness of the proposed system. It can be seen that on one side the number of implemented feature detection and path planning algorithms will grow up and cover more and more path planning scenarios and possible geometries. But on another side there are no guaranties that the available algorithms can always produce a valid output tool path for any provided input geometry. It means that the proposed system will be able to generate useful output only for a subset of all the problems and that the number of problems that can be solved will be relatively small at the beginning of development.

One of possible solutions for this problem is described in this work. The idea is to develop a robust multi-axis tool path planning algorithm, which can be applied for any possible geometry and produce a reasonably optimal valid tool path. This algorithm does not have to be extremely efficient or fast but the most important quality for it is to be able to produce a valid tool path for any input geometry if it is feasible from a geometry point of view. The proposed automated tool path planning system would use this algorithm as a

last resort in cases where there are no known efficient algorithms for selected features or where there are no detected features. Based on the idea of continuous improvement it is obvious that this algorithm will be used more often at the beginning of development and less often after adding more efficient algorithms. The algorithm developed in this work fits the desired requirements and will be described in further chapters.

Another important fundamental problem is related to parallel processing. As described above, parallel processing has become a main processor industry trend and there are no known solutions that can allow further growing of CPU clock frequency and the increasing of serial algorithms' performances without a significant breakthrough in physics, material science and processor manufacturing. As a result, even in 10-20 years current serial algorithms will not become much faster. But this is only one side of a problem. On the other side, performance of modern CAM systems is barely good for everyday usage i.e. it is possible to perform multiple tool path planning generation iterations for relatively simple geometry or few iterations for complex geometry in a reasonable time (some hours), but there is no way to use the same algorithms for the hundreds and thousands of tool path planning iterations required for the proposed automated tool path planning system. And although multi-core processors have been available on the market already for 8 years, modern CAM systems still have very limited support of parallel processing, which usually requires a user to run multiple independent tasks manually. In the case of 2-cores it still can be a reasonable solution but with modern 6- and 8-core processors it becomes extremely inefficient.

The reason for the absence of parallel processing support in modern CAM systems is related to the way geometry is represented. Traditionally Computer Aided Design (CAD) and CAM systems use boundary geometry representation (BREP) developed back in 1970s. The BREP has a lot of advantages that were extremely important during the second part of 20th century; especially the support of extremely high accuracy with relatively low computational and memory requirements. It provides the best set of tradeoffs between accuracy, memory usage and required amount of calculations on a serial processor for most geometry operations required by CAD and CAM systems. Although BREP is a good geometry representation, it has some significant drawbacks that are becoming more important today with spreading of multi-core processors. One important drawback of BREP is the complexity of geometry operations from a human point of view. Even reasonably simple operations like Boolean subtraction or an intersection between a plane and a compound surface represented by BREP require a lot of complex mathematical calculations which usually cannot be represented as a set of simple independent operations. This drawback has two important results: the development of CAM systems becomes quite complicated with BREP and it is not possible to use data parallelism for parallel processing support. The data parallelism and its comparison to task parallelism will be given in the "Background" chapter but the main difference is related to how work is divided between multiple cores. In case of data parallelism it is quite easy to split work between many cores without significant effort from a developer. In opposition to data parallelism, task parallelism requires developers to split work manually, which is a much more complicated problem, especially for a high

number of cores. For example one of the most popular geometric modeling kernels used in modern CAD/CAM systems called “Parasolid” has recently started support “thread-safety” which means that developers can run multiple editing tasks on multiple cores. And although it is definitely a good trend, development of software systems, which can really use many cores, with manual load balancing requires a tremendous effort and usually cannot be done in a research environment.

The idea behind a solution for the parallel processing problem is actually quite simple: use another geometry representation, which provides a different set of tradeoffs between memory consumption, computational requirements and accuracy but supports parallel processing on data level and can be scaled efficiently. This work presents results of the research project about automated tool path planning and also results of a search for a new geometry representation, which can efficiently replace a traditional boundary representation and solve existing parallel processing problems. Since the BREP is a good tradeoff between accuracy, memory, computational requirements, complexity and scalability, it is easy to assume that in order to reduce complexity and improve scalability another geometry representation may take more memory and/or computational resources for the same level of accuracy. At the same time the facts are that modern processors are barely fast for CAM systems using traditional BREP and performance of CPUs is growing quite slow. Five years ago, it appeared that there was no way to solve the problem. Now, it seems to be the same way - but the solution has actually come from the gaming industry.

One of the most important aspects of games is the quality of the graphics. In order to render images faster, the computer graphics industry starting in the 1980s has been using specialized hardware called Graphics Processing Units (GPU). In the early stages of computer graphics and gaming industries, GPU was just a chip with some predefined rendering algorithms implemented in the hardware. But the gaming industry required more realistic graphics and more flexibility of hardware implemented algorithms. As a result, at the beginning of the 2000s GPU had gotten the support of special programs called shaders written by software developers in addition to predefined hardware algorithms. Increased flexibility requirements forced GPU manufacturers to make their processors more and more general and as a result it has become possible to do General Purpose calculation on GPU (this approach is called GPGPU). More information about GPU architecture, GPGPU approach and GPU performance will be given in the "Background" chapter but it is important to notice 2 things: GPU is a naturally highly parallel and theoretical GPU performance is a several hundred times higher than serial CPU performance. For example theoretical performance of the fastest modern CPU and GPU is shown in Table I-1. It can be seen that the theoretical performance difference between serial programs and parallel programs that use SIMD approach on CPU is 81x and parallel programs on GPU is almost 1500x faster than serial programs on CPU.

Processor name	Performance (SP GFLOPS)
Intel i7-3960X (Serial performance @ 3.9GHz)	3.9
Intel i7-3960X (Parallel SIMD performance @ 3.3GHz)	316
NVidia GTX690 (Parallel performance)	5621

Table I-1: Fastest CPU and GPU performance

The shown theoretical possibility of performance improvement in the case of parallel algorithms proves that parallel processing is a crucial part of any modern software system. It can also be seen that a transition from serial CPU algorithms to parallel algorithms, which can run on GPU, may provide a performance improvement comparable to the past 30 years of continuous CPU performance growing. The GPU actually may provide the additional computational resources needed in the case of new geometry representations which will replace BREP and add support of parallel processing. Although it may look like GPU is a perfect solution and that all modern software should run on it, the difference in CPU and GPU architectures does not allow a simple porting of algorithms from one platform to another. More details about architectural differences and GPU algorithm design challenges will be given in the "Background" chapter but it is important to notice that in order to achieve theoretical performance limits, algorithms and data structures have to be designed especially for GPU and, in most cases, this is not a trivial problem. The current research actually provides the geometry representation including data structure and algorithms especially designed for highly parallel GPU architectures, which supports data parallelism and allows performing of all operations in parallel without a significant effort from a developer. Data parallelism means that the development of parallel tool path planning algorithms is significantly easier and developed algorithms can scale even to multi-GPU systems as will be shown later.

Work structure

This work describes the research of algorithms, data structures and geometry representations that can be used for efficient milling process simulation and tool path planning accelerated by GPGPU approach. The information is provided in approximately chronological order, so that the research path and key decisions made during the research project can clearly be seen. All required background information about CNC milling, parallel processing and GPGPU approach is provided in the "Background" chapter, which also describes past research in the milling area and gives information about modern GPU architectures required for understanding GPU algorithms development challenges. The entire work is divided in two main areas: 3-axis milling and 5-axis milling. Although 3-axis milling can be described as a subset of 5-axis milling, the approach used for 3-axis tool path planning and simulation is similar and allows easier showing of some important concepts of GPU accelerated milling before going to 5-axis. The entire research can also be divided into two other areas: milling simulation and path planning, which may look like independent areas, but it will be shown that generalized tool path planning approach cannot be implemented without integration of tool path planning and milling simulation algorithms into one system. As result of this double subdivision, 4 main structures of this work are "3-axis milling simulation", "Tool path planning for 3-axis milling", "5-axis milling simulation", "Tool path planning for 5-axis milling" that correspond to described research areas. The chapter "Conclusion and recommendation" at the end provides a summary of the entire research and describes

future research possibility of the developed technology. The last part of this work provides references to books, papers and other resources used in this work.

II. BACKGROUND AND RELATED WORK

CNC milling

CNC milling has progressed in the last 40 years from fully mechanical machine controls, punch cards and paper tapes to modern fully computerized controllers, programmed via variants of G-code programming languages. Programming these machines has advanced from inefficient handwritten programs to powerful CAM systems capable of generation complex multi-axis trajectories, based on strategies selected by operator and precise virtual milling simulation.

Significant research has been focused on key areas such as tool path planning, tool orientation selection, and selection of tool geometry. Many researchers have addressed tool path planning using traditional methods such as iso-planar [3-5] or iso-parametric approaches [6]. Results of these approaches generate paths that achieve certain accuracies, or surface characteristics, but that may not be optimal with respect to other process parameters, such as production time. In order to improve performance of traditional methods, the iso-scallop approach was introduced by Suresh and Yang [7] and Lin and Koren [8]. It produces a constant scallop height of a machined surface. Popularization of 5-axis milling and milling of non-parametric surfaces has resulted in the development of new approaches resolving specific 5-axis problems and further reducing milling time. These approaches can be classified [9] as curvature matched milling [10-12], isophote based method [13-15], configuration space methods [16, 17],

region based tool path generation [13], compound surface milling [18, 19] and methods for polyhedral models and cloud of point [20, 21]. With respect to tool orientation selection, traditional methods such as fixed orientation, principal axis methods [22] or multi point milling [23] have been developed. Furthermore, in the past 10 years, more advanced path planning methods such as the rolling ball [24, 25] and arc intersect methods [26] as well as earlier C-space based approaches [16, 27] were successfully deployed. Furthermore, research addressing tool geometry selection [28, 29], and implementation of automatic tool selection in commercial products does not exist or is very limited when addressing optimized tooling parameter selections. While significant progress has been achieved over the last several decades, a plethora of issues to be addressed that will reduce production time and improve / guarantee component quality still exist.

Throughout the literature, it is clear that computation time is a major limitation of most, if not all, of the proposed algorithms. One solution for this problem is the employment of high performance computing, in particular the GPU (Graphical Processing Unit) platform to accelerate the processing. Development and popularization of a general purpose GPU (GPGPU) approach and platforms like Compute Unified Architecture (CUDA) have resulted in promising results for deploying GPGPU functionality in a manufacturing environment. Tukora and Szalay presented an approach for GPGPU accelerated cutting force prediction [30]. Hsieh and Hsin proposed a GPU accelerated particle swarm optimization approach for 5-axis flank milling [31]. Furthermore, new approaches for geometry representation used in CNC area were

recently proposed. Guang and Ding proposed employing a quadtree-array for representation of a workpiece in 3-axis milling [32]. Li and Yao used an extended octree for cutting force prediction. Zhao and Wang presented a GPU accelerated approach for Boolean operations on polygonal solids. Wang and Leung described the use of layered depth-normal images for solid modeling of polyhedral objects [33]. All of this research demonstrated the value of parallelized processing in milling operations.

Geometry representation

One of the most fundamental concepts in the CAD/CAM area is the geometry representation. There are several fundamentally different approaches for representing geometry such as Boundary Representation (b-rep or BREP), Constructive Solid Geometry (CSG), volume sampling, height map, sweeping, implicit representation and other approaches. Many of them have multiple implementations based on different data structures such as arrays, lists or trees and unit elements such as voxels, surfaces, planes or triangles. Traditionally modern CAD/CAM systems use solid modeling engines based on BREP but also support other techniques such as CSG or sweeping volumes. In opposition to CAD/CAM world, the game and art industries usually work with triangular meshes since they provide a different set of tradeoffs which is more appropriate for these applications.

The BREP approach uses limits for representing a shape. It represents a boundary between material and empty space by a set of connected surface elements. Surface elements are usually represented by NURBS (Non-uniform rational B-spline) surfaces or

by other analytical surface descriptions. In additional to geometric data the BREP stores topological information including faces (bounded portion of a surface), edges (bounded portion of a curve) and vertexes as shown on Figure II-1.

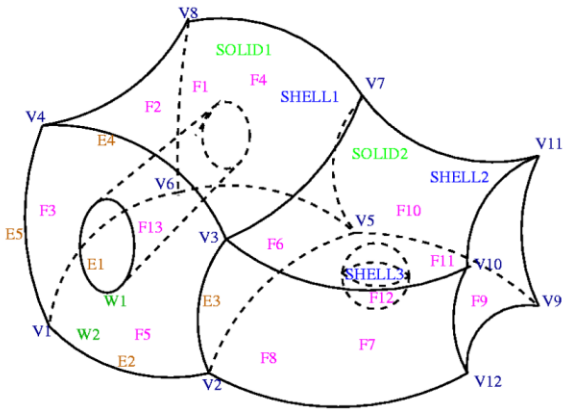

Figure II-1: BREP example [34]

A special case of a BREP, where all faces are planes, is called a polygonal mesh. The triangular mesh can be described as a special case of BREP as well or as a polygonal mesh where all faces are represented by a set of triangles as shown on Figure II-2.

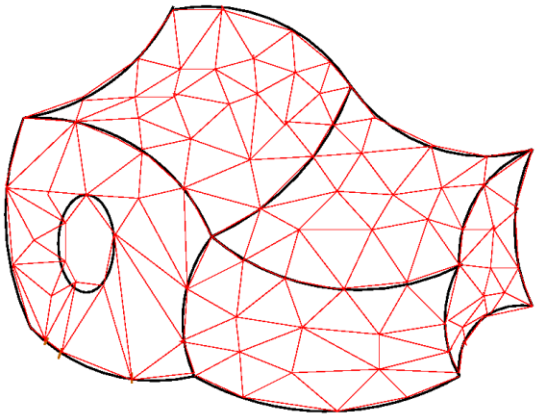

Figure II-2: Triangular mesh example [34]

The triangular mesh representation is widely used in computer graphics and can be rendered extremely quickly and efficiently by Graphics Processing Units (GPUs).

In opposition to BREP the CSG approach uses Boolean operations between simpler objects in order to create a complex solid. The CSG approach does not require storing additional topological information but the pure CSG approach can represent a limited set of shapes. As a result it is usually used in combination with BREP approach which is used for describing CSG primitives.

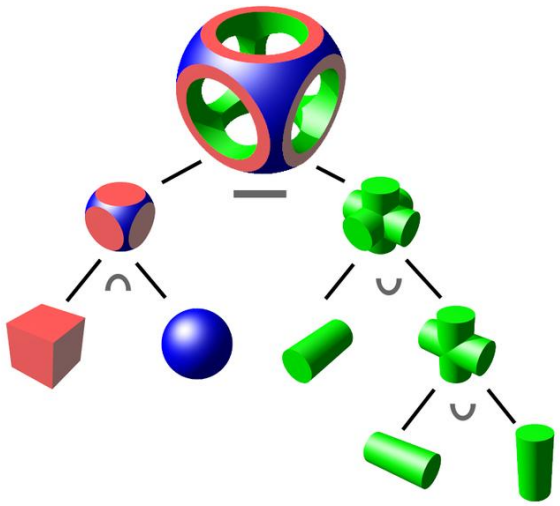

Figure II-3: CSG example [35]

One approach that is completely different from BREP is representing a volume itself, and not a boundary surface. Volumetric approaches usually subdivide an entire space into smaller areas called voxels or cells. Every volumetric element stores volume sampling data which may contain information such as material density, distance to the closest surface, color or something also. Based on volume subdivision, it is possible to notice two ways of sampled approaches: regularly and irregularly. This way of

subdivision also affects a selected data structure used for storing sampling data. For example, a regularly sampled volume data is usually stored in 3-dimensional arrays (this geometry representation is called “voxel model” and volume elements are called “volumetric pixels” or “voxels”). In case of irregularly sampled volume data, tree-like data structures are usually used for as a storage, for example Octree (Figure II-4) or k-d tree.

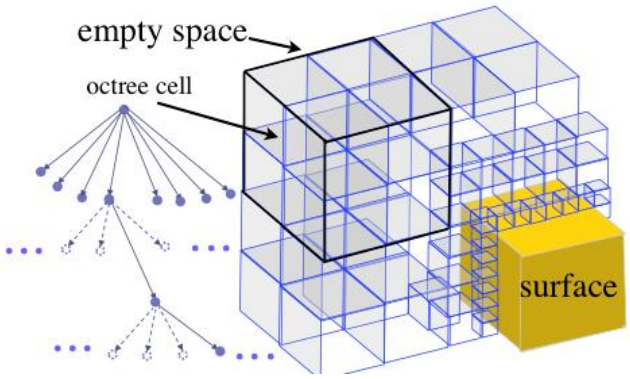

Figure II-4: Octree example [36]

Geometry representations described above provide different tradeoffs between precision, memory usage, parallelization and complexity but they are very general purpose and can represent any possible shape. In contrast to them, the height map geometry representation is not capable of representing any possible geometry but provides an interesting set of tradeoffs and can be useful in tasks like 3-axis milling (with some limitations which will be mentioned later). The height map (or z-map) represents a surface by storing sampled distances from a base plane to points of a represented surface. The distance sampling data can be stored in a 2d array or a tree-like structure such as quad-tree as shown on Figure II-5.

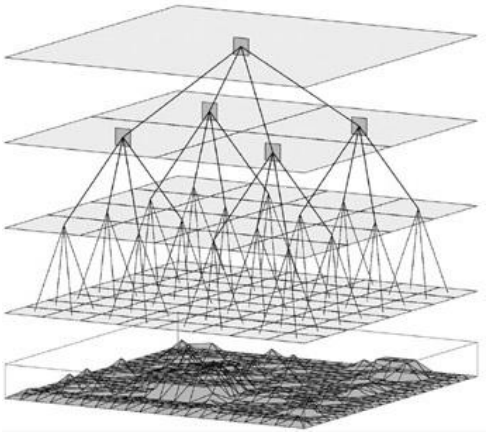

Figure II-5: Quad-tree height map example

Milling simulation

Milling simulation today is a critical component of the milling process that allows safe usage of machines, prevents collisions, saves material and also allows the selection of better milling parameters. Many researchers have being working in this area since the 1980s and have developed several different simulation techniques. It is important to notice some of the most popular approaches described in published works.

In the earliest days of milling simulation area and limited computational resources Boolean operations on solids was a main simulation tool. For example in 1983 Bertok and Takata [37] used it for the prediction of a cutting torque and in 1986 Tim Van Hook [38] described a system for rendering a solid milled by a cutting tool following an NC path. Usage of Boolean operations on a solid has the benefit of producing a very accurate result and a perfect image with low computational requirements for a small number of tool motions. The drawback of this approach, however, is a dependency on the number of

operations required for image rendering on a number of tool motions which can be very high in real NC programs.

In opposition to Hook in 1993, Hsu and Yang [39] used an isometric projection and a height map data structure for 3-axis real-time milling simulation. This approach guarantees an independency of rendering performance from a number of tool motions although it provides only an approximate result with a predefined resolution and does not provide a natural way for multi-axis simulation. Although as Roth and Ismail [40] showed in 2003 it is possible to use a height map for multi-axis milling by the continuous generation of height maps for each tool orientation. A different solution based on the single voxel model for representing a workpiece was presented in 2000 by Jang and Kim [41]. The concepts of primitives voxelization process similarly used by Jang and Kim was published earlier in 1997 by Cohen-Or and Kaufman [42].

One of the crucial components for all described methods is the calculation of the swept volume of a tool. One of the first papers on swept volume calculation was published by Wang and Wang [43] in 1986. A newer approach for the APT tool was described by Bohez and Minh [44] in 2003. Although all mentioned that simulation approaches are quite different and use different data structures, almost all of them are pure geometric simulation techniques.

Another class of milling simulation is an actual physical simulation with the finite element method described in the work of Ozel and Tugrul [45] in 2000 and in the newer work of Rai and Xirouchakis [46] published in 2008. Although the finite element approach provides a much more accurate simulation and allows the measurement of

many physical parameters like tool temperature or tool load, it has two important problems. The first problem is a need of physical parameters of material, tool and machine which are not always available and may be hard to measure. Another problem is related to a computational time. Modern processors cannot achieve even a real-time simulation with a relatively coarse grid, which makes finite element simulation a useless tool for manufacturing and limits its use to scientific research projects.

It is important to notice that most of the latest researches related to milling simulation lies in areas like error prediction and compensation, like the work of Uddin and Ibaraki [47] published in 2009 or Cortsen and Petersen [48] published in 2012, web-based simulation described in the work of Hanwu and Yueming [49] published in 2009, unification of manufacturing resources description proposed by Vichare and Nassehi [50] published in 2009, and quad-tree-array based workpiece representation used in the work of Li and Ding [32] published in 2010.

Parallel processing and GPGPU

It is well known that most popular computer processors as we see them today were developed in 1980s, and since that time there were two main sources of increasing their performance: growth of clock frequency which directly increases performance because it allows performing more operations per second; and growth of transistor number and circuit complexity which allows performing more complicated commands and many commands per clock cycle. It is also well known that the physical limitations of existing manufacturing processes and processor technologies do not allow further

significant increasing of a clock frequency and increasing number of transistors in a processor becomes more and more complicated as well. Since increasing the clock frequency is not an option anymore and it may be impossible to continue increasing transistors number soon, at least without a significant breakthrough, it is important to look at other possible ways of increasing available computational performance which mainly lies in the area of more efficient usage of existing resources.

In order to understand how to use existing resources efficiently, it is important to understand that tradeoffs have to be solved by processor developers, which is basically how to use available transistors. In general, for a given number of transistors there are two extreme ways to resolve a main tradeoff: make a processor that can perform one very complicated command per clock cycle; or make a processor that can perform many very simple commands per clock cycle. In the real world all existing processors are somewhere in between. For example the Central Processing Unit (CPU), used for performing most operations in modern computers, can perform few complicated commands per clock cycle (and actually can perform a few times more simple commands) and Graphics Processing Unit (GPU), used for 3d graphics calculations, can perform many relatively simple commands per clock cycle. It is interesting that new generation of CPUs can perform more and more commands per clock cycle and new generations of GPUs can perform more complicated commands with fewer limitations, so both CPUs and GPUs are becoming closer from an architecture point of view.

Although the tradeoff described in the previous paragraph is not just one and there are many other tradeoffs related to memory subsystem, branch prediction, command

scheduling and others, the described one is one the most fundamental and important. Based on this explanation it is easy to see that CPU is more generally purposed and more algorithms may achieve good performance since CPUs can perform more complicated commands specific for each algorithm and algorithms actually do not need to provide many commands for each clock cycle. In opposition to this situation, GPU can perform only simple commands and only algorithms which use simple commands and can perform many commands at the same time will achieve high performance. What is even more important is that these algorithms will run on GPU much faster than on CPU. This situation makes sense since CPU is designed for any possible applications like browsers, games, video players, scientific applications, engineering applications and all have to achieve good performance. GPU, however, is designed specifically for 3d graphics that require many simple independent math calculations. Although a GPU may perform only specialized tasks, these tasks running on GPU may achieve hundreds times faster performance than they would running on CPU (for example modern desktop CPU may perform up to 4 billion floating point operations per second (or 4 GFLOPS) for serial algorithm or up to 192 GFLOPS for highly optimized parallel algorithms and GPU may perform up to 5621 GFLOPS for GPU-optimized algorithm) and an attempt to get similar performance boost for all applications is a goal of General Purpose calculations on GPU (GPGPU) technology which allows running general purpose applications on GPU.

Although GPGPU may look like a great solution for all performance problems, it only allows running non-graphics code on GPU, but does not change its architecture. Now developers have to find a way to use GPU hardware more efficiently. The main

problem here is how to provide enough commands to GPU on every clock cycle. In the case of serial processing on CPU only one command of algorithm is given on every clock cycle, which is exactly how all algorithms are usually designed. In the case of GPU, hundreds or even thousands of commands have to be given and these commands have to be independent from each other because they will be performed concurrently or in parallel. This becomes a problem since usually the commands in algorithms use results of previous commands and process data continuously. In order to solve this problem new algorithms and data structures for representing processing data have to be selected or developed that allow issuing many independent commands every clock cycle and somehow combining results of their work and designing especially for GPGPU purpose.

GPU architecture and OpenCL

The previous part describes the importance of parallel processing and the tradeoff that processor manufacturers have to resolve. Although the need of highly parallel algorithms is the main result of using highly parallel architectures for GPUs it is not the only one. The GPU memory and work scheduling subsystems are also significantly different from their CPU analogs and this difference has to be considered in an algorithm design phase since inefficient memory usage and significant control path branching result in extremely high performance penalties in opposite to traditional CPUs. In order to understand how to design efficient GPGPU algorithms it is important to understand the architecture of modern GPUs that perform these algorithms and available development tools and concepts.

Before going into discussion of GPU architectures it is also important to notice that there are three major GPGPU platforms on the market today: CUDA from NVidia [51], DirectCompute from Microsoft [52] and OpenCL from Khronos Group [53]. The CUDA is a proprietary NVidia technology that works only on NVidia GPUs. It was the first commonly used GPGPU technology mainly because it was a result of a significant and successful effort to make a GPGPU development easier. In opposition to CUDA, OpenCL was developed by Khronos group as an open standard for heterogeneous computing that may work on many possible devices with different architectures. At the current moment all major processor manufacturers have added OpenCL support and released OpenCL SDKs for their processor which means that it is possible to run the same code on several different platforms. Although an ability to write the same code for different devices may significantly simplify a development process the significant difference between architectures requires optimization of code for each architecture or even device separately. The Direct Compute is the latest technology developed by Microsoft as a part of DirectX that supposed to compete with OpenCL. In order to popularize DirectCompute and make it easier to use there was developed the C++ AMP extension that allows running C++ code with minor changes on GPU. For this work the OpenCL was selected since it is an open standard supported by all major chip makers which may become a main standard used for GPGPU computing in future. The OpenCL programming language is based on C99 standard. It adds the additional concept of a kernel – functions running on GPU, memory spaces corresponding to different physical memory locations and some other features which allow access hardware resources.

In this work almost all algorithms were implemented in OpenCL and run on GPUs with NVidia Fermi architecture, and this platform will be discussed (all values will be given for NVidia GeForce GTX580). Although there are some major differences between NVidia, AMD and Intel GPU architectures most of the concepts and ideas behind GPU architectures design are the same and this discussion can be generalized to all available GPUs.

From the OpenCL [54] point of view every computing system contains a set of Compute Devices (CD) which are GPUs in case of GPGPU technology used in this research; every Compute Device contains a set of Compute Units (CU) which are Streaming Multiprocessors in used CUDA architecture and every Compute Unit contains a set of Processing Elements (PE) which are CUDA cores as shown on Figure II-6.

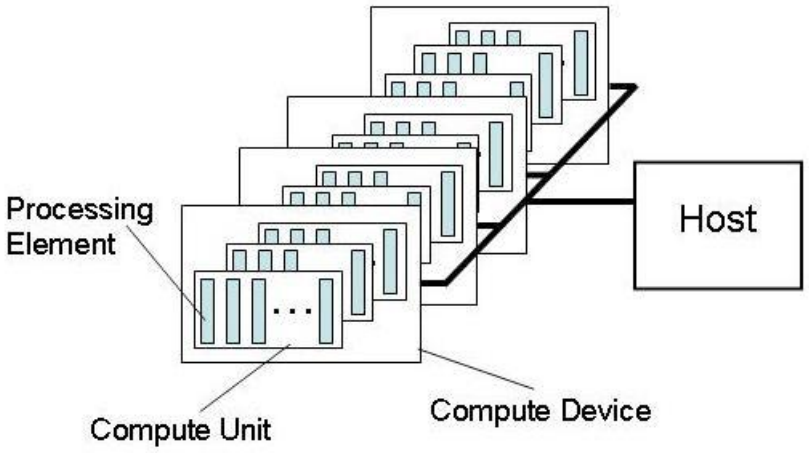

Figure II-6: OpenCL platform model

For example one of the computing systems used in this research had 3 Compute Devices (2x GeForce GTX580 and 1x Quadro 6000) with total number of 46 Compute Units and total of 1472 Processing Elements.

At the same time from the memory model point of view there are Global, Constant, Local and Private Memory spaces as shown on Figure II-7. Global and Constant memories are physically allocated in GPU memory which has a relatively high throughput (~200Gb/s) but very high latency (~800cycles), although Constant memory has an additional cache which allows efficient reading of the same value by multiple threads. The Local memory is physically stored inside of GPU chip and every CU has access to an individual Local Memory storage. This memory type has much lower latency (~10cycles) and relatively high bandwidth (~1Tb/s) but the size of it is very limited (~48Kb/CU). The Private memory is the fastest available data storage which represents CU registers which are divided by all PE and only accessible by one PE. In modern GPUs there is also available L2 cache (768Kb/CD) used for caching Global memory access and part of Local memory storage is used for L1 cache (16Kb/CU).

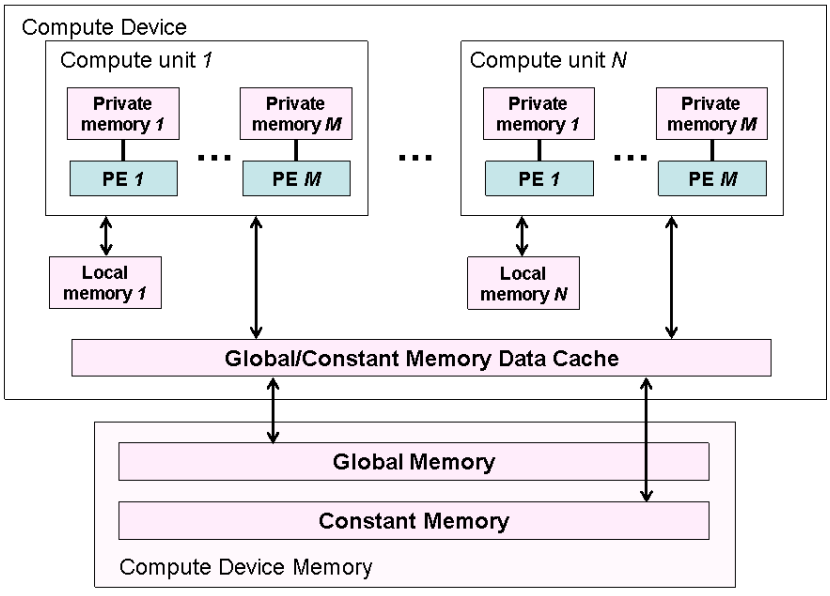

Figure II-7: OpenCL memory model.

From the programming point of view GPU processes a grid or N-Dimensional Range (with up to 3 dimensions) of Work Items as shown on Figure II-8 where all Work Items are combined into N-Dimensional work groups.

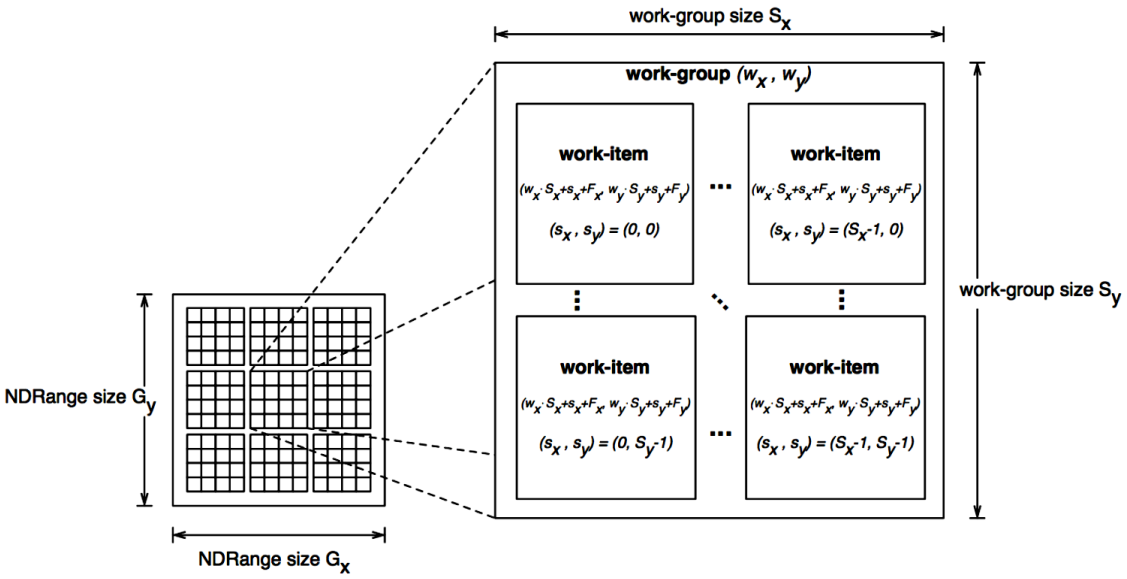

Figure II-8: OpenCL threads grid

For each work item, GPU launches a light-weight thread that performs a selected function called “kernel”. Since the number of command schedulers on each Compute Unit is much less than a number of Processing Elements, multiple PEs are combined in a group (32 elements) called “warp” (“warp” is the term used by NVidia, AMD uses the term “wavefront” for their architecture, that actually has value 64) and all PEs in this group perform the same command on different work item data elements. This approach is called SIMD (Single Instruction, Multiple Data) and it allows development highly parallel processors which can process many data elements per clock cycles. The important drawback of this approach is a significant penalty in the case of code

branching, it is easy to see that if some threads in a warp follow one branch of code and other follow another branch they have to wait for each other since they can perform only one command at a time. This drawback means that efficient algorithms need to have a low control flow divergence inside warps.

Another important limitation of GPUs is related to the high global memory latency which can be up to a thousand clock cycles. In order to hide this latency GPU runs much many threads that it can process at a time and switches between them in order to process available data while other threads are waiting for loading data. It means that a number of running threads has to be much higher than a number of processing elements in order to hide GPU memory latency and this number may need to be as high as tens of thousands in opposite to few threads on CPU.

The last limitation to be mentioned is also related to a memory subsystem. As it was mentioned before, physical limitations do not allow significantly increasing clock frequency for modern processors but the same limitations affect also memory chips and memory manufacturers need to use a workaround. One of the most popular ways is similar to processor technologies – use parallel processing or parallel reading/writing in case of memory. In order to achieve high throughput required for GPU many data elements or words are loaded from or stored to memory in one memory access operation. Usually it is implemented in the way that a linear block of words is accessed in one memory operation (this is a limitation of a memory controller complexity) and the number of words is equal to number of threads in a warp so each warp thread can read or write a word in one memory command. This approach works quite well and allows

achieving extremely high memory bandwidth, but only if all threads access a continuous block of memory. If threads access words at completely random memory addresses this process is serialized and multiple memory access commands are issued which results in a significant performance penalty.

The described list of three GPU architecture limitations is not a full list, but even they can reduce performance by many orders of magnitude. In order to understand the importance of optimization and GPU specific algorithm and data structure design it may be useful to look on the difference between most efficient and most inefficient programs from the described limitations point of view. The code branching limitation can reduce the program up to 32X if all threads follow different branches, the linear memory access limitation may also result in up to a 32X slower performance if all memory commands have to be issued 32 times. Memory latency limitation may result in up to 800X slower performance if processors have to wait ~800cycles for the next data element all the time if there are not enough running threads. It is easy to see that the difference between the most efficient and the most inefficient algorithms may almost reach a 1000000X times just due to three described GPU architecture limitations. It is obvious that real algorithms are usually not so inefficient but even an order or two orders of magnitude of performance degradation which are quite common results of optimization are extremely important.

III. 3-AXIS MACHINING SIMULATION

3-axis milling is the most popular CNC milling technology. Successful and efficient 3-axis milling is not trivial, often requires multiple iterations and has to be simulated to ensure that the machine tool does not crash due to tool path errors.

There are currently many simulation software systems available for 3-axis milling on the market. Some of them use GPU acceleration for rendering processes but to the author's knowledge, there are no systems that employ the GPGPU programming approach for both simulation and rendering operations even though modern GPUs have extremely high theoretical computational performance and general purpose programming ability. Traditional central processor units (CPUs) are reaching performance boundaries due to physical limitations and a parallel GPU based approach is attractive for developing new high performance simulation systems. Although the GPU has significant promise, it requires a new design approach using highly-parallel algorithms and data structures that vary significantly from those that are presently employed in the traditional milling simulation field.

This chapter describes the developed 3-axis milling simulation system based on the developed parallel algorithms for simulation and rendering. The presented set of algorithms is based the height map data structure and implemented with GPGPU approach. There will be also presented experimental milling simulation results and simulation accuracy analysis. In addition to algorithm presentation there will be a

discussion about methodology for algorithm parallelization and selecting parallel friendly and especially GPU friendly data structure.

Height map representation of a machined workpiece

The selection of the right geometry representation for simulation is the most fundamental and critical part of any geometry processing software. A geometry representation has to satisfy accuracy, memory usage and computational requirements but a critical additional requirement in this research is the ability to use parallel processing for geometry editing and rendering.

The geometry processing operations used in milling simulation are: geometry rendering and geometry editing. Triangular geometric representations are the most widely used for rendering. GPUs are specifically designed for rendering triangular meshes since this process can be efficiently parallelized and even implemented in hardware as it was done in the early history of the gaming industry. Although triangular meshes allow high performance rendering, they are relatively complex from the editing perspective. The geometry editing during milling simulation can be represented as a set of Boolean operations between workpiece and tool swept volume. If the workpiece is represented by a triangular mesh, each Boolean operation requires location of existing triangles (workpiece surface), calculation of a new surface geometry, triangulation of the new surface and updating the existing list of triangles. Although some smart tree-based localization algorithms can be used for solving the triangle location problem, other parts of this algorithm require a significant amount of calculations and cannot be easily

parallelized which is a significant limitation. While multiple Boolean operations may be parallelized, this is only possible when editing different areas and, more importantly, it requires a significant amount of synchronization and complex memory management. In addition, processing different triangles in parallel, as it is done during the rendering process, is not efficient in the case of continuous editing when many edits are applied simultaneously and cannot be used to simulate a long program in parallel fashion. The use of triangles also requires complex memory management due to the unknown number of triangles generated by each surface change.

It is important to identify two main use cases for a milling simulator. First, a "continuous simulation" scenario is used when a user is interesting to see machine motions and find collision. This scenario requires simulation of a short tool motion between rendered frames since a user wants to see all tool positions and smooth continuous tool motion. Second, "fast simulation" scenario is used when a user wants to see a final result of a milling process. In this case a long list of tool motions (or even an entire trajectory) is simulated between two rendered frames.

These opposite objectives represent a fundamental tradeoff significantly affecting the editing algorithm and require development of two independent algorithm approaches since a general algorithm that scales well in a very large range of number of editing operations may not satisfy both objectives sufficiently. In the many edits scenario, it is acceptable to perform some data pre- or post-processing, which takes a constant amount of time. However, this time is separated between multiple edit operations and does not significantly affect the rate at which edits are applied. In contrast to the many edits

situation, a single simulation edit scenario requires as short as possible single edit processing time because pre- or post-processing time is not hidden by multiple edit operations (the pre- or post-processing time usually does not rely on the number of data elements and it becomes very small from a per element point of view in case of many data elements). Another important limitation of single edit situation is a way of parallelization because if an algorithm is designed only to process multiple edits in parallel, it is difficult to provide enough work for multiple computational devices when the number of applied edits is low. For these reasons, a triangular geometry representation is a good choice for rendering but is not a good choice for parallel editing operations.

A natural fit for 3-axis CNC milling simulation is a height map. The height map is a data structure that represents a surface as a 2D array of distances from a base plane to the target surface in direction of a surface normal (a simplified 1D height map is represented by values of H1...H5 on Figure III-1). The reason it is "natural" is because in most cases, a 3-axis machine is removing material only from one side (top for vertical machines). Although there are some cutting tools used in the industry that can remove material under top surface areas, they are beyond the scope of the current research where the main goal is exploring parallel algorithms for milling simulation. For all other 3-axis situations, it is possible to represent a machined workpiece as a height map.

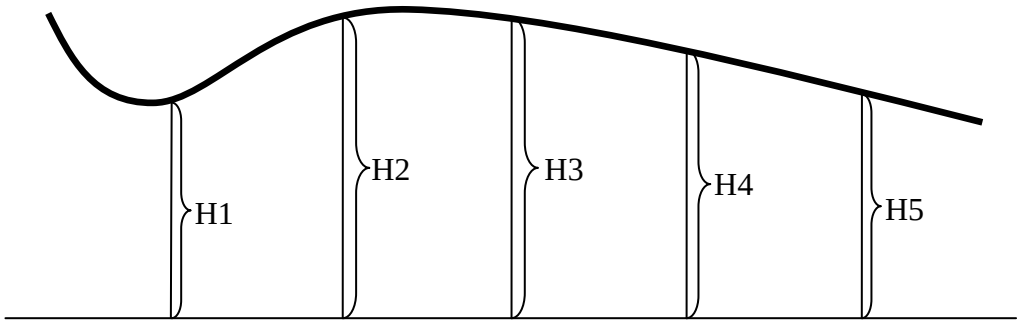

Figure III-1: 1D height map

A 2D height map array is stored in GPU memory in OpenCL memory space and is accessible to OpenCL kernels. For this work, the top plane of a workpiece is considered as a base plane for a height map and the normal is directed up, so all values in machined areas are negative. However the height map represents only a set of points on a real machined surface and parts of surface between known points are approximated by linear interpolation of neighboring points.

Workpiece rendering

In opposition to the triangular mesh, the height map allows implementing efficient parallel editing algorithm, which will be described later, but does not have good algorithms for rendering. Since an efficient direct rendering of a height map usually is not feasibly, a rendering is done indirectly by converted a height map into a triangular mesh for which there are known efficient hardware accelerated rendering algorithms. This approach solves two problems at the same time: first it allows using GPU hardware for efficient rendering and also provides a “free” linear interpolation of surface areas between points. From a parallel programming point of view the converting process is also

quite good since there is always known a number of triangles and all triangles for a mesh can be generated completely independent.

The described indirect rendering process is shown by Algorithm III-1.

```
1  For each height map point in parallel:
2  |  Generate two triangles
3  |  Estimate triangle normal based on neighbor points
4  |  Add triangle vertices and normal to a buffer
5  Render a list of generated triangles
```

Algorithm III-1: Height map rendering

Generally, there are three main steps:

1. Triangles generation
2. Normals estimation
3. Triangles rendering

Each pair of triangles generated for each point represents an approximated surface around a height map point. Their vertices have the same coordinates as a main point and 3 neighbors:

$$1: (x_{X,Y}, y_{X,Y}, z_{X,Y}), (x_{X+1,Y}, y_{X+1,Y}, z_{X+1,Y}), (x_{X+1,Y+1}, y_{X+1,Y+1}, z_{X+1,Y+1}) \quad \text{(III-1)}$$

$$2: (x_{X,Y}, y_{X,Y}, z_{X,Y}), (x_{X,Y+1}, y_{X,Y+1}, z_{X,Y+1}), (x_{X+1,Y+1}, y_{X+1,Y+1}, z_{X+1,Y+1}) \quad \text{(III-2)}$$

Where $(x_{X,Y}, y_{X,Y}, z_{X,Y})$ represents physical coordinates of a height map point with (X, Y) logical coordinates.

Although real normal vectors for each surface point cannot be extracted from a height map representation, they can be estimated based on height values. For simplicity

in this work, lighting calculations use normal vectors of generated triangles which are estimations of a surface between height map points. These normal vectors can be calculated as a cross product of triangle edge vectors:

$$e_1 = (x_{X,Y}, y_{X,Y}, z_{X,Y}) - (x_{X+1,Y}, y_{X+1,Y}, z_{X+1,Y}) \quad \text{(III-3)}$$

$$e_2 = (x_{X,Y}, y_{X,Y}, z_{X,Y}) - (x_{X+1,Y+1}, y_{X+1,Y+1}, z_{X+1,Y+1}) \quad \text{(III-4)}$$

$$n = e_1 \times e_2 \quad \text{(III-5)}$$

After generation of a list of triangle vertices and their normal vectors, this list can be rendered by OpenGL on available GPU in a traditional way. Figure III-2 shows an example of a rendered simulation result.

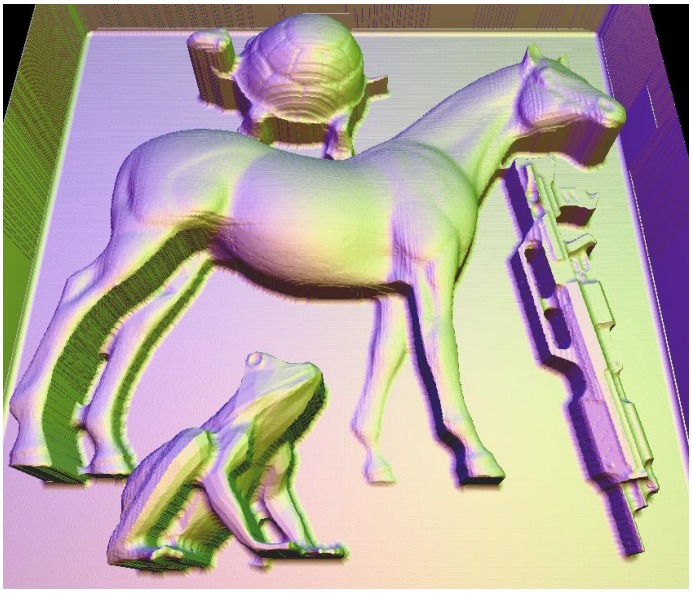

Figure III-2: Height map rendering example

From the algorithmic point of view, all three described steps required for rendering the height map are straightforward. However, it is important to mention that the

implementation and performance of these algorithms on current hardware have some limitations. In this research, the simulated results are rendered using the open source rending API OpenGL and a main limitation is related to the method of sharing data between OpenCL and OpenGL. Current hardware does not allow the same buffer to be used by both languages and requires copying vertex data buffer from one context to another on GPU. Although using OpenCL-OpenGL interoperability extensions allows eliminating copying data through host (and very slow PCIex), data is still copied inside GPU memory. As result there is a constant time overhead due to memory copy operation. Another limitation is related to multi-GPU configurations. In contrast to OpenCL, which allows control device data storage and kernel execution, OpenGL does not provide any control (except extensions for professional cards) of where the geometry is stored and rendered. OpenGL even performs some synchronization between devices automatically. As a result, rendering performance of multi-GPU systems may be significantly slower than a performance of single GPU systems due to additional and often useless data transfers between multiple devices. These issues are not critical for traditional single-GPU systems but there is no general way to scale performance efficiently for multi-GPU systems without considering other geometry representation approaches and rendering algorithms. This clearly defines opportunities for improved architecture elements for OpenGL.

Generalized cutter representation for 3-axis milling simulation

The previous discussion explained the need for indirect height map rendering and its method of implementation. But the real strength of the height map geometry representation is parallel milling simulation. Before explaining the details of the simulation algorithm it is important to describe how machine tool geometry is stored. This research is currently limited to 3-axis milling simulation with rotary cutting tools (without tapered tool support). Although there are many ways to represent a cutter, (*e.g.*, a triangular mesh or CSG object) it is obvious that any rotary cutting tool can also be represented as a half of a curve that is a result of intersection of a cutter and a plane which contains a cutter axis (Figure III-3).

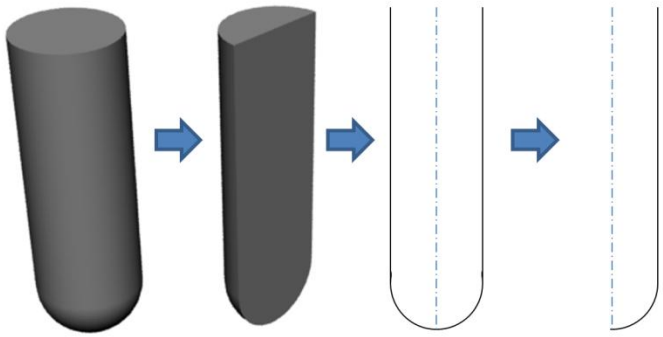

Figure III-3: Cutting tool intersection

This curve can be represented analytically and described in Automatically Programmed Tool (APT) language format as it is often done in traditional CAM systems or also can be represented as a 1D height map shown on Figure III-4 where N is the number of points representing a cutter.

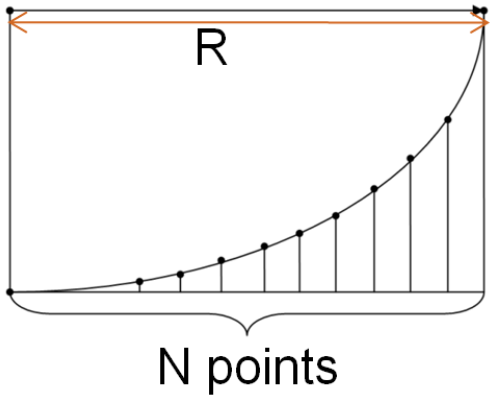

Figure III-4: Cutting tool height map representation

For the purpose of this research, the height map representation was selected not for geometry processing or algorithm purposes, but because it lends itself well to the GPU architecture. An analytical description of a cutting tool as a curve usually requires trigonometric functions that are quite slow on the GPU, especially if accurate but non-hardware versions are used. As result a height map with resolution of 1024 points for cutter and linear interpolation of intermediate points was selected to represent the cutting tool.

3-axis milling simulation algorithm

The height map and generalized cutting geometry are used to simulate the milling process. Simulation allows the machined surface geometry to be represented without actual milling. The milling process is simulated by calculating and removing material by the generalized cutting tool at every point of a tool path. For 3-axis milling, the simulation process is the sequential update of height map values by the minimum value between existing values and distances to a cutting tool.

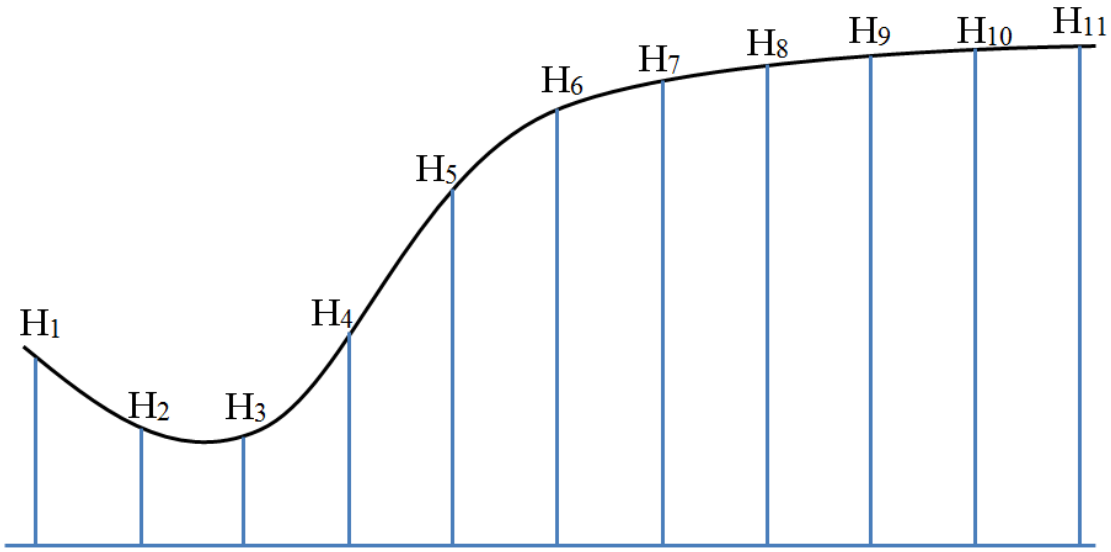

Figure III-5: Height map updating process - before editing

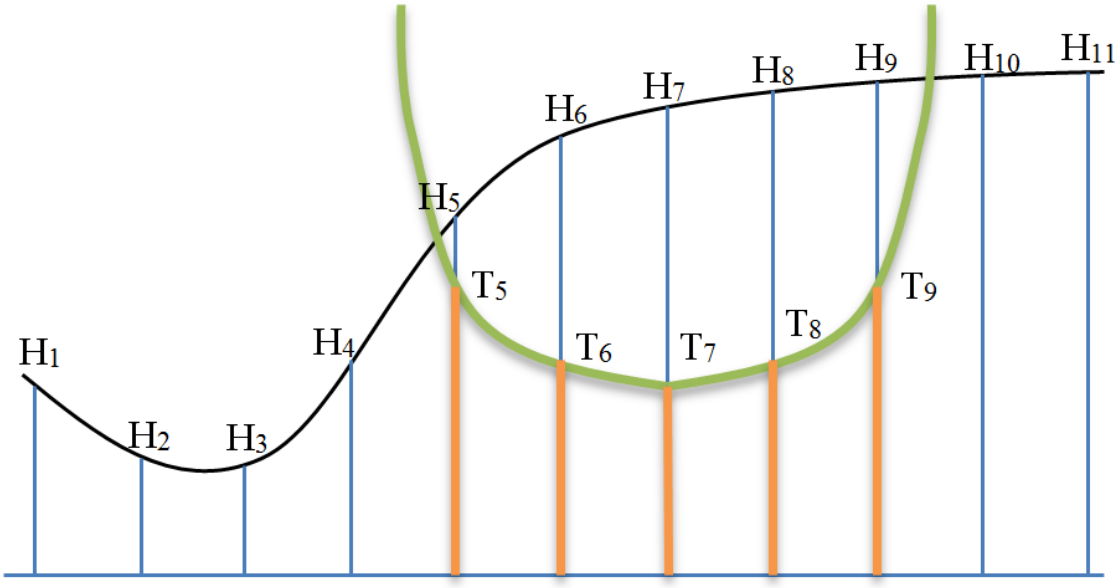

Figure III-6: Height map updating process - editing

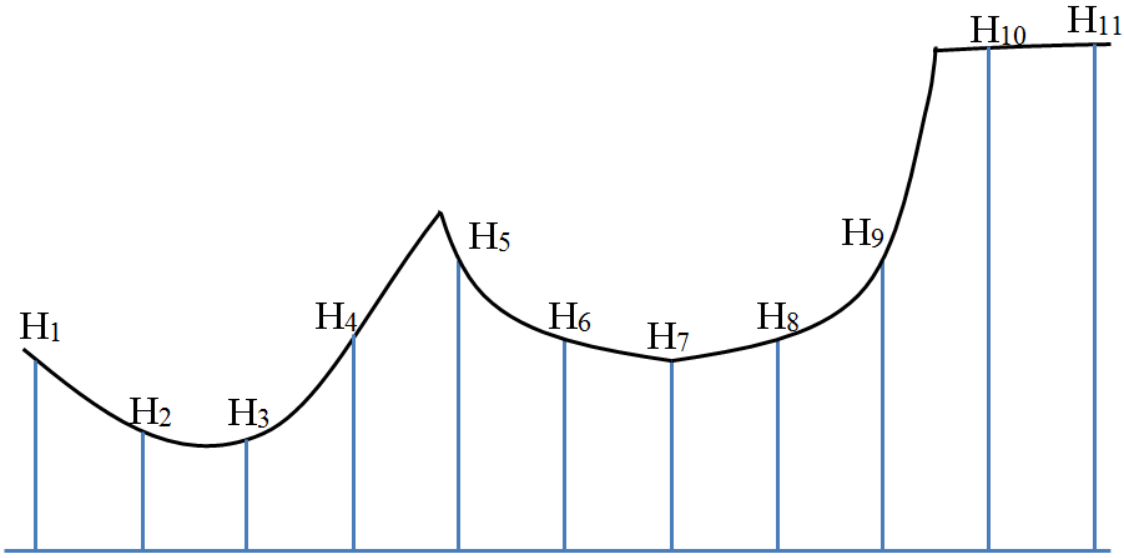

Figure III-7: Height map updating process - after editing

Figures above demonstrate a process of updating height map values for a simplified 1D height map. The Figure III-5 shows an original surface and height map values H1…H11 which represent this surface. The Figure III-6 shows a tool and appropriate distances to a tool surface T5…T9. The Figure III-7 demonstrates a result of an editing operation with new surface and new height values H1…H11. A single iteration of an editing process for a single cutter position can be described by the equation:

$$H_i = \min(H_i, T_i) \tag{III-6}$$

It is important to notice that the calculation of each height map value uses only a previous value and a distance to a tool surface and it is completely independent from other values. For simulation of an entire tool path with multiple tool locations it becomes a bit more complicated:

$$H_i = \min(H_i, T_{i,1}, T_{i,2}, \dots, T_{i,n}) \quad \text{(III-7)}$$

Where $T_{i,1}, T_{i,2}, \dots, T_{i,n}$ are distances to a tool surface for the same logical height map location and multiple tool positions. The algorithm for implementing the described approach is shown by Algorithm III-2.

```
1  For each height map point in parallel:
2  |  Retrieve current height value and store as a Current Value
3  |  For each tool position:
4  |  |  Calculate tool surface height value at current height map point
5  |  |  If new height value is smaller than the Current Value:
6  |  |  |  Replace the Current Value by new height value
7  |  |  Update height map value by the Current Value
```

Algorithm III-2: Material removing simulation

The expression (III-7) can also be written in another ways:

$$H_i = \min\left[\min\left(H_i, T_{i,1}\right), \min\left(H_i, T_{i,2}\right), \dots, \min\left(H_i, T_{i,m}\right)\right] \quad \text{(III-8)}$$

It is mathematically identical to the original expression but represents a completely different approach for parallel implementation of the same concept as shown by Algorithm III-3.

```
1  For each height map point in parallel:
2  |  For each tool position in parallel:
3  |  |  Calculate tool surface height value at current height map point
4  |  |  Perform atomic operation:
5  |  |  |  Update the height map value with a minimum of existing and new value
```

Algorithm III-3: Material removing simulation second approach

In case of form (III-7) each thread processes all tool positions for one logical height map point and selects the minimum value. In case of (III-8) each thread processes only one pair of logical height map point and tool position and then compares its own result to results of other threads. The tradeoff between these approaches is amount of calculations and synchronization versus parallelism. The second approach obviously has to perform much many min operations than the first one but can run much more threads with easier tasks and offers higher granularity parallelism. Another important issue is a requirement of additional synchronization between threads, like atomic memory operations, in case of the second scenario because multiple threads may work together on the same logical height map point as shown on Figure III-8. The effect of the implemented collision avoidance techniques on simulation performance due to additional synchronization will be described later in the performance analysis section.

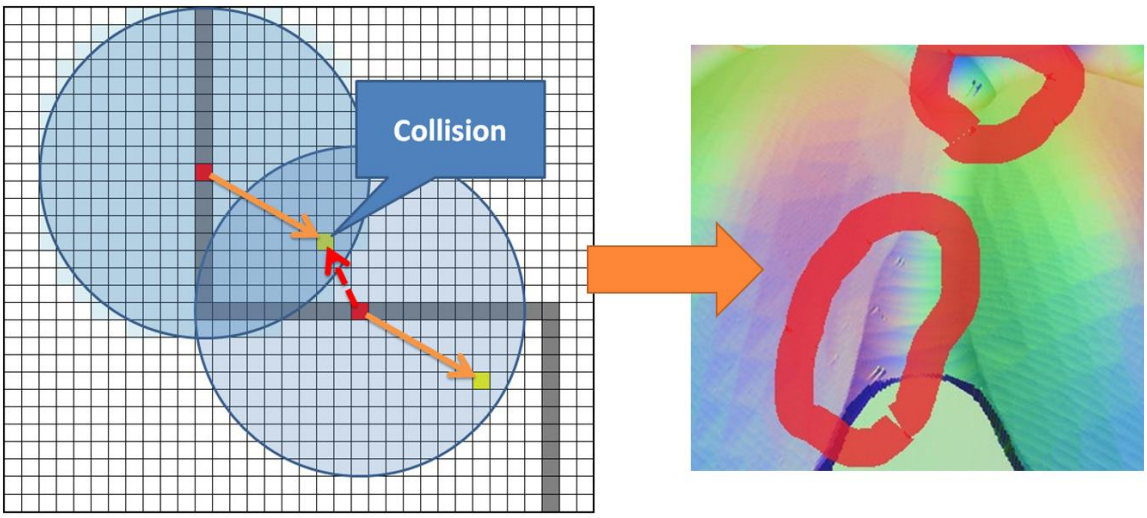

Figure III-8: Collision example

In the current work the second approach, described by equation (III-8), was selected since it provided slightly better performance on existing NVidia Fermi architecture. Although in case of this work the selected approach showed better performance, this tradeoff significantly depends on hardware and has to be considered independently for different architectures since performance of synchronization primitives, thread group granularity and command throughput may be very different.

Experimental 3-axis simulation results

The described 3-axis milling simulation and rendering algorithms were implemented in C++ and OpenCL during the research project and tested on multiple tool paths. The experimental simulation results are presented in the ensuing text and figures.

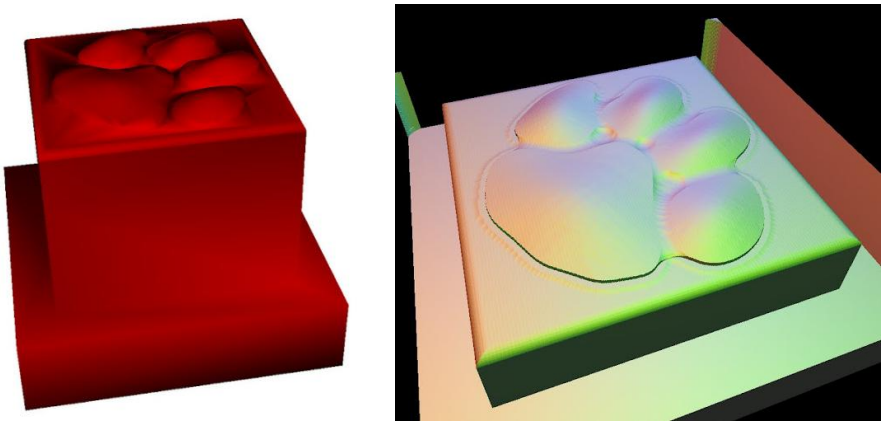

a) Original model b) Simulation result

Figure III-9: Test model “Tiger paw”

a) Original model b) Finishing result (1/16” ball-end)

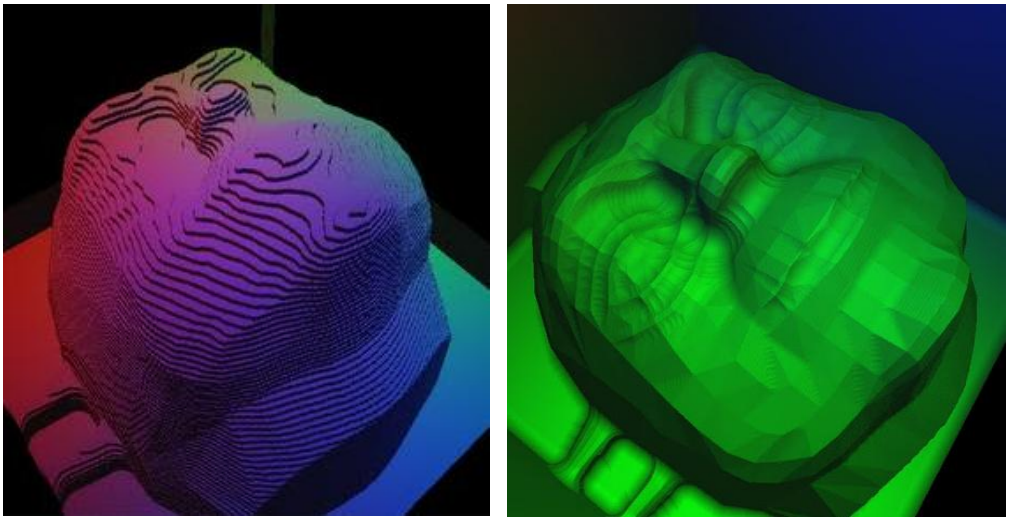

c) Roughing result (1/4” flat-end) d) Finishing result (1/16” ball-end)

Figure III-10: Test model “Yoda”

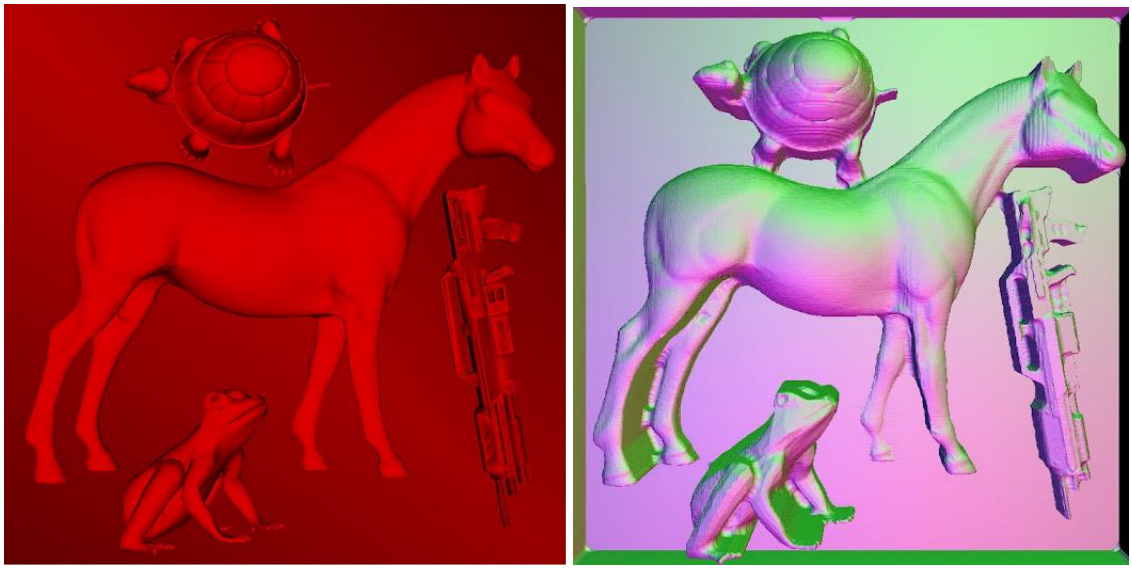

a) Original model b) Finishing result (1/16” ball-end)

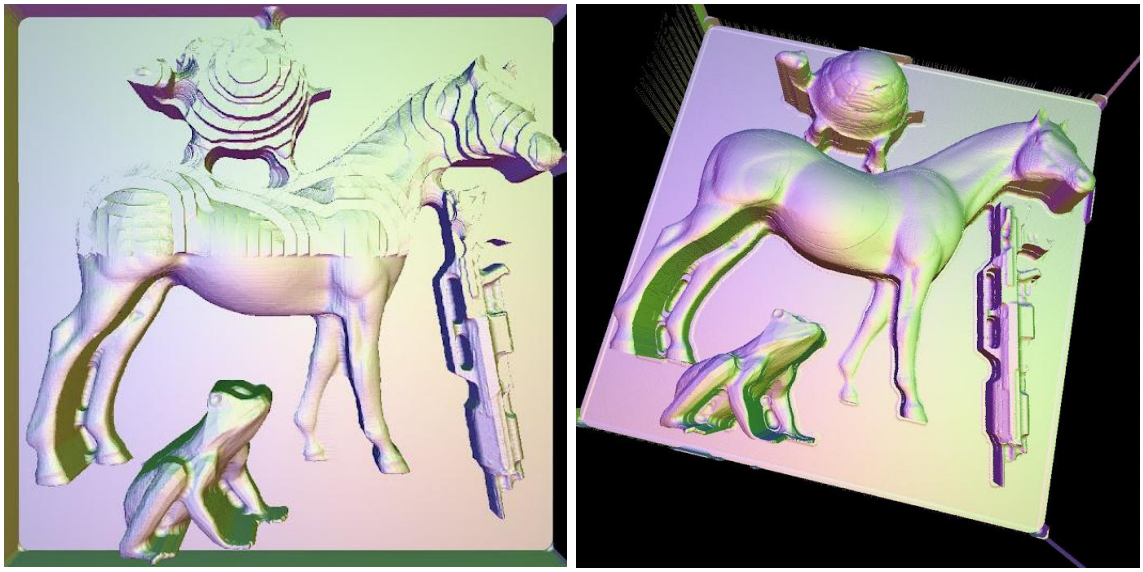

c) Half way finishing d) Finishing result (1/16” ball-end)

Figure III-11: Test model “Zoo”

a) Original model

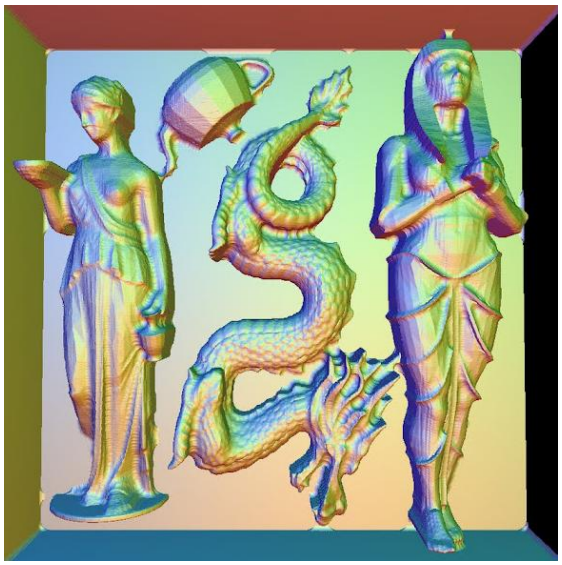

b) Finishing result (1/16” ball-end)

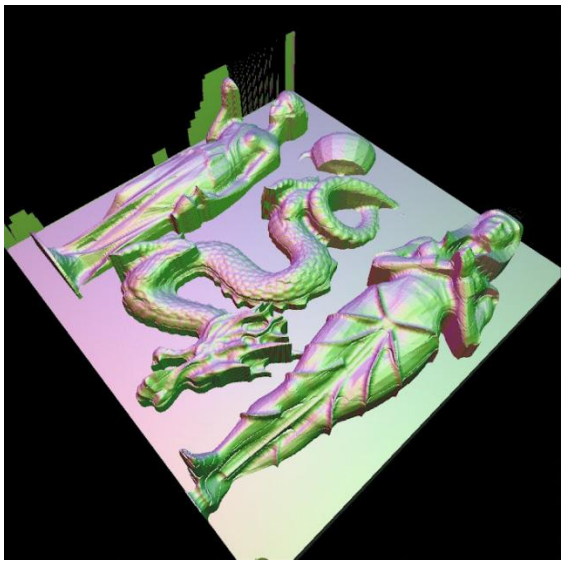

a) Rotated model

b) Finishing result (1/8” ball-end)

Figure III-12: Test model “Sculptures”

Demonstrated results show that the height map geometry representation model can successfully be implemented on modern graphics processors for milling simulation with high accuracy. Although there are no efficient techniques for direct rendering of a height map, converting to the triangular mesh allows efficient rendering and also can be accelerated by the GPU. It is important to note that the height map does not represent vertical surfaces as well or as accurately as horizontal surfaces. This is the reason there are some color artifacts on vertical walls. These artifacts appear at places with a high difference between neighboring height map point's values. These differences result in a poor normal estimation and incorrect surface color rendering. Increasing the height map resolution will help with this problem but it will result in increased processing time. The complexity of height map processing is proportional to the square of the resolution and results in significant performance and memory penalties as discussed in the performance analysis section.

Milling simulation and rendering performance

The main goal behind using parallel processing and GPUs for calculation is obviously getting better performance and scalability. The performances of all the described simulation algorithms were implemented on both CPU (Single threaded version) and GPU (Parallel OpenCL version) for comparison. The testing results are shown on Figure III-13.

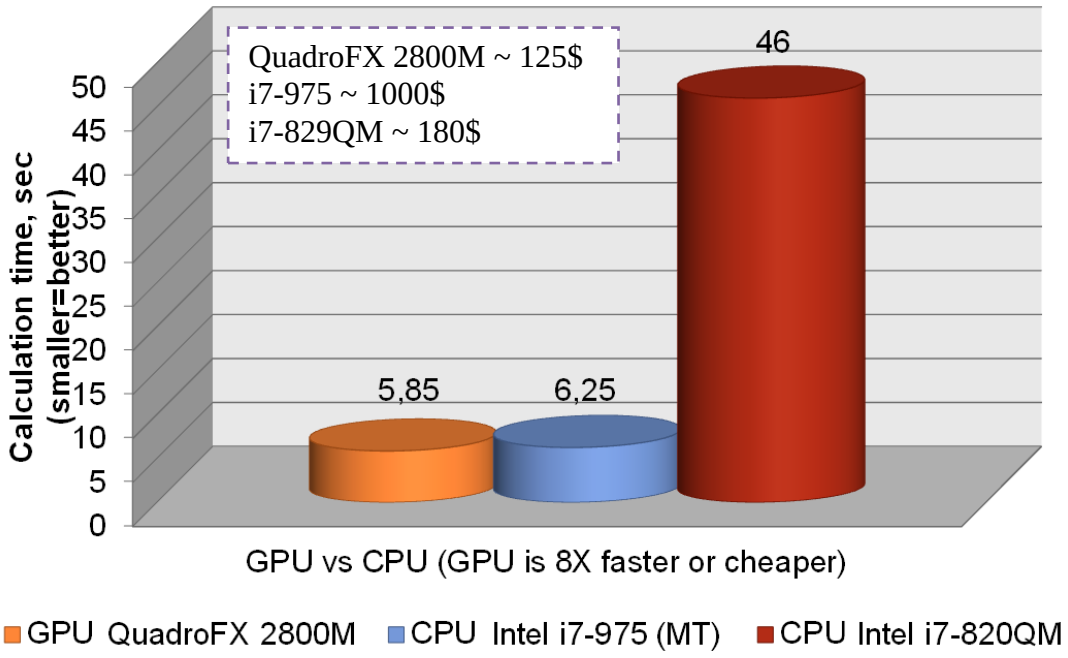

Figure III-13: CPU vs. GPU simulation performance

Performance testing was performed on a Dell Precision M6500 mobile workstation with the Intel i7-820QM CPU (4 cores, 1.73 GHz) and an NVidia Quadro FX2800M GPU (96 CUDA cores, 1.5 GHz) with a 2048x2048 height map resolution. When comparing hardware, it is important to consider cost. In order to estimate prices (because the hardware used is only available for OEMs and its prices are not publically available) the prices of similar retail GPU and CPU hardware costs with very similar performance were recorded:

- NVidia QuadroFX 2800M ~ NVidia GTS 250 ~ $125
- Intel i7-820QM ~ Intel i5-650 ~ $180

This comparison shows that the parallel algorithm running on the low-end GPU with the lower than the CPU price provides 8X better performance than the non-parallel

algorithm on the CPU. In order to make comparison more interesting, the fastest available hardware on the market (at the time of the comparison) is the "Intel i7-975" CPU with a price of ~$1000. The performance of the algorithm was estimated by assuming utilization of all available cores and linear performance growth. Since the performance of the CPU was linearly extrapolated, and the linear performance scaling is the maximum theoretically achievable result, it is accurate to say that the best CPU available on the market can only achieve the performance of the low-end GPU which is ~8X cheaper. The demonstrated result shows that GPUs may provide a significantly better performance for the same task than the best available multi-core CPUs if the right parallel algorithm is employed.

In contrast to the CPU, the work is always divided into groups or blocks on the GPU. Each GPU contains multiple multiprocessors with many cores. Selection of the best block size is an important performance optimization step. Figure III-14 shows that the implemented simulation algorithm works faster with larger group sizes. It also shows that there is the relatively constant performance penalty due to the collision avoidance algorithm which performs the additional synchronization between threads for preventing collisions.

Another important factor is the dependency of the entire simulation time on a number of path points processed per iteration (Global size) as shown on Figure III-15.

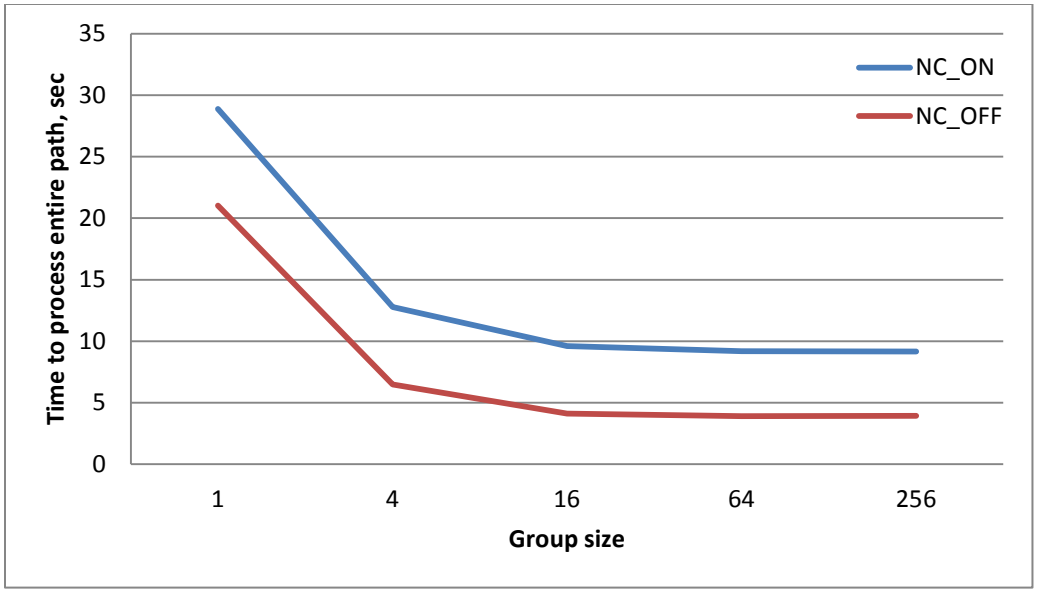

Figure III-14: Performance vs. Group size (global size = 8k)

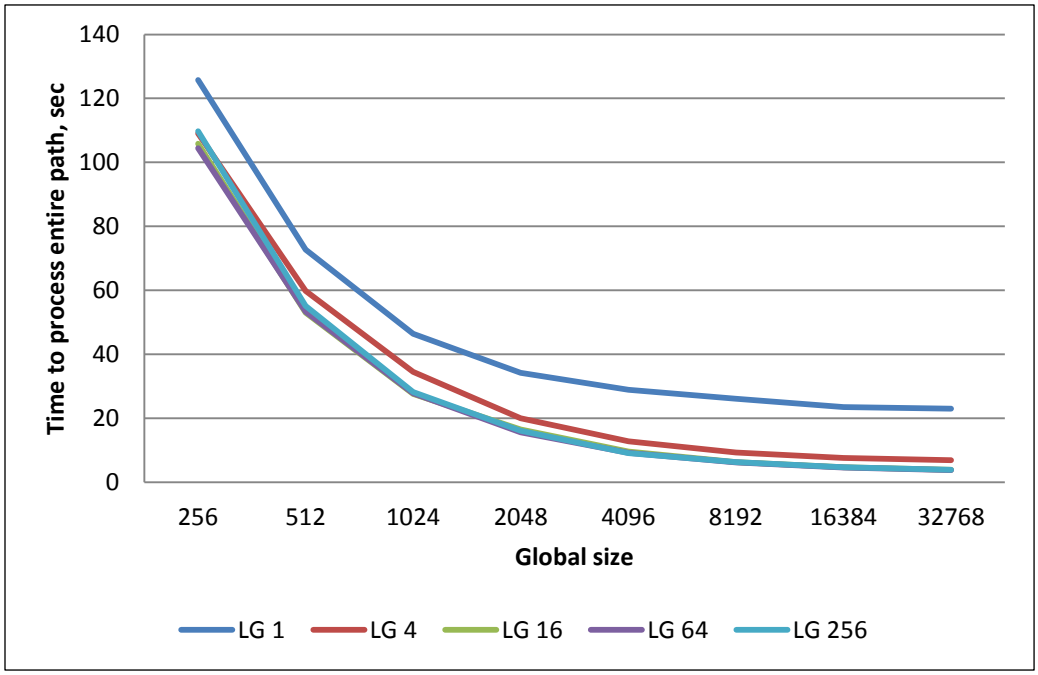

Figure III-15: Performance vs. Global size

Larger global sizes result in much faster simulation due to better utilization of the GPU workload. It also shows that the GPU provides good performance only in situations when the number of processed path points (or working threads) is high enough to load the entire GPU and to hide the memory access latency. Figure III-16 shows that the high number of working threads may completely hide the cost of the additional synchronization required for the collision avoidance algorithm.

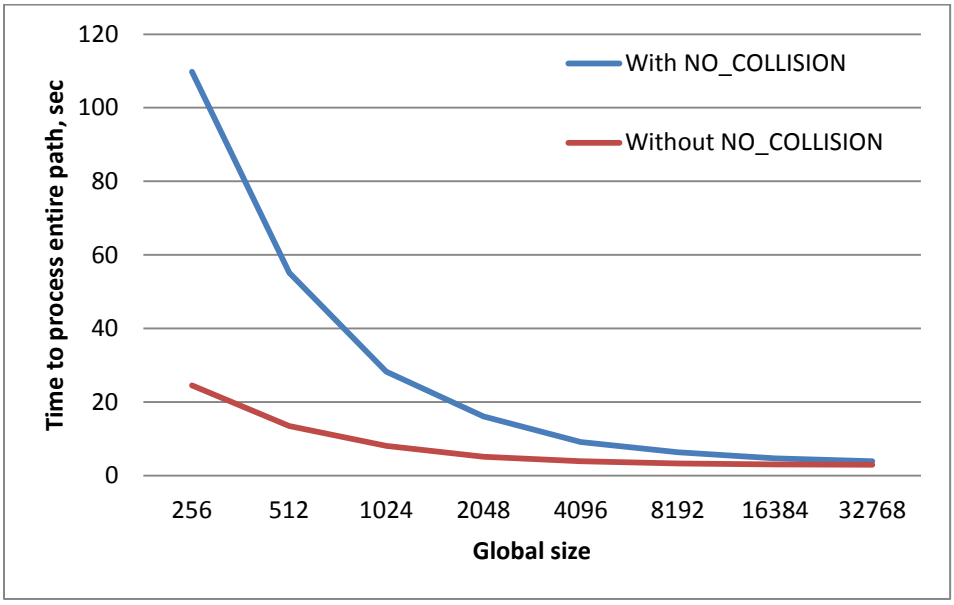

Figure III-16: Effect of collision avoidance on performance

The most important conclusion about the GPU performance is that it has to have enough work and enough threads running in parallel to show good results. Although the GPU may yield excellent performance results if it has enough work to do, the opposite statement is also correct and the performance can be very poor if there is not enough work as shown on Figure III-17.

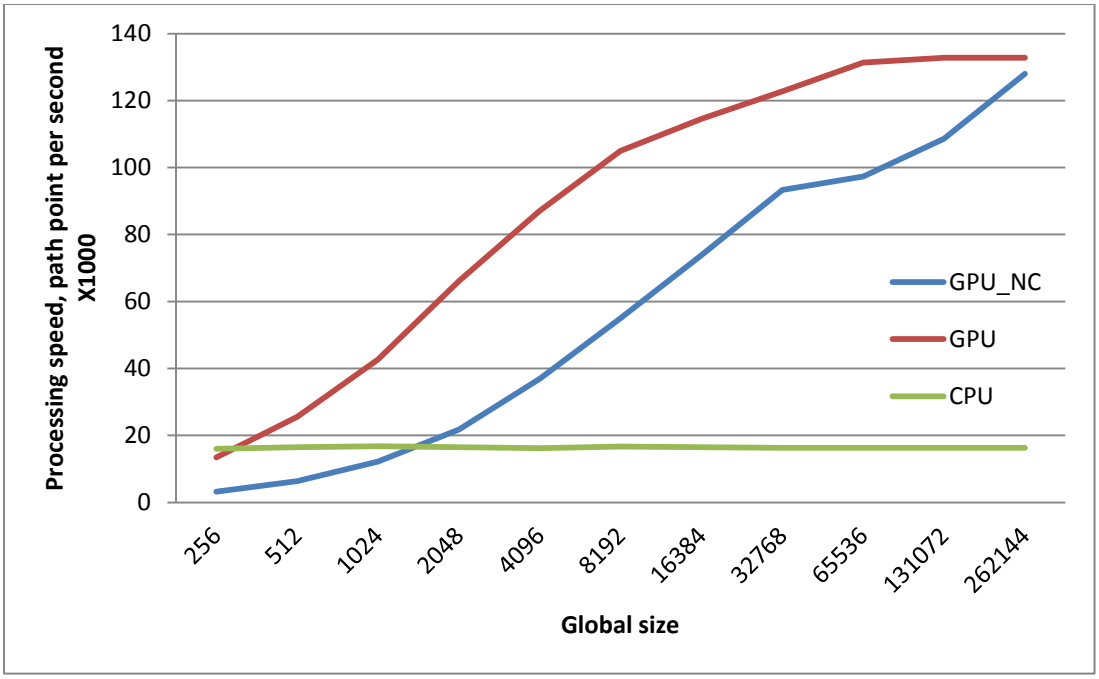

Figure III-17: Simulation performance vs. Global size with CPU

It is easy to see that in the case of only 256 path points per iteration the GPU simulation performance is lower than the single threaded CPU performance. However, its performance constantly grows with growing global size (number of processed path points) until it saturates at 32k-64k points per iteration.

There is a quadratic dependency between the resolution per side (symmetric height map is used for simplicity in this research) and the performance. The simulation performance was measured for different height map resolutions and the same tool path. During the measurements, the global size of 1024 points per iteration and the local size 64 were used.

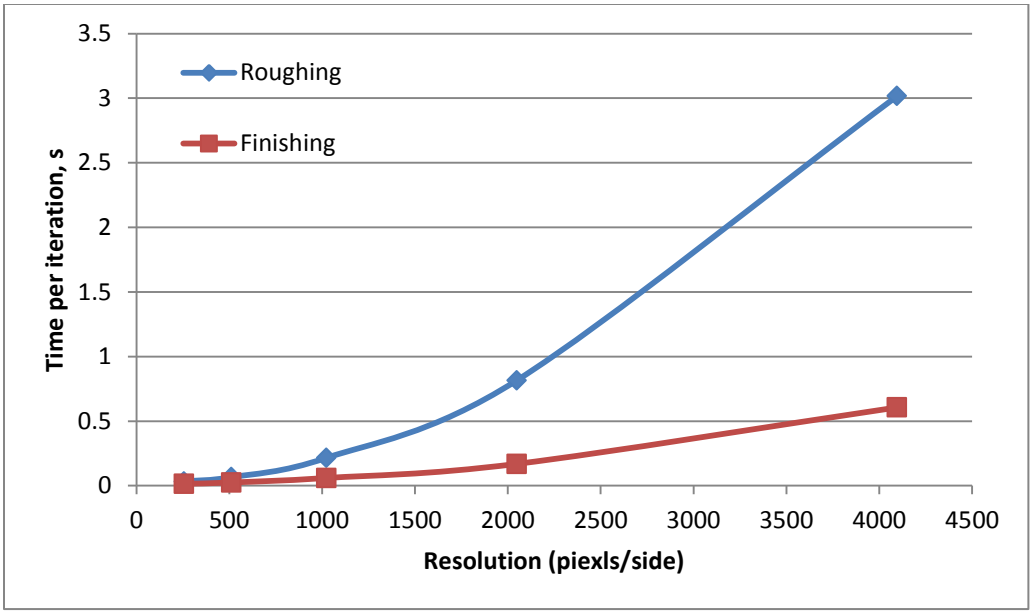

Figure III-18: Rendering vs. Resolution

Figure III-18 shows results of these measurements for roughing and finishing tool paths. The noticeable difference in the performance is the result of different memory access patterns. In case of the finishing tool path, with a zigzag topology, only a small area of the height map is accessed during iterations. The reason for this is that the position of all path points is along a short line segment when the tool moves from one side to another. In contrast to finishing, the roughing path requires tool movement in a relatively random way from a memory controller point of view because the path topology depends on the target geometry and cannot be described as a list of long linear motions and linear memory access operations. As result the memory access pattern becomes non-linear. This results in a much lower memory subsystem performance and the slower simulation.

Although the simulation performance results demonstrated on the Figure III-18 show a strong quadratic dependency, the total simulation time contains multiple components. As mentioned previously, the implemented simulation process includes:

- simulation (actual editing of the height map),
- map generation (converting the height map into the triangular mesh),
- rendering (actual rendering of the triangular mesh by OpenGL)

The independent performance results of each step for different resolutions are shown on the Figure III-19.

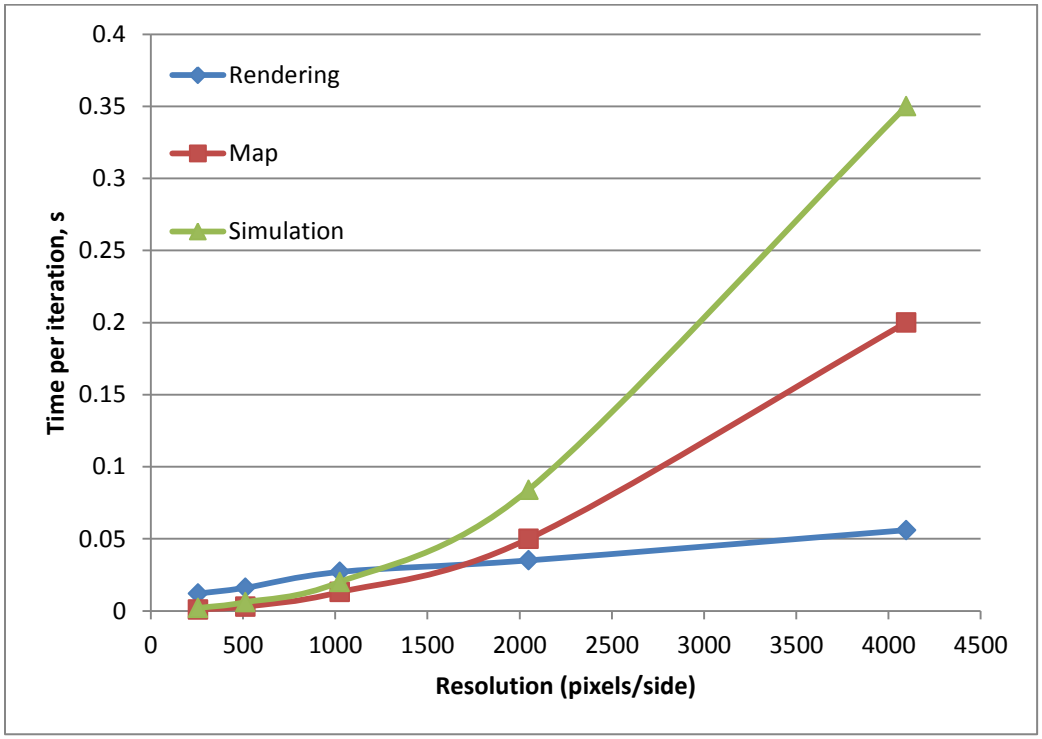

Figure III-19: Simulation components vs. Resolution

It is apparent that for low resolutions (<2048) the main part of the simulation time is the rendering time. However, at higher resolutions the rendering process does not show a quadratic performance dependency and becomes a minor part of the final result.

The second longest part of the current simulation implementation is the generation of the triangular mesh. The process of a mesh generation is very simple from a computational perspective. The primary time consumption is due to memory transfer operations. The problem with memory transfers is because OpenCL and the OpenGL do not share memory and memory must be transferred from the GPU to the host and back. Although the pure OpenCL specification does not allow sharing buffers there is the OpenCL-OpenGL interoperability extension available. It significantly improves data sharing performance. This extension replaces two memory transfers operations over the PCIEx bus by a single memory copy operation inside the GPU memory that works much faster. The performance benefit from the usage of the OpenCL-OpenGL interoperability extension is shown in Figure III-20.

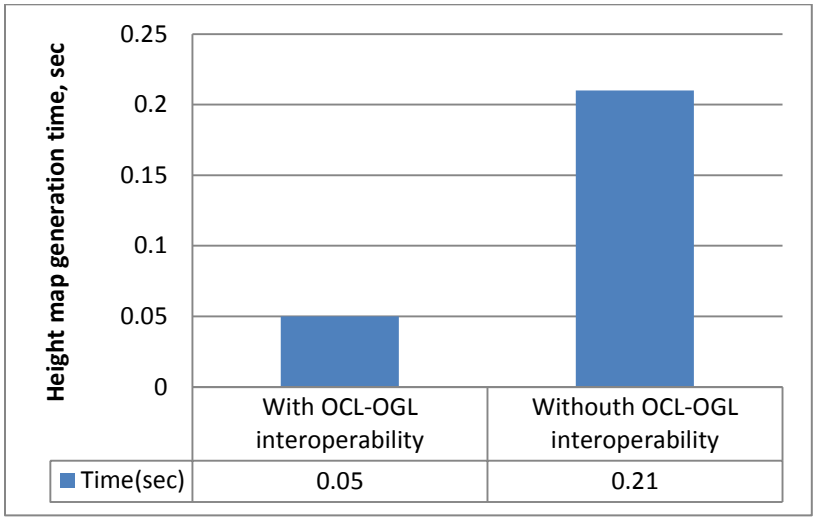

Figure III-20: OpenCL-OpenGL interoperability improvement

Accuracy analysis

There are two main sources of geometric errors in the proposed simulation: the simplified cutter representation and the height map used for workpiece and cutter geometry representations.

The cutter in this work is represented as a solid with no geometric information related to the flutes (Figure III-21). As this work is a pure geometric simulation, there is no need to calculate physical properties of a cutting process that requires flute information. There is also no practical way to know actual flute orientation at each time point due to unknown initial condition and variation in a spindle speed. As result, simulation of individual flutes does not make the simulation more accurate (but it will require significantly more computational resources) and it is safe to assume that a cutter is a body of rotation due to high spindle speeds.

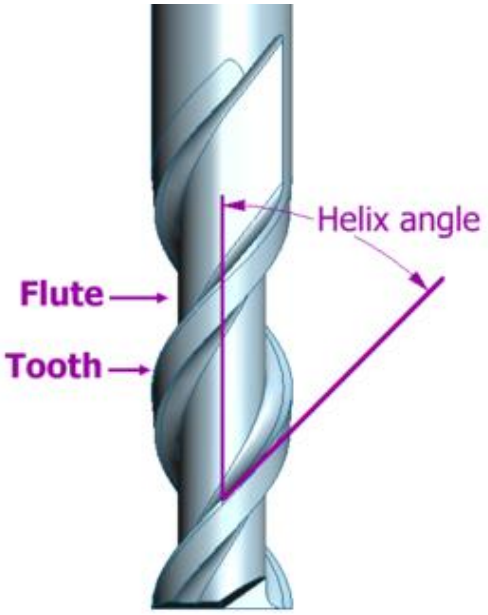

Figure III-21: Cutter parts description

In order to estimate the geometric error of the height map, it is important to select the appropriate metric. Since the height map is used in this work, the difference between an approximated height and an analytically calculated height is used. This approach may yield inaccuracies as the measurement direction is in a single direction as opposed to the standard measurement which is normal to the surface.

Since the cutter in this work is represented as a body of rotation a 1D height map representation is employed. For a ball end cutter, the minimum distance between analytical and approximate surface can be represented as a difference between actual and interpolated cutter radius (Figure III-22). Figure III-23 shows dependency of maximum and mean error values on a number of interpolation points for both methods ("Y" – height, "R" – radius). It is easy to see that used in this work 1024 interpolation points result in less than 0.001% average error for both methods.

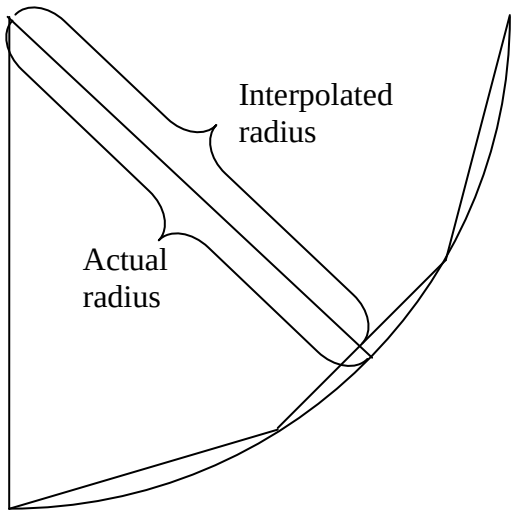

Figure III-22: Difference between actual and interpolated radiuses

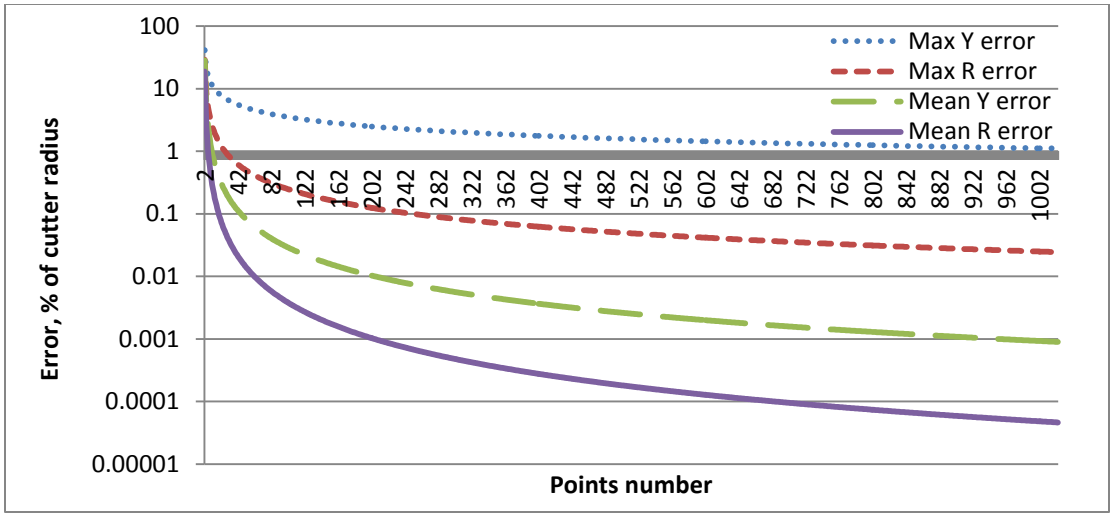

Figure III-23: Cutter interpolation error based on points number

At the same time, the relatively high maximum error value measured by the height method can be explained by limitation of a method itself. Figure III-24 demonstrates that the error value grows up at the end of a cutter. It is exactly the point when error measurement happens in a direction that is almost parallel to a surface and the measurement itself has a high error.

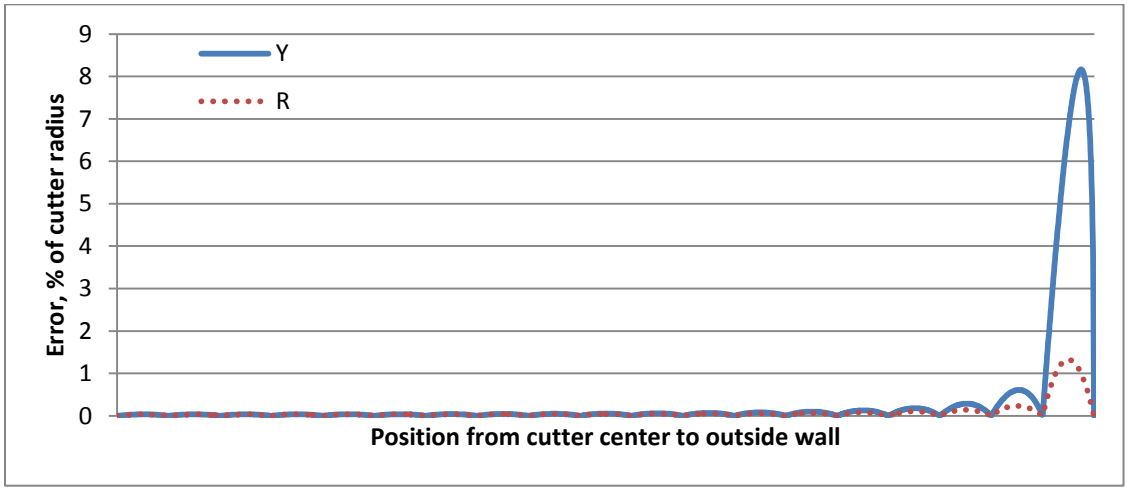

Figure III-24: Cutter error based on position

In addition to the cutter representation, a workpiece is also represented as a height map. But, in opposite to a ball end cutter, calculation of an error distance between analytical surface and approximated surface for a general shape is not a trivial problem and it is out of scope of this work. At the same time using just a height difference is not really useful since it will produce wrong results for vertical walls with large error values. However it is possible to estimate boundaries of geometry error values. The height map data structure stores exact surface point positions for each grid point. As result error can appear only between grid values and cannot be larger than a distance between grid points. Assuming that a workpiece size is 500x500x500mm and a height map resolution is 4000x4000, it is easy to calculate that the maximum possible error cannot exceed 180 microns. Based on the relations between maximum and average errors given for a ball-end cutter approximation, it is safe to assume that in most cases an average error will not exceed 2 microns which is better than the resolution of existing machines.

The last possible source of geometric errors is actually the rendering process or, more precisely, conversion of a height map into a triangular mesh. In order to prove that this conversion does not increase geometric error it is important to notice that it is lossless since all existing surface points are preserved during a conversion process. At the same time, since flat planes are used for representing surface between height map grid points, this conversion is nothing more than a linear interpolation process that cannot introduce an error higher than described earlier.

Discussion

In this chapter the developed 3-axis milling simulation system and underlying parallel algorithm were described and evaluated based from the performance and accuracy points of view. Additionally there were described rules and recommendations for GPGPU algorithms design and selecting data structures.

The described work has demonstrated the possibility of using graphics processors for the CNC milling simulation and possible performance benefits. The experimental results show up to 8X performance improvement over a traditional processor even without careful tuning of the GPU code. This is an excellent starting point especially considering the fact that the GPU performance is not limited by clock frequency as much as the CPU and that GPU performance continues to improve at a much faster rate than that of the CPU. It is also important to note that the algorithms and data structures traditionally used in the CAM area may be not the best choice for GPGPU oriented applications.

The GPU programming brings many additional limitations and tradeoffs some of which do not exist in CPU programming or do not affect performance significantly. The most important tradeoff for parallel programming and especially for GPU programming is the selection of the parallelization methodology. In the case of the CNC milling simulation, the most obvious and easiest way is to process multiple path points (or segments) in parallel. This approach is sufficient from a mathematical perspective if the required synchronization is implemented properly. It also usually works well on both the CPU and the GPU when the simulation of an entire tool path is executed. However, the

approach does have a significant limitation as the maximum number of threads cannot be higher than the number of processing path points during iterations. Thus, in the case of a continuous simulation, when only few path points are processed between neighbor frames, the GPU performance will be quite poor (even worse than CPU performance in extreme cases). This is the case as there are not enough threads to hide the memory access latency and to load all GPU cores. At the same time, CPU performance will be almost constant in this situation since it needs only one thread per core. This limitation may require development of different GPU algorithms for different use cases such as the continuous simulation or the fast simulation to a final result. In contrast to the GPU, there is only one algorithm required for the CPU in order to get good performance in both scenarios.

Another important difference between CPU and GPU programming is the importance of the optimization process. For example, selection of the optimal algorithm parameters or the memory access pattern usually cannot significantly increase the CPU performance. At the same time, a non-linear memory access, multiple divergent control branches or a wrong group size can decrease the GPU performance by three orders of magnitude and make the GPU performance inferior to that of the CPU.

It is also important to note that the CNC milling simulator requires implementing two conceptually opposite operations: visualization and data editing. The difference between them is the fact that the visualization does not change data and requires reading as fast as possible but the editing process requires changing data as fast as possible and does not consider efficient reading. Every data structure is a tradeoff between efficient

visualization and efficient editing. For example, the triangular mesh is perfect for visualization because rendering algorithms are implemented in graphics hardware. However, it is not easy to change the triangular mesh, especially in parallel. The height map is an example of the opposite tradeoff, it is extremely easy to edit it in parallel but there are no known ways to render it efficiently. In the described work, the best properties of both data representation approaches and computational resources were used to create a hybrid approach. The results of this approach were relatively good but the penalty for using different data structures is the time required for converting from one to another. There is also another limitation related to the multi-GPU support and the data synchronization performed by OpenGL driver but this issue will be solved by future drivers. Synchronization will become extremely important in the case of development of a more complicated multi-GPU system.

IV. TOOL PATH PLANNING FOR 3-AXIS MACHINING

The previous chapter showed that a GPU can be efficiently used for acceleration of a 3-axis CNC milling simulation based on the height map geometry representation. This chapter continues exploring the area of 3-axis CNC milling by showing possible GPGPU accelerated solutions for tool path planning. This chapter also describes GPU accelerated 2d contour offset path planning algorithm based on a simple but easy parallelizable 2d bitmap data structure for roughing tool path generation. In addition to a tool path planning algorithm the optimization approach for connecting tool path components based on a topology tree processing will be presented. Finally a GPU accelerated finishing tool path generation algorithm based on cutter shifting approach and earlier discussed height map data structure will be discussed as another example of utilization of the height map data structure for geometry processing on GPU.

The performance evaluation section will provide information about path planning performance for different models, although there will be no comparison between CPU and GPU because the algorithms developed are designed for GPU and cannot run on CPU directly. At the same time, a direct comparison between different tool paths planning algorithms on different hardware does not make sense due to the different amount of calculations. Although there will be no direct CPU vs. GPU comparison of the same algorithm, it will be easy to see that developed path planning algorithms provide great performance relatively to commercial CAM systems.

GPU accelerated 2d contour offset roughing path planning algorithm

The common first step of the milling process is the removal of a vast amount of material which does not make the surface by a large flat-end tool. This process is called "roughing" and a tool follows a roughing tool path. Since a part surface is usually not milled during this step it does not require a very high tolerance but requires a maximum possible material removing rate and constant tool load. It is easy to see that both material removal rate and tool load depend on depth of cut, angle of engagement and feed rate. There are a lot of research works [55-58] done in the area of optimization of these three parameters offline and online based on material properties, geometry, force response and other parameters. But for this work a simple assumption that all of them have to be constant is done since the topic of interest for this work is parallel processing and GPGPU technology application for tool path planning.

With the assumption about constant depth of cut, it is easy to see that material will be removed by layers with the distance between the layers equal to the depth of cut value. It also means that all layers are completely independent and an entire target 3d model can be represented as a set of 2d bitmaps with only two possible values per element as shown on Figure IV-1. (More complicated scenarios with 3 possible values per element will be actually discussed in further chapters.)

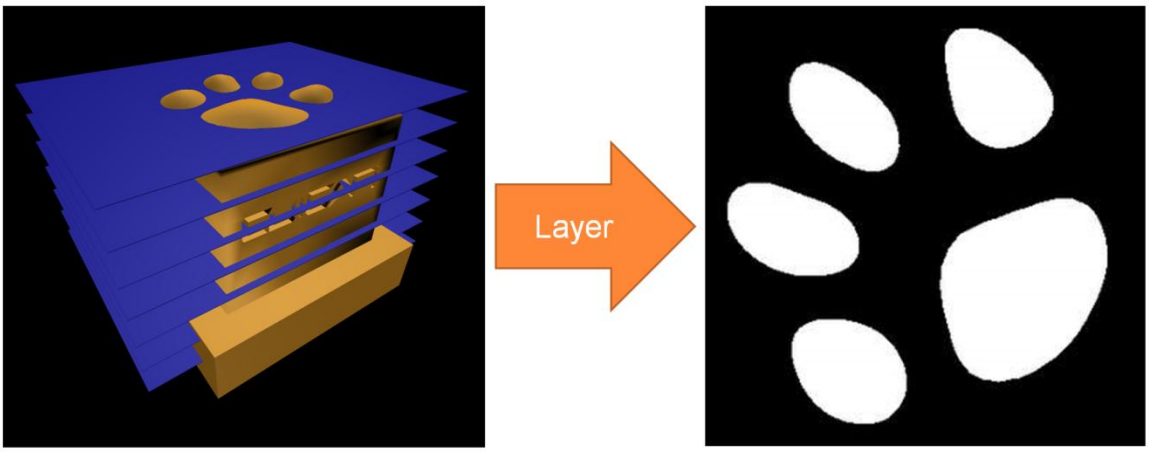

Figure IV-1: Part slices

The white color on the bitmap represents areas with part material that cannot be removed and the black color accordingly represents areas with material that has to be removed. Considering usage of a flat-end rotary cutter that is controlled by a center position it is possible to construct an area where tool center can go. This area can be constructed by offsetting each white (target material) region by a tool radius distance as shown on Figure IV-2.

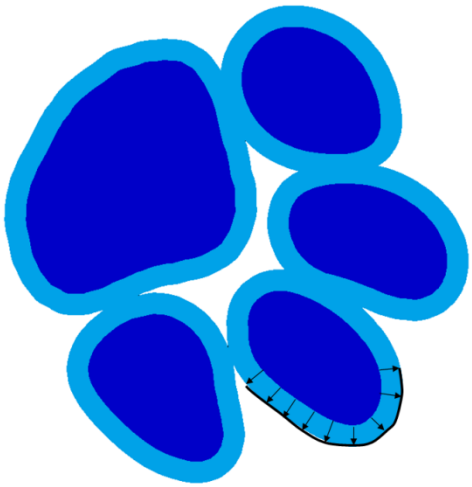

Figure IV-2: Contour offset

The same contour offset approach can be used for the generation of a roughing tool path. In this case it is applied iteratively and shape contours are used as a tool center trajectory as shown on Figure IV-3 where red lines represent tool path components and green lines represent rapid tool movements between different areas connected by a special algorithm. The approach for optimization of tool path components connection which uses a topology tree and process path components from multiple layers will be described in the next part.

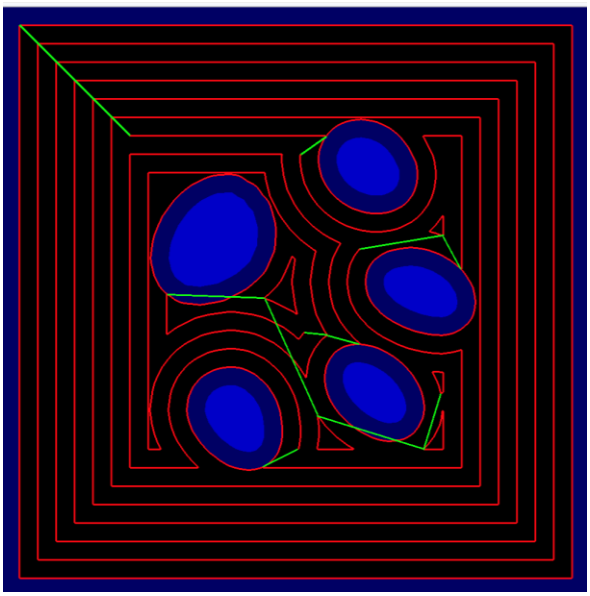

Figure IV-3: Iterative roughing tool path

Although the tool path generation process is iterative there are still two major options for parallelization. The first possible approach is processing different layers in parallel, since they are independent. This approach is suitable for multi-core CPU or multi-GPU systems but the number of layers is usually not high enough for loading all hundreds or even thousands of GPU cores. The second possible approach is processing

each bitmap pixel independently by many threads on GPU. For this work, the second approach was selected mainly because it offers much better scalability and parallelizability although in the case of multi-GPU systems both approaches can be combined together and provide even better performance.

The entire contour offset path planning algorithm has 3 main parts:

1) Edge detection
2) Expansion
3) Continuous path generation

The edge detection was implemented similarly to a Sobel filter [59] with a threshold: each pixel value is compared with 4 neighbors and in case of at least one neighbor with different value it is marked as an edge. In case of GPU implementation every pixel is processed by an independent thread and threads in a warp process continuous range of pixels. The edge detection algorithm is shown by Algorithm IV-1.

```
1   For all bitmap pixels in parallel:
2   |   For all 4 neighbors:
3   |   |   If neighbor value is not equal current pixel value:
4   |   |   |   Mark current pixel as boundary
```

Algorithm IV-1: Edge detection

The expansion algorithm is a bit more complicated and can be implemented by two different strategies: thread per input pixel or thread per output pixel. In case of the first strategy each thread processes one edge pixel and mark all output bitmap pixels if a distance between a selected edge pixel and current output pixel is less than expansion radius. The second approach is the opposite of the first. Each thread selects an output

pixel and tries to find an edge pixel around selected output pixel. If there is at least one edge pixel closer than an expansion value, the selected output pixel is marked. It is also possible to combined both approaches and run one thread per combination edge-output pixel. In the case of this combination it is possible to guarantee that amount of work done by each thread is bounded to a relatively small number of operations which is important for GPU implementation since it does prevent it from extensive branching. Although these ways of implementation are quite different they basically provide different solutions for the tradeoff between amount of calculations, number of divergent branches and memory access patters. For this work the pure second approach with one thread per edge pixel was selected (as described by Algorithm IV-2) since it provided the best performance on NVidia card with Compute Capability 1.1 but other GPU architectures or even GPUs of the same architecture may perform very differently and require another implementation for the best performance.

```
1   For each edge pixel in parallel:
2   |   For pixels in range [x-r:x+r, y-r:y+r] (x, y - edge pixel position, r – offset distance):
3   |   |   If distance to pixel is less than the offset distance:
4   |   |   |   Mark this pixel
```

Algorithm IV-2: Edge expansion

The continuous path generation, which is the last step of the roughing algorithm, was implemented on CPU since it is a pure iterative algorithm that cannot be divided into many independent parts and it does not take a lot of time relatively to other roughing path planning steps. This algorithm starts with a random edge pixel and tries to find an edge neighbor of this pixel. If there an edge neighbor exists it is saved to a list of pixels and

become a new selected pixel. This process continues iteratively while it is possible to select a neighbor edge pixel. At the end it starts with another random edge pixel and performs the same process until all edge pixels are processed. Since it is not known if a randomly selected pixel is on the end of a continuous path, when the algorithm cannot find a neighbor near the current pixel it tries to find one near the beginning of a current segment and connect both segments correctly. Steps performed during the continuous path construction are shown by Algorithm IV-3

```
1  While there are non-processed edge pixels:
2  |  Create a new path list
3  |  Select a random edge pixel
4  |  While there are non-processed neighbors:
5  |  |  Select a random neighbor
6  |  |  Mark selected pixel as processed
7  |  |  Save selected pixel to a list
8  |  If initially selected pixel was in the middle of a path:
9  |  |  Repeat steps 4-7 for another part of a path and place results in the same list
```

Algorithm IV-3: Continuous path construction

The next part will explain a possible optimization technique for connecting multiple path components into one continuous tool path with relatively short movements between different path segments.

Tree based algorithm for path components connection optimization

One of the most important parameters of the roughing tool path planning algorithm is the milling time. It contains time of material removing and moving of cutter

from one position to another. Since the material removal rate is usually a constant value it is easy to see why the best path requires continuous material removing all the time without cutter movement between different areas.

A machine removes material layer by layering in different areas with the described roughing path planning algorithm, as result roughing path contains a lot of path components for each layer and machine needs to move cutter from one area to another if they are not connected together. This movement between different areas of each layer costs extra milling time and may become a significant part of entire roughing time for some specific part geometries. One of solutions for this problem is optimization of order of sub paths while generating a roughing path automatically. There are many ways to connect paths generated after the processing of each layer. The simplest way is to connect all path components for each layer and process all layers sequentially. This way is easy to implement and it works quite well in modern software but if a part contains some deep holes machine has to move cutter from one whole to another. Figure IV-4 and Figure IV-5 illustrate this situation. Movement from area A to area B requires to move the tool up and down 5 times. The same situation exists with area C. As a result processing of such part layer by layer requires too many useless motions.

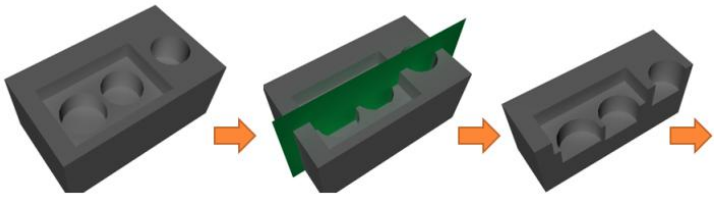

Figure IV-4: Slicing test part

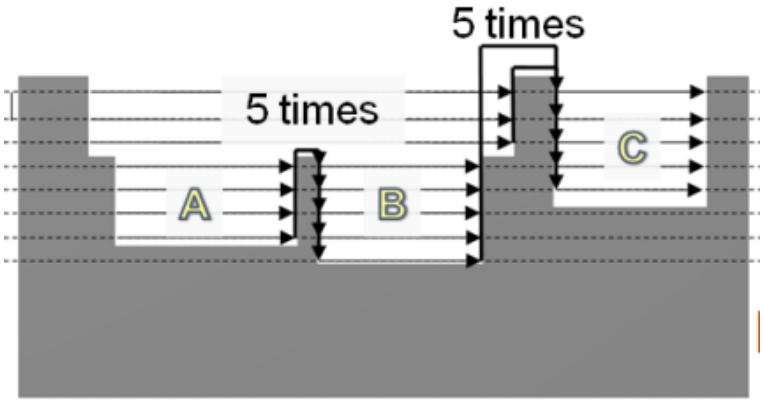

Figure IV-5: Not optimized tool path

The developed approach allows solving this problem. It is based on the fact that it is not possible to remove more material on each layer before removing material on previous layer, or it is not possible to remove material from any point of any layer without removing of materials on top of this point from a previous layers (this algorithm does not work with some special cutter which allow to do it with some limitation). It is possible to say that each layer is a sub-layer of previous layer and it is possible to construct a tree of layers (Figure IV-6).

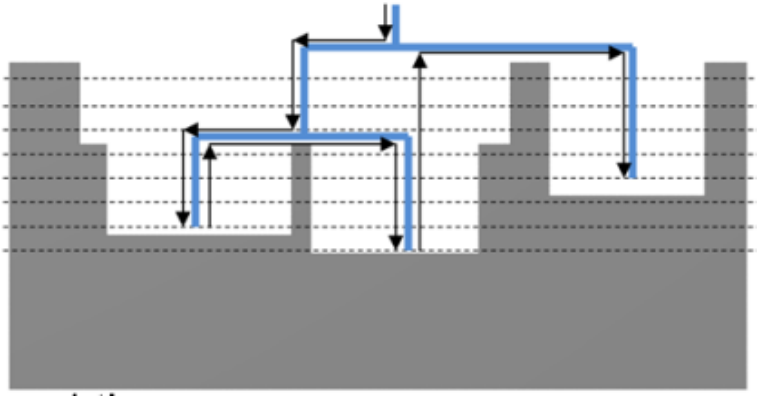

Figure IV-6: Generated tree

A standard tree processing algorithm may be used for generating a sequence of sub-paths. The algorithm starts with an area at the top level and checks all sub-areas on the next layer, than it does the same operation recursively for each sub-area. When an area does not have any sub-areas algorithm generates a roughing path for it and connect it to a path of previous sub area. It generates the best path by processing layers and minimizing useless movements because this path takes only one movement for moving tool from one area to another (Figure IV-7).

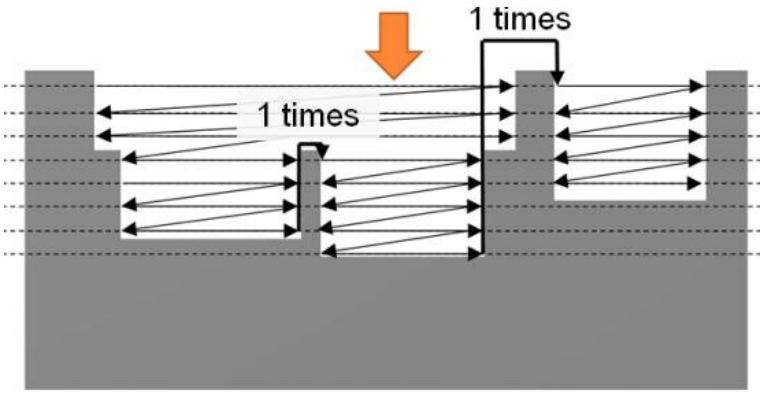

Figure IV-7: Optimized tool path

This algorithm (Algorithm IV-4) can be used for optimization of paths for 3-axis machine as well as for lathe machine and even for some specific 5-axis machine paths if it is possible to represent them as a tree. It is also possible to optimize result path with selecting the best order of area processing. In this case a set of classic Traveling salesman [60, 61] problems for the distances between areas for each section has to be solved. The solution of them will give the shortest path between different areas and minimum roughing time as result.

```
1   For each layer:
2   |   Find all independent regions
3   |   For each region:
4   |   |   Create a tree node associated with this region
5   For each layer from bottom to top:
6   |   For each region:
7   |   |   For each region of previous layer:
8   |   |   |   If current layer region has common pixels with previous layer region:
9   |   |   |   |   Add an edge between their nodes
10  Use depth-first tree traversal algorithm for generating a sequence of regions
11  For each region in sequence:
12  |   Generate roughing tool path
```

Algorithm IV-4: Tree optimization

The algorithm was tested on a real machine and in the simulator (Figure IV-8), which was described in the previous chapter. It can be seen that it allows processing each area separately and saves time for movement from one area to another, since it processes every region completely before going to a next one.

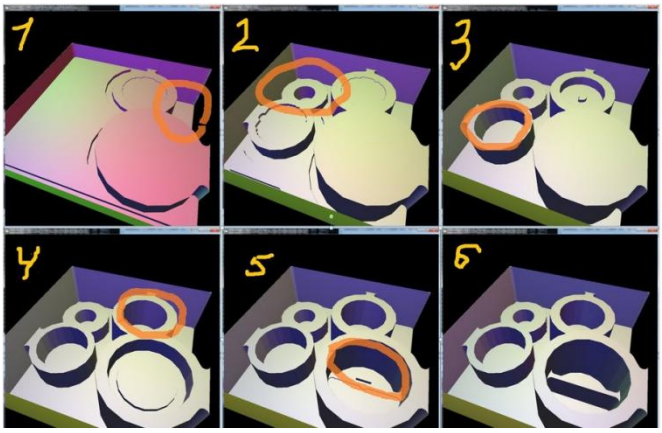

Figure IV-8: Tree optimization testing result

GPU accelerated shifted zigzag finishing path planning algorithm

Previous parts have described the parallel implementation of the contour offset roughing path planning algorithm and the tree based approach for optimization of path components connection. Although in real-world scenarios the next milling step is often a semi-finishing operation, it is not too different from roughing from an algorithmic and parallel processing point of view. Since this research is not interested in semi-finishing, this part goes directly to the finishing operation and its implementation.

In this work the tool offset finishing generation algorithm with a zigzag topology tool path was selected for researching of GPU implementation. The main idea of this approach is to separate 2d tool path topology and actual tool position calculation into two independent problems. Generation of a 2d tool path is not computationally complex problem and it may be done quite fast on traditional CPU. As a result 2d tool path generation is not particularly interesting for this research and a simple zigzag tool path generated on CPU is used for finishing tool path generation. On the other side, calculation of an actual tool position in 3d space, which can be reformulated as calculation of a tool height or Z coordinate since 2d position is known, is much more complicated computational problem which requires a lot of resources. The idea of the tool offset approach is to start with a known 2d tool position and a random tool height at which tool may intersect a surface or does not touch it at all and find an offset required for moving a tool at a position when it exactly touches a surface as it is shown on Figure IV-9.

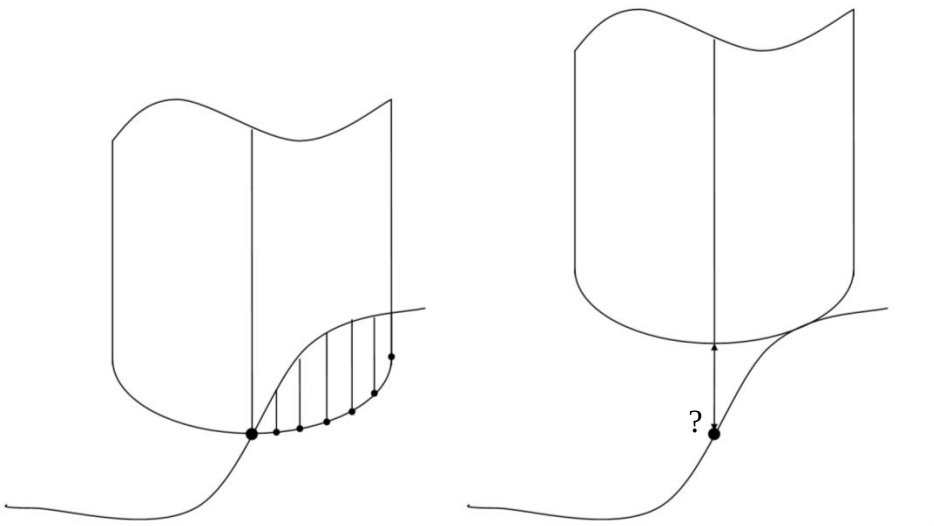

Figure IV-9: Tool offset

It is easy to see that the offset distance is equal to maximum vertical distance between a target surface and a tool surface. At the same time the distance between surfaces at every point can be expressed as a difference between height values of these points as shown on Figure IV-10. Considering usage of the height map geometry representation described earlier a tool offset value for each 2d tool position can be expressed as:

$$dH = \max_{i \to n}(H_1 - T_1, \dots, H_i - T_i) \qquad \text{(IV-1)}$$

Where n is a number of height map test points is, H_i is a height value of a target surface and T_i is a height value of a tool surface.

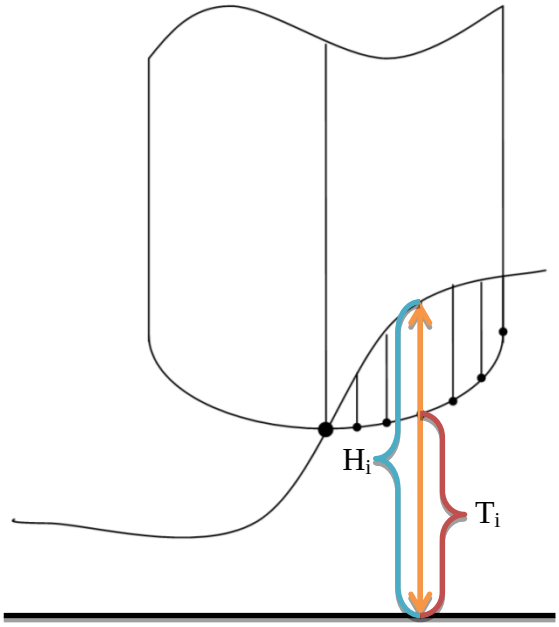

Figure IV-10: Distance between tool and target surfaces

In order to generate a finishing tool path for an entire surface tool offset, distances have to be calculated for every point of an initial 2d tool path.

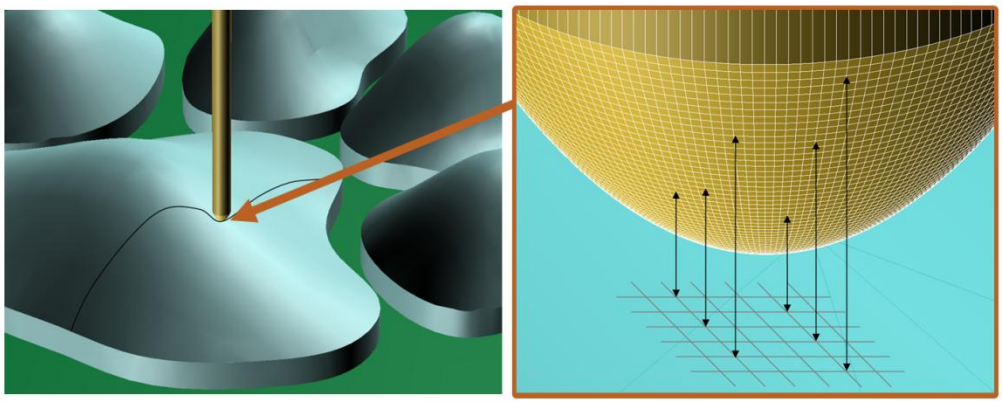

Figure IV-11: Required testing points.

As Figure IV-11 shows, it requires testing every tool surface point for every path point which results in many billions of test points. Considering the fact that all path point

offsets are completely independent and the offset calculation algorithm is very simple, from the mathematical point of view this problem is a perfect fit for parallelization and GPGPU implementation.

In this work the described algorithm was implemented on GPU with C++, OpenCL and OpenGL. The OpenGL is used during the first step for a very fast construction of a height map from an input STL model by rendering a triangular mesh with orthogonal projection and extracting Z-buffer values which represent a height map (Figure IV-12).

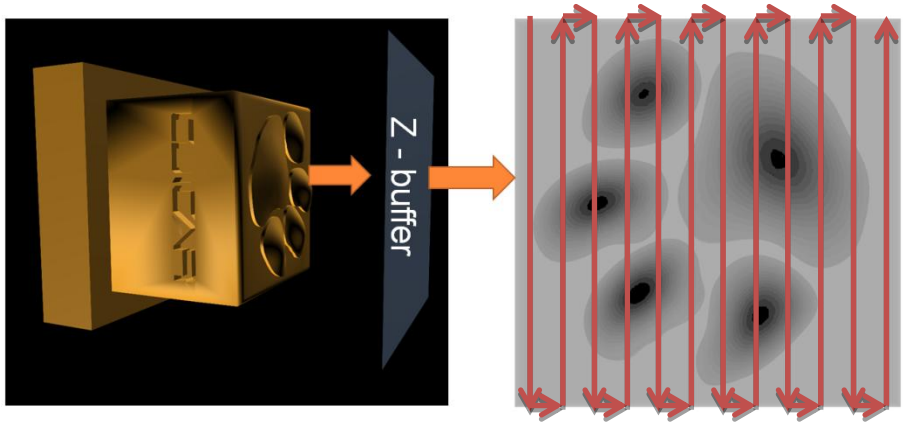

Figure IV-12: Height map generation with zigzag 2d path

On the second step, C++ code is used for generation of a 2d zigzag tool path and OpenCL is finally used for generation tool offsets for every 2d tool path point. The implemented version of the OpenCL code utilized independency of multiple path points from each other for parallelizing algorithm execution. Each OpenCL thread selects a 2d path point and processes all cutter surface points by calculating a maximum difference between a target surface and a tool surface. The result is saved to a global memory

without additional synchronization since all dependent calculation happens in one thread. The complete finishing tool path planning algorithm is shown by Algorithm IV-5.

```
1  Generate 2D zigzag path with zero tool height (Z coordinate) at each point
2  For each 2D path point in parallel:
3  |  Initialize the tool offset value with some a large negative value
4  |  For each tool surface point:
5  |  |  Calculate a difference between tool and target surfaces point heights
6  |  |  If the difference is greater than the stored tool offset value:
7  |  |  |  Replace the offset value by the calculated difference
8  |  Use the maximum difference as a new tool height value
```

Algorithm IV-5: Finishing path planning

Since CNC machines require control by G-code commands there was also developed a simple post-processor that converts a sequence of tool center coordinates into a list of G-code commands accepted by the used Okuma machine and also performs some optimizations of a sequence like the detection of straight lines represented by multiple points and replacing it with a single command in order to reduce an output file size.

Experimental 3-axis path planning and milling results

During the research project, developed path planning algorithms were implemented by using C++, OpenCL and OpenGL with support of GPU acceleration and performed on Dell Precision M6500 mobile workstation (GPU: NVidia Quadro FX2800M with 96 CUDA cores @1.5GHz, CPU: Intel i7-820QM, 4 cores @1.73GHz). Implemented algorithms were used for generation tool paths and G-code programs that

were tested by performing both simulation in developed simulator and milling on the Okuma MB-46VE CNC milling machine. A set of randomly selected complex 3d models in STL format available on the Internet was used as the input for path planning algorithms. In this part of the research, project collisions between tool holder, machine components and workpiece were not considered and manually avoided by selecting proper tooling and fixtures (collision avoidance will be described in following chapters during a discussion about 5-axis orientation selection). All milling experiments used 1/8" flat-end cutting tool for roughing and 1/16" ball-end cutting tool for finishing and were performed with two different types of plastic. Figures on pages 85-87 demonstrate both the simulation and milling results of the performed experiments.

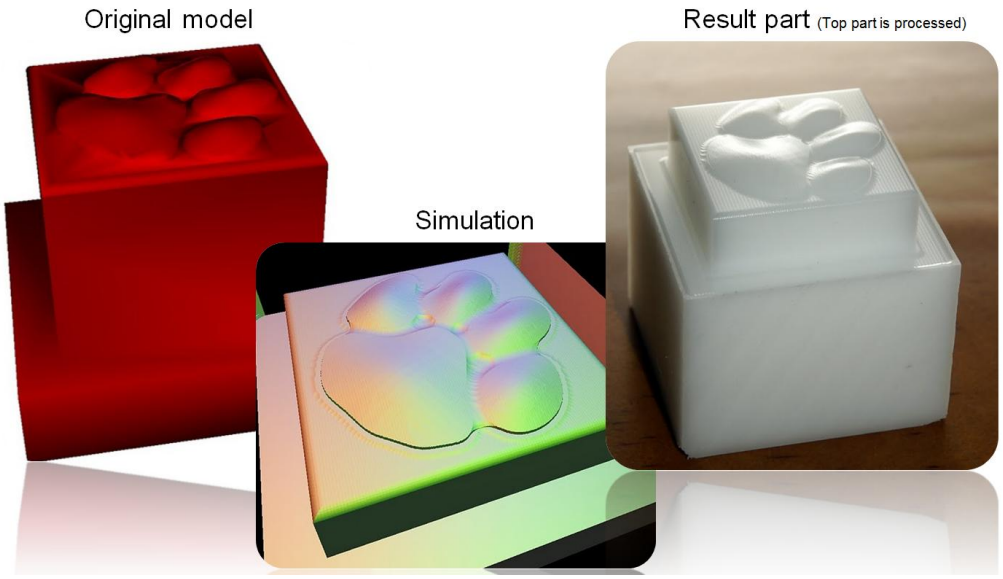

Figure IV-13: Experimental milling results for the "Tiger paw" model

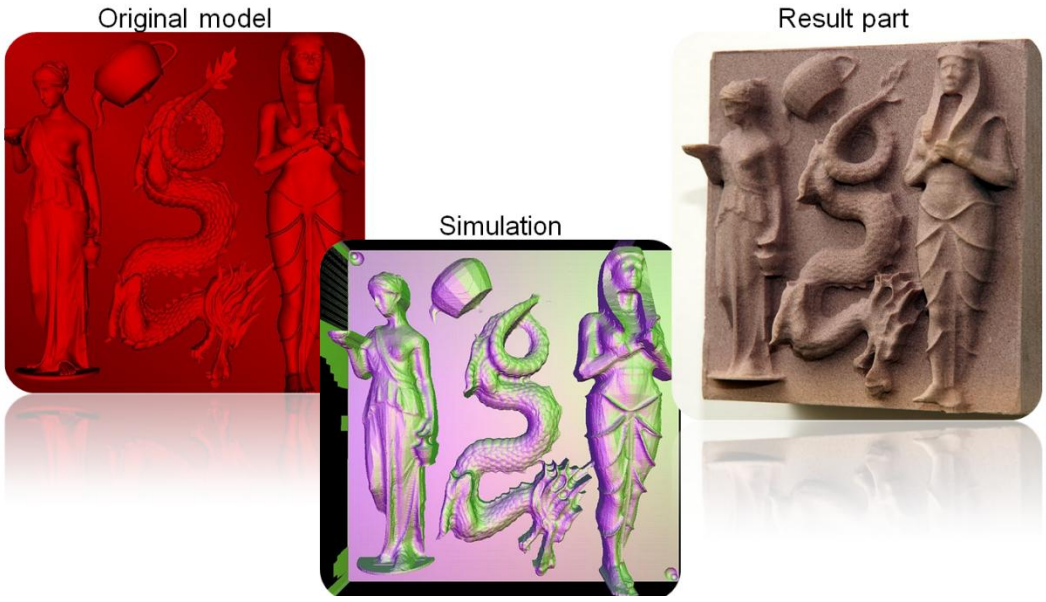

Figure IV-14: Experimental milling results for the “Sculptures” model

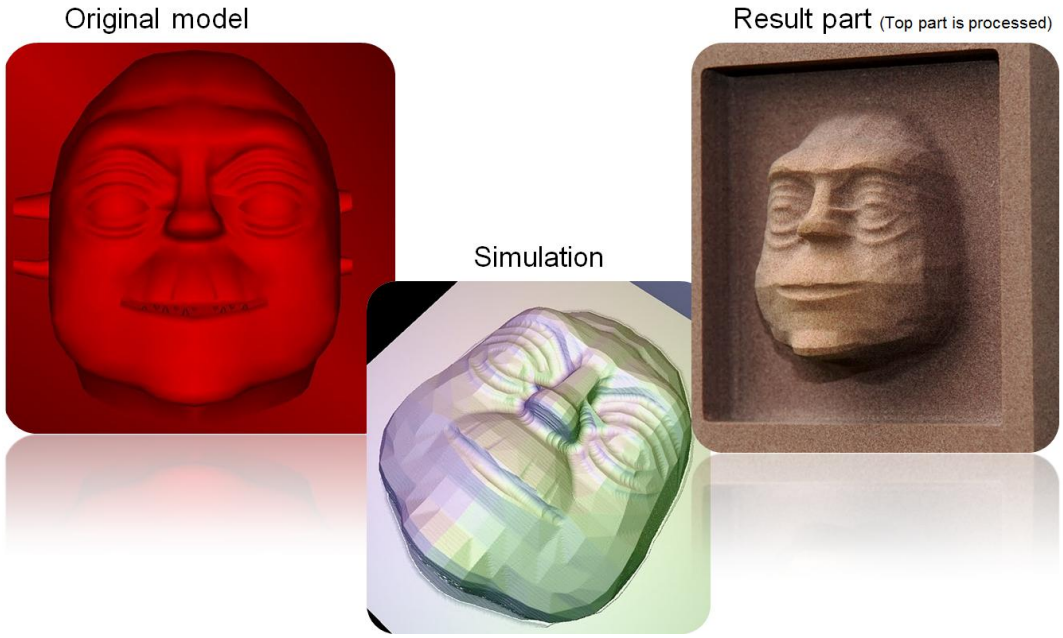

Figure IV-15: Experimental milling results for the “Yoda” model

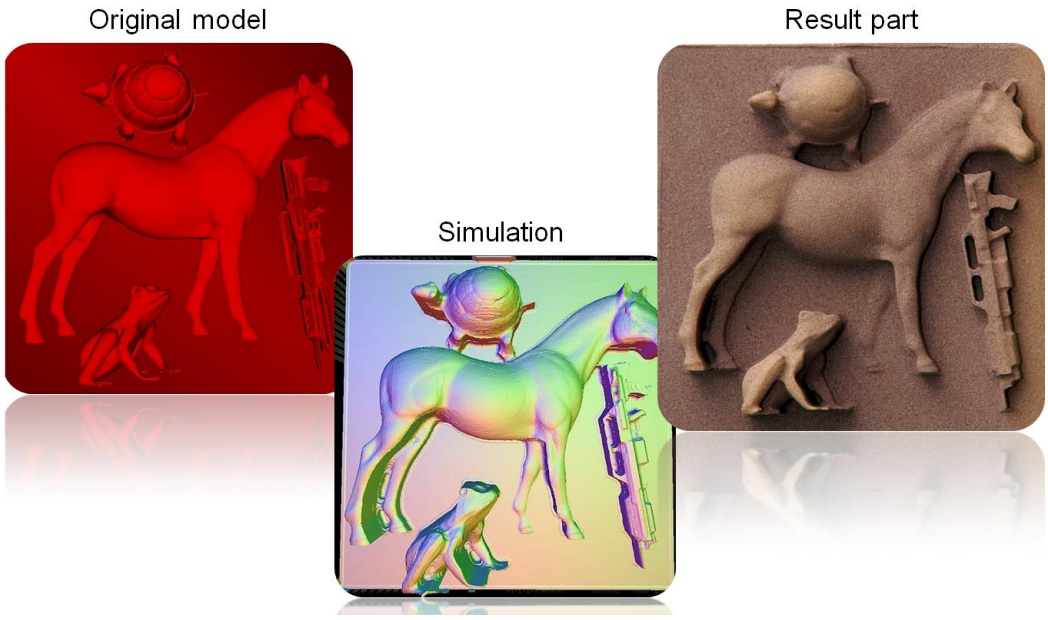

Figure IV-16: Experimental milling results for the “Zoo” model

Discussion

In this part of the work, a set of popular algorithms were redesigned in order to implement them on GPU and demonstrate a possibility of using GPU for tool path planning calculations. The experimental simulation and milling results show that the tool trajectories generated by GPU are valid and can be used for actual milling. At the same time GPU implementation of path planning algorithms show that traditional approaches for representing and processing geometry may be not the best choice for GPU and there is a need for replacing them by other GPU-friendly geometry representations and algorithms.

It is important to notice that the height map data structure used allows path planning for 3-axis machines with some limitations only. There are known techniques that allow using multiple height maps for 3+2-axis milling but there is no way to do more general 5-axis path planning without significant changes to a geometry representation and algorithms. Although a height map is not suitable for 5-axis milling, it is one of the best candidates for geometry representation that can be easily processed in parallel, and it may make sense combining more complicated data structures for 5-axis milling with some special cases like pocket milling or initial roughing operations processed with a height map.

V. 5-AXIS MACHINING SIMULATION

5-axis CNC milling is not as popular today as the 3-axis milling mainly due to its complexity. Two additional degrees of freedom make the tool path planning process much more complicated. They also significantly increase a chance of a collision in case of a path planning error. And from the mechanical point of view it is much harder to make 5-axis machines as rigid as their 3-axis analogs. Although two additional axes bring a lot of problems and complexity, they also bring a lot of freedom and possibilities. For example, the 5-axis milling may significantly decrease a number of setups and related positioning errors. And what is most important is that 5-axis milling can significantly decrease the milling time and produce better surface quality by using a more efficient tool orientation and a shorter tool path. But in order to use benefits of the 5-axis CNC milling the tool path planning process has to be automated or at least significantly simplified.

This chapter discusses one of the most important parts of the tool path planning process – the milling simulation. The milling simulation is used for two different areas. From one side it is an important component of a tool path planning process since continuous simulation allows selection of a safe tool orientation and save time by processing only areas that contains material. From the other side, the simulation process is extremely important for verification of a generated tool path in safe virtual environment before using it on a real machine.

The problem with 5-axis simulation is its complexity from the mathematical and the computational points of view. As it was showed in previous chapters the

computational problem can be solved by using GPUs for calculations. But in the case of the 5-axis simulation there are no known highly parallel algorithms and data structure that can be used in GPGPU approach. The 5-axis workpiece cannot be naturally represented by a height map as it was done in the 3-axis milling and there are no known geometry representations that can be efficiently edited in parallel on GPUs, provide good performance and memory usage. As a result there is a need for a specially designed data structure and highly parallel simulation algorithms especially designed for 5-axis milling simulation.

During this research project, a new volume representation was developed as well as a set of algorithms for the 5-axis CNC milling simulation that can run on multi-GPU systems. Although the described system is designed for 5-axis CNC milling, it is quite general and can also be used for simulation of multi-axis machines with more than 5 axes.

This chapter describes the developed volume representation, the used data structure, rationale behind its design and discusses its properties. It also provides information about developed highly parallel algorithms used for rendering and editing and the algorithms performance evaluation. Finally it describes experimental simulation results and discusses the efficiency of the performance scalability on multiple GPUs.

Geometry representations and data structures evaluation

As was mentioned in one of previous chapters, selection of a right geometry representation and an underlying data structure is a key component of a geometry

processing system. In the case of the 5-axis milling simulation workpiece geometry is not limited as much as in the 3-axis milling and the height map representation used earlier in this work does not fit naturally for the new purpose. It means that a new geometry representation has to be selected or specially designed for this work.

Before going into discussion about possible solutions it is important to define a set of features and properties that a new geometry representation has to provide.

- First of all it has to be able to represent any possible geometry with high precision and without topological limitations by using a reasonable amount of memory.
- From the parallel processing point of view, an underlying data structure has to provide an ability to render and edit geometry in parallel with a high level of parallelism without significant synchronization overhead.
- From a scalability point of view it is important to be able to split a model between multiple devices with very limited communication channels.

It is important to note that scalability and parallel processing are more important than performance of serial algorithms for processing this data structure since. In contrast to CPU, GPU performance grows over time and not limited too much by physical limitations. So it is much easier to increase the available performance linearly just by using more GPUs or using newer processors if a geometry representation can be scaled efficiently. Now, existing geometry representations can be evaluated based on the formulated requirement.

The most popular in the CAD/CAM field, BREP geometry representation obviously meets the accuracy and memory usage criteria but fails both parallelization and scalability requirements. The problem with parallelization and especially GPGPU processing of BREP is related to the mathematical complexity of the surface elements representation and an absence of spatial boundaries of surfaces elements. For example, there are no boundaries on a number of surfaces that represent a given workpiece surface region. A region can be represented either by a single surface or by a thousand of surfaces. It means that there is no way to guarantee a high number of elements that can be processed independently in parallel and provide enough GPU load. Possible differences in a mathematical description of surface elements make the situation even worse since even independent surface elements cannot be processed by the same algorithms. It results in inefficient GPU utilization since multiple threads in the same warp have to wait for each other and cannot process elements concurrently.

The triangular mesh represents the tradeoff between the geometry accuracy and the surface representation complexity. It can be viewed as the BREP with surface elements simplified to planes connected to exactly three neighbors (triangles). Using triangles allows using the same algorithm for processing all surface elements. It results in much more efficient geometry processing on GPU, especially in the mesh rendering process, but it does not help with the geometry editing issues that the BREP has. In addition the approximation of a surface by triangles requires extremely large amount of memory for achieving high precision.

In contrast to boundary geometry representations like BREP and triangular mesh, the volumetric geometry representations have a completely different set of tradeoffs. Probably one of the simplest volume representations is the voxel model. Voxel model subdivides an entire volume into a 3-dimensional grid of independent elements called voxels. Each voxel has a value that may represent some properties of that area of volume such as distance to the closest surface, amount of material or simply a presence of material. The most important voxels property from the GPGPU point of view is their independence. It means that each voxel can be processed completely independent from other voxels and it can be done in parallel on multiple devices. Another important property of the traditional voxel model is the fact that a volume is sampled regularly. It means that there is a constant predefined number of voxels for a given volume and a given resolution. And it results in a very simple memory management. Although the voxel model looks like a perfect choice for GPGPU computing, since it has both parallelizability and scalability, it has an extremely important drawback. An amount of memory required for storing the voxel model is proportional to a third power of the model resolution. It makes completely unfeasible using it for precision tool path planning without additional algorithms that can overcome this limitation. For example, a 500mm cube represented with 2micron resolution as a voxel model will require ~14PetaByte of space for storage. This is approximately the same as an entire Google or AT&T process every day and it is definitely not feasibly for CAM applications.

In contrast to the regularly sampled voxel model, that provides perfect parallelizability and scalability, there is a class of irregular sampling volume

representation approaches. Usually irregularly sampled approaches are represented by trees such as the octree with constant cells ratio or the k-d tree with a variable cells ratio. Irregularly sample models provide a tradeoff between memory requirements, parallelizability and complexity of a memory management process. They need much less memory than the traditional voxel model, but a tree processing is usually implemented by recursion algorithms which are not well suitable for GPU processing since GPU kernels cannot launch other kernels (this feature is not available in GPUs currently available on the market at least). Tree processing on GPU is a tradeoff between the number of kernel launches (which is equal to a tree height) and the overhead required for launching each kernel and work planning. On one hand higher (or deeper) trees provide better resources usage and may provide higher accuracy and on another hand every additional level requires another kernel launch and jobs planning time. An additional problem of all tree based algorithms is the memory management. In the case of CPU processing, there is virtually no significant memory allocation or releasing penalty, and every thread can manage its memory independently. But there is no such natural mechanism for GPU and the implementation of a memory management system can significantly increase an algorithm complexity, and add extra performance penalties. Although irregularly sampled volume representations have significant drawbacks related to GPU computing, and their implementation itself is not trivial, it is important to note that they still provide a high level of parallelizability and scalability. It means that an irregularly sampled volume represented by a tree can be a good starting point for designing a data structure for

GPGPU accelerated simulation and tool path planning but there are additional changes required since available implementations cannot be efficiently ported to GPU.

Approach	Z-map	BREP	Trian. mesh	Voxel	Octree
General	Bad	Good	Good	Good	Good
Accuracy	Average	Good	Average	Bad	Average
Memory	Average	Good	Average	Bad	Average
Rendering	Average	Average	Good	Average	Average
Editing	Good	Bad	Bad	Good	Average
Scalability	Good	Bad	Bad	Good	Average
Complex	Good	Bad	Good	Good	Average

Table V-1: Geometry representations comparison

Developed irregularly sampled volume representation

As was mentioned above, existing geometry representation approaches provide a wide range of tradeoffs between accuracy, memory usage, parallelizability and scalability but do not offer a perfect choice for GPU-computing. As results it is possible to note that there is a need for a specially designed geometry representation and a corresponding data structure that can be used for the 5-axis CNC milling simulation and tool the tool path planning process.

Based on the geometry representations evaluation it is easy to see that volumetric approaches are better suited for parallel processing than surface based approaches, mainly because of independence of volume elements which can be processed independently and predictability of a workload. It is also more natural for the milling simulation to represent

a volume since the actual physical process is the volume removing process. It is also obvious that the regularly sampled volumetric approach (such as the voxel model) cannot be used due to memory requirement, and that there is a need for an irregularly sampled representation. However even irregularly sampled tree-based representations cannot achieve a BREP level of accuracy with reasonable memory requirements. For example, considering the representation of a 500mm cube with 2 micron elements (as an example of a work area and accuracy found in modern 5-axis machines) and 1 byte per element, a simple part would require ~350Tb (6 sides * (500 mm /side / 0.002 mm)^2) of data just for surface representation without considering a data structure overhead. It is much more than modern personal computers can store and process in a reasonable time. It also means that the available volumetric geometry representations will always have a limited precision in comparison to the actual machine precision. From one side it may look like it is a fundamental limitation that cannot be overcome. But from another side there are not so many use cases with a real need of the extremely high accuracy. It may be more efficient to use data structures with lower accuracy and some workarounds for these special cases.

After accepting the fact of accuracy limitation for volumetric data representations, the next step is to make a decision about the tradeoff between memory usage, accuracy and parallelizability. There are two main relations between these parameters. First, more complicated data structures provide higher accuracy for a given amount of memory. Second, deeper trees provide more efficient memory usage for a given accuracy. Relatively complicated data structure with non-predictable density such as k-d trees are

less suitable for this research due to GPGPU specific load balancing (the problem similar to the BREP) and editing problems. Although generally they provide higher efficiency, their processing algorithms are more complicated, often have non-linear memory access patters and have a higher branch divergence. These properties result in significant performance penalties on modern GPUs. As a result, it is possible to note that considering the existing GPU architectures the designed data structure has to be as simple as possible. One of the simplest possible tree-based volumetric representations is a tree with nodes where each node represents a regularly sampled volume and a list of references to its children. The octree is a classic example of this type of geometry representations with 8 children per node.

One of the most important steps is the selection of a number of children and amount of geometrical data stored in each tree node. It is easy to see that a higher children number reduces memory usage efficiency (in an extreme case a tree becomes a voxel model) and a tree depth for a given accuracy. But it is also important that a geometry processing can be efficiently parallelized by processing each child of a node concurrently. If this is done by a warp, it makes memory access more efficient by storing children data in a continuous memory block which can be read linearly in one memory access operation. Considering the amount of geometrical data stored in a node it is possible to say that more data approximates geometry better but uses more memory. On one side of this tradeoff, each node contains a complete mathematical description of all geometry elements. And on the other side, it is possible to use only one bit to store information about presence of material in a nodes volume (or store a byte that describes a

distance to a surface or material density as it is done in the traditional voxel model). The first approach is similar to the BREP and has similar problems. Complete geometry description requires using complex algorithms and complicated memory management since it is not possible to predict a content of a node after editing. The opposite approach is actually much more GPU-friendly because the amount of data is constant, geometry processing algorithm is much simpler and all nodes use exactly the same geometry processing algorithm.

Based on the described tradeoffs there was designed a volumetric data structure for the GPGPU accelerated multi-axis CNC milling simulation and the tool path planning (Figure V-1). The developed geometry representation is a 2-level hybrid of the tree and the voxel model. It uses a 3d array of cells that represents a regularly sampled volume. Each cell stores 2 bits of geometrical data (similar to voxel model) and a pointer to an array of 4096 children (similar to a tree). Cells children (called "subcell") represent a regularly sampled (16x16x16) volume and store 2 bits of geometrical data but do not store pointers to their children. 2 bits geometrical data is used for 3-color scheme for geometry representation. They represent 3 possible states of a cell or subcell:

- Cell is completely filled by material
- Cell is completely empty
- Cell state is unknown and it probably contains a boundary

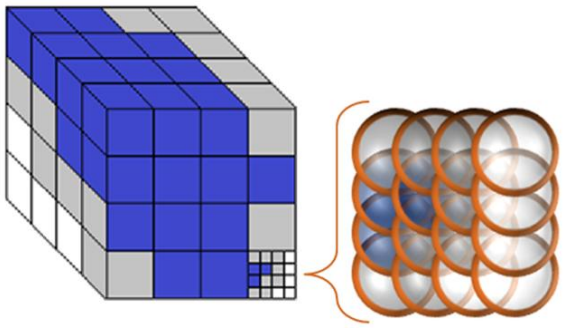

Figure V-1: Developed geometry representation model

In contrast to traditional cubical voxels, cells or subcells represent spheres circumscribed around traditional cubes calculated by volume subdivision.

The Figure V-2 demonstrates a surface representation example with the 2D version of the described geometry representation and square cells.

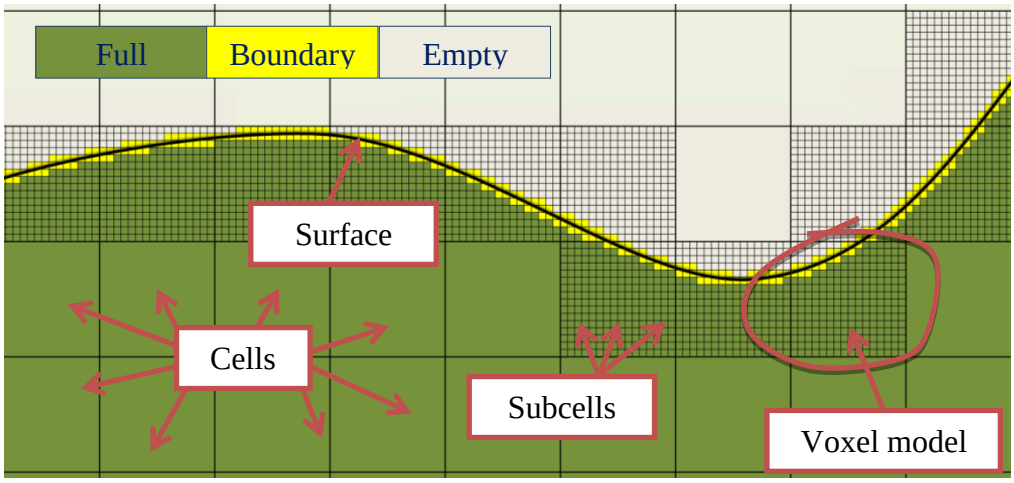

Figure V-2: 2D example of the developed model surface representation

From a hierarchy point of view, it can be viewed as a 2 level tree as shown on Figure V-3. It is important the low level nodes that represent subcells are stored in voxel models. But information about high level nodes is stored in a list. As result, links between

nodes are not really stored anywhere as it is done in traditional trees but the model still has a tree like hierarchy. First level links are represented by indexes in a cells list and second level links are represented by indexes in voxel models. This approach allows saving a significant amount of memory relative to a traditional linked tree based approach.

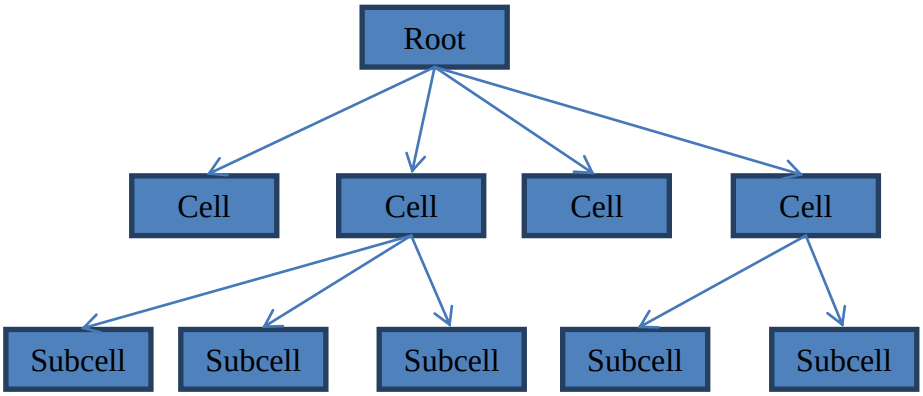

Figure V-3: HDT hierarchy

From a memory point of view, the developed model looks like the diagram shown on the Figure V-4.

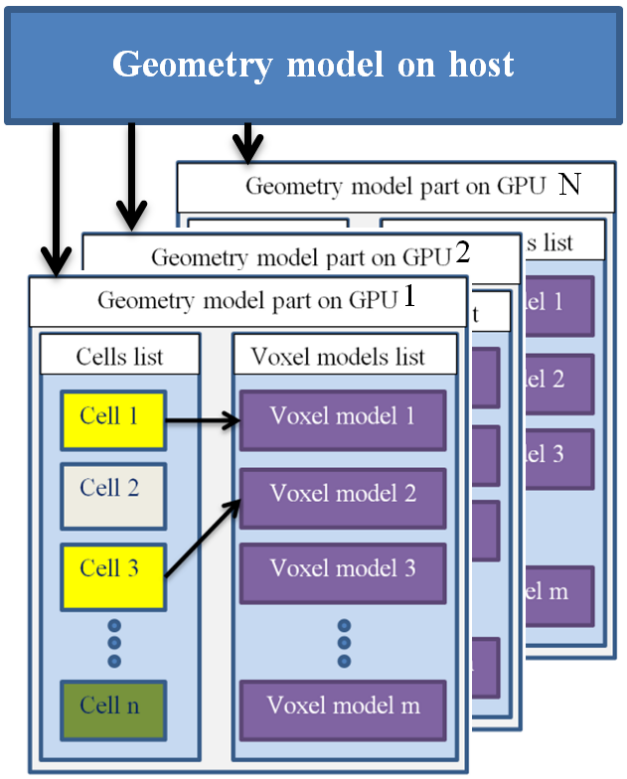

Figure V-4: Developed geometry model from a memory point of view

The rationale behind the selected design is an attempt to combine parallelizability and scalability of the voxel model and memory efficiency of tree based geometry representations. The 2-level design provides much better memory efficiency than the voxel model but almost does not affect performance. With a high enough number of children all their data are stored in continuous 1KB blocks of memory that can be efficiently read and each cell is processed by a warp. The reason for the selection of the 2bit geometry representation and spherical cells is an attempt to use as simple as possible geometry processing algorithms with the lowest number of branches. Further parts of this work will describe geometry editing and rendering algorithms and the importance of

spherical cells for making them simpler. 2 bit data structure also allows increasing resolution almost twice with the same memory usage in opposite to the traditional voxel model (1 byte per voxel). The used design also achieves great scalability. Since all cells are completely independent they are stored on multiple GPUs (and possibly on multiple computers) and processed independently with the almost linear performance improvement. The multi-GPU scalability will be also discussed later in this chapter.

Although the detailed performance evaluation will be provided later in this work, it is important to note that the designed data structure showed great parallelizability and scalability. The 3-GPU configuration successfully simulated and rendered in real-time a workpiece represented with the resolution of 6000^3 which is not feasible for a traditional voxel model due to memory usage.

Tool motion representation for 5-axis milling simulation

Before describing actual milling simulation algorithms it is important to discuss a machine tool representation since it significantly affects material editing algorithms. One of the most popular tool models used in researches is a generalized tool model shown on Figure V-5 and described by Chiou and Lee [62]. It contains three main parts: lower and upper cones and a torus component. The benefit of this model is an ability to represent a wide range of popular cutters with the same model. For example, a ball-end mill can be represented by completely eliminating both cones or a flat-end tool can be represented by eliminating torus component.

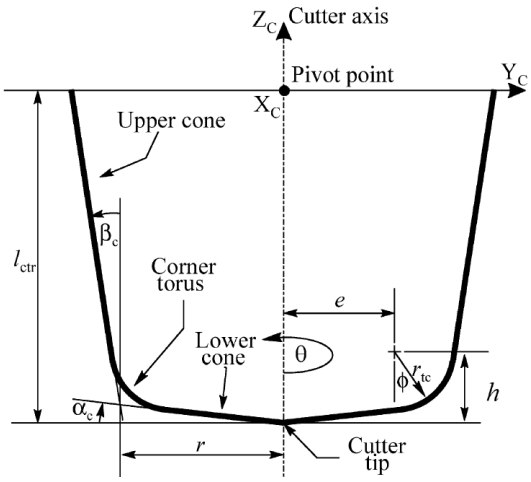

r: the cutter radius,
r_{tc}: the cutter corner radius,
e: the radial distance from the cutter axis to the cutter corner center,
h: the distance from the cutter tip to the cutter corner center as measured along the cutter axis,
α_c: the angle from a radial line through the cutter tip to the cutter bottom, $0 \leq \alpha_c < 90°$,
β_c: the taper angle between the cutter side and the cutter axis, $-90° < \beta_c < 90°$, and
l_{ctr}: the cutter length measured from the cutter tip along the cutter axis.

Figure V-5: Generalized tool model [62]

At the same time this model is not the best solution for a GPU-oriented simulation system. In order to understand why it is not the best choice it is important to look on description of 5-axis motions of this tool. Chiou and Lee [62] provide solutions for swept profiles of a torus (V-1) and cones parts (V-2), (V-3). It is easy to see that the depicted solutions have many trigonometric functions. It means that actual computing kernels will have to calculate quite many trigonometric operations which are quite slow on modern GPUs especially if full precision is used.

$$P_{\text{swept,torus}}(s,t) = [Trans(p_{\text{pvt}}(t))][Rotz(\theta_{\text{C}}(t))][Rotx(\theta_{\text{A}}(t))] \begin{bmatrix} (e + r_{\text{tc}}\sin\phi^*_{\text{T}})\cos\theta^*_{\text{T}} \\ (e + r_{\text{tc}}\sin\phi^*_{\text{T}})\sin\theta^*_{\text{T}} \\ -l_{\text{ctr}} + h - r_{\text{tc}}\cos\phi^*_{\text{T}} \\ 1 \end{bmatrix} \quad \text{(V-1)}$$

$$P_{\text{swept,UC}}(s,t) = [Trans(p_{\text{pvt}}(t))][Rotz(\theta_{\text{C}}(t))][Rotx(\theta_{\text{A}}(t))] \quad \text{(V-2)}$$
$$\begin{bmatrix} (e + r_{\text{tc}}\cos\beta_{\text{c}})\cos\theta^*_{\text{UC}} + c^*_{\text{upper cone}}(l_{\text{ctr}} - h + r_{\text{tc}}\sin\beta_{\text{c}})\tan\beta_{\text{c}}\cos\theta^*_{\text{UC}} \\ (e + r_{\text{tc}}\cos\beta_{\text{c}})\sin\theta^*_{\text{UC}} + c^*_{\text{upper cone}}(l_{\text{ctr}} - h + r_{\text{tc}}\sin\beta_{\text{c}})\tan\beta_{\text{c}}\sin\theta^*_{\text{UC}} \\ -l_{\text{ctr}} + h - r_{\text{tc}}\sin\beta_{\text{c}} + c^*_{\text{upper cone}}(l_{\text{ctr}} - h + r_{\text{tc}}\sin\beta_{\text{c}}) \\ 1 \end{bmatrix}$$

$$P_{\text{swept,LC}}(s,t) = [Trans(p_{\text{pvt}}(t))][Rotz(\theta_{\text{C}}(t))][Rotx(\theta_{\text{A}}(t))] \quad \text{(V-3)}$$
$$\begin{bmatrix} c^*_{\text{lower cone}}(e + r_{\text{tc}}\sin\alpha_{\text{c}})\cos\theta^*_{\text{LC}} \\ c^*_{\text{lower cone}}(e + r_{\text{tc}}\sin\alpha_{\text{c}})\sin\theta^*_{\text{LC}} \\ -l_{\text{ctr}} + c^*_{\text{lower cone}}(e + r_{\text{tc}}\sin\alpha_{\text{c}})\tan\alpha_{\text{c}} \\ 1 \end{bmatrix}$$

Although the presented solution can be used, and it does provide the generalized tool support, this work is oriented on a search for GPU-friendly solutions. As result, there was selected a tool representation approach similar to the Constructive Solid Geometry. A tool is represented as a set of simple geometry shapes such as spheres, cylinders, planes. And a swept volume of each simple shape is also a simple shape. For example a sphere makes a swept volume that can be described by two spheres and a cylinder. A

cylinder at the same time makes a swept volume that can be described by a prism and two cylinders.

It is important to notice an important assumption made in this work: true 5-axis motions can be approximated accurately by a set of 3+2 axis motions. Although it is not generally true, true 5-axis motions are not as popular as 3+2 axis motions even on 5-axis machines. And even in case of true 5-axis motions only a tip of a tool is used most of the time and the assumption is valid in this case. At the same time the selected approach can be used for representing true 5-axis motions but swept volumes of simple shapes in this case become much more complicated and they are not discussed in this work.

The selected tool representation approach has multiple benefits. First of all, very simple geometric tests can be used for detection if a cell or subcell is completely inside or outside of a tool swept volume. Another benefit is the even higher possible parallelizability since different tool swept volume components can be processed completely independently. For example, formulas (V-4), (V-5) show how a cell can be tested.

$$f = f_s \cup (f_{cb} \cap f_{cs}) \tag{V-4}$$

$$f_s = |C| < (R - r)$$

$$f_{cb} = (C - rN) \cdot N > 0$$

$$f_{cs} = |C - (C \cdot N)N| < (R - r)$$

$$f = [|C| < (R - r)] \cup \left[\left((C - rN) \cdot N > 0\right) \cap \left(|C - (C \cdot N)N| < (R - r)\right)\right]$$

$$e = e_s \cup (e_{cb} \cap e_{cs}) \tag{V-5}$$

$$e_s = |C| > (R + r)$$

$$e_{cb} = (C + rN) \cdot N < 0$$

$$e_{cs} = |C - (C \cdot N)N| > (R + r)$$

$$e = [|C| > (R + r)] \cup \left[\left((C + rN) \cdot N < 0\right) \cap \left(|C - (C \cdot N)N| > (R + r)\right)\right]$$

f represents a Boolean value, which means that a cell is fully inside of a swept volume and *e* represents that a cell is completely outside and not affected by this tool movement. It is noticeable that all operations in these formulas are very simple and actually implemented in GPU hardware. Formulas represent geometric tests for a steady tool. Although, in case of actual movements, these formulas will get additional components and become a bit more complicated. . As it is shown on Figure V-6 a 3+2 axis tool movement will create an additional prism and cylinder. All geometric tests for these shapes will still be efficient since almost all of them are based on hardware implemented vector operations.

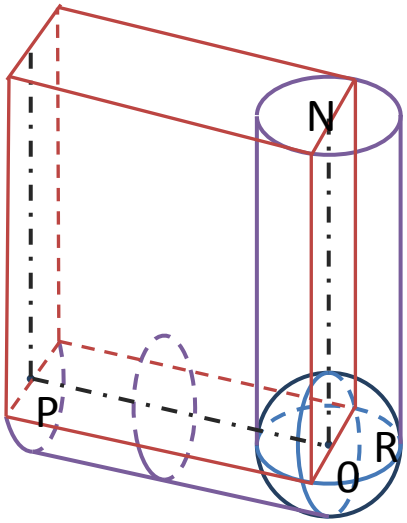

Figure V-6: Ball-end tool swept volume model

5-axis milling simulation based on irregularly sampled volume

The previous part describes the selected tool representation and the reasons why it is better to use a CSG based tool model than a traditional generalized cutter representation. This part goes forward and discusses implementation of the developed geometry representation and the material removing simulation algorithm. It is based on the assumption that there are known solutions for determining if a spherical cell is completely inside, outside or on the boundary of a tool swept volume one of which is shown in the previous part.

The implementation of the developed geometry representation model (called Hybrid Dynamic Tree or HDT) contains 3 main parts: array of cells, pool of subcells and a memory map. In contrast to a traditional voxel model, which stores all cells information in a 3d array, the HDT uses a constant length list (implemented as 1d array) where every element contains coordinates of a cell, cell value and a reference to a subcells node. The rationale behind this way of storing data is improving of the data structure scalability. During a data structure initialization time an entire space that has to be represented is regularly subdivided into cells as it is done in a voxel model. Then, based on the number of computing devices (in the current implementation, GPUs), each cell is randomly mapped to a specific device and the generated map is stored for using during initialization of other data structures on the same computer. Random mapping with uniform distribution guaranties that every device gets a reasonable equal amount of work (cells to process) for any possible spatial distribution of edited cells. This fact is a key component for the efficient load balancing of multi-GPU configurations. The developed

implementation actually divides cells based on an estimation of a device performance for improving load balancing of systems that have multiple different GPUs as it is shown on Figure V-7.

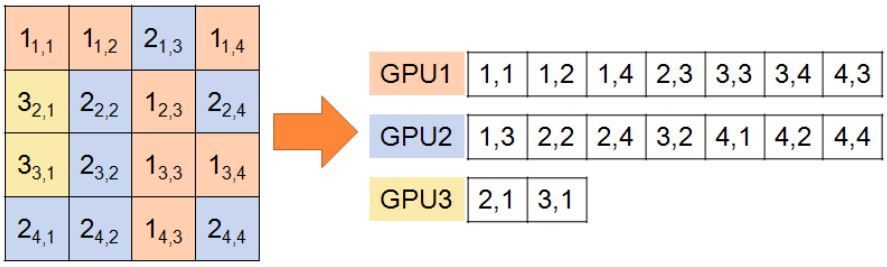

Figure V-7: Multi GPU load balancing

Every cell contains the complete information required for cell editing or rendering and can be processed completely independent from other cells. It is required for better scalability since each computing device needs to store only a subset of all cells and does not need information from other cells. It significantly reduces traffic between host and GPUs since each GPU has all required information in its own memory.

During a milling simulation the simulator processes a sequence of tool movements. Each tool movement is represented as a set of geometric primitives and each GPU calculates if there are cells intersecting one or more of these primitives. Generally each GPU performs a set of geometric tests, similar to those described in the previous part, in order to determine if a cell is intersected or hovered by a tool movement swept volume. If a cell lies completely inside of a tool swept volume, it is marked as an empty cell and its subcells node is released (if it was a boundary cell). If a cell is intersected by one or more tool swept volumes it is added to a list of cells that have to be further processed. The Algorithm V-1 demonstrates the first part of the simulation algorithm.

```
1   For all cells in parallel:
2   |   For all tool motions:
3   |   |   Calculate intersection between cell and swept volume
4   |   If cell lies inside of at least one tool swept volume:
5   |   |   If cell is full:
6   |   |   |   Mark cell as empty
7   |   |   If cell is boundary:
8   |   |   |   Mark cell as empty and add to a list for subcells cleaning
9   |   Else:
10  |   |   If cell is intersected by swept volume:
11  |   |   |   If cell is full:
12  |   |   |   |   Allocate memory for subcells from a memory pool
13  |   |   |   If cell is not empty:
14  |   |   |   |   Add cell to a list for subcells processing
15  For all cells in cell cleaning list:
16  |   Mark all subcells as full
17  |   Return memory allocated for subcells to a memory pool
```

Algorithm V-1: First part of the machining simulation process

```
1   For all cells in subcells processing list in parallel (per multi-processor):
2   |   For all subcells in cell in parallel (per core):
3   |   |   For all tool motions:
4   |   |   |   Calculate intersection between subcell and swept volume
5   |   If subcell lies inside of at least one tool swept volume:
6   |   |   Mark it as empty
7   |   Else:
8   |   |   If subcell is intersected by at least one swept volume and subcell is not empty:
9   |   |   |   Mark it as boundary
```

Algorithm V-2: Second part of the machining simulation process

The second part (shown by Algorithm V-2) of the material removing algorithm is the processing of subcells. During processing cells each GPU generates a list of cells intersected by a swept volume. This list is used for selecting subcells that have to be further processed. The algorithms performs the same set of geometric tests to each subcell and determines if a subcell is completely inside of a swept volume, completely outside or interested. Subcells that lie completely inside of a swept volume are marked as empty. Subcells intersected by a swept volume are marked as boundary if they were completely full by material. The Table I-1 shows the possible cell value changes based on results of geometric tests.

Cell \ Swept volume	**Inside**	**Intersected**	**Outside**
Full	Empty	Boundary	Full
Boundary	Empty	Boundary	Boundary
Empty	Empty	Empty	Empty

Table V-2: Cell value changes

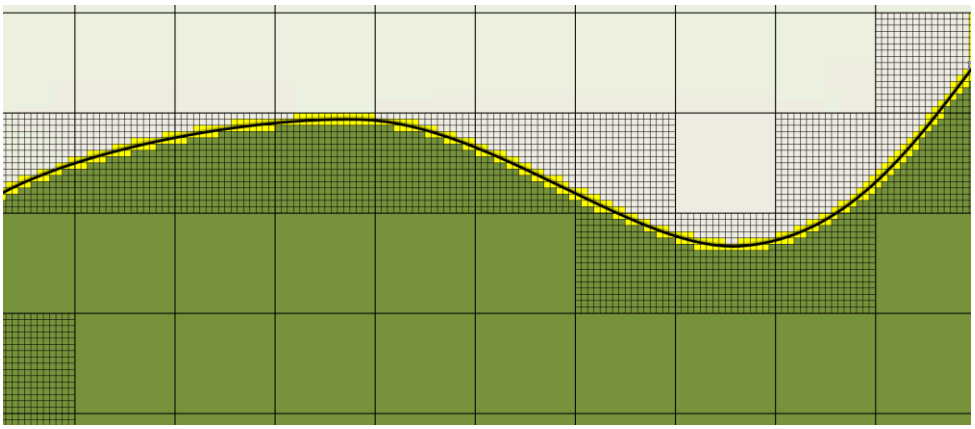

a) Initial surface representation

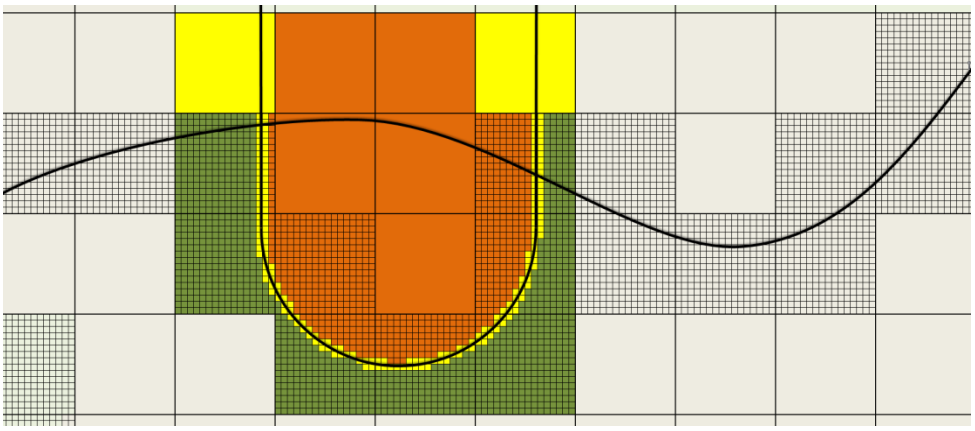

b) Results of intersections between cells and a tool swept volume

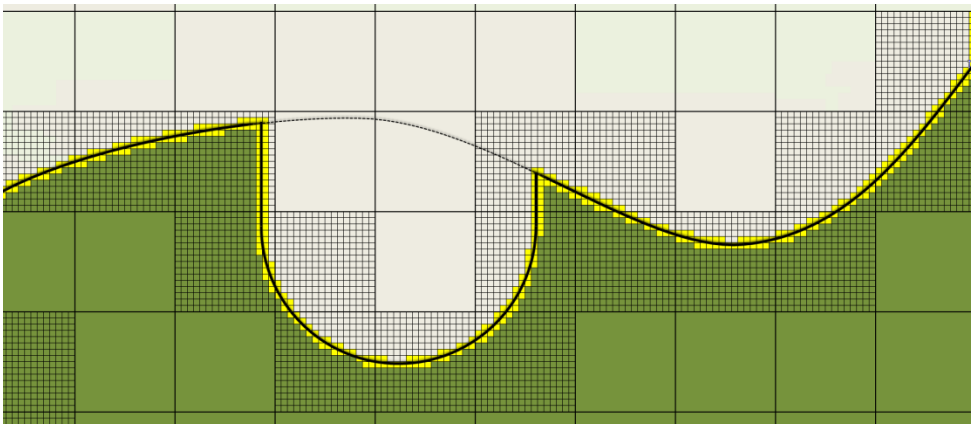

c) Geometry model after machining simulation

Figure V-8: Machining simulation process shown on 2D geometry model

The Figure V-8 demonstrates the machining simulation process and different states of the underlying geometry representation model. The first part “a” demonstrates an initial state of a geometry model that represents a surface, green color represents cells with material and yellow color represents boundary cells. The second part “b” shown a tool swept volume (just a slice of it in case of this 2D example) and calculated intersection results between cells and tool swept volume. Here, the orange color

represents the cells that lie completely inside of a swept volume. These cells will be removed. The green color in this case represents the cells that lie completely outside of a swept volume; they will not be affected at all. The last part “c” represents a geometry model state after machining simulation. It is easy to see that that some cells have been subdivided into subcells since they contain surface now and some cells which earlier contained subcells are completely empty.

Although the subcells value updating algorithm is relatively simple and straight forward, it is important to notice some GPU-specific implementation details. Each cell contains an array of 16x16x16 subcells and each subcell is represented by 2 bits. The selection of these parameters is critical since they determine both performance and memory efficiency. In this work each block of subcells is processed by an independent warp for decreasing data exchange between warps and eliminating additional synchronization. It means that all of the warps in a work group are completely independent and use internal synchronization without any memory access barriers for improved performance. From another side each thread in a warp read a 32 bit integer that stores a consequent block of 16 subcell values as shown on Figure V-9, processes it and stores updated values back. It results in perfectly linear and efficient memory reading and writing operations which are extremely important due to GPU memory controller limitations. This is possible because all of the subcells are independent from each other and their values can be updated in private memory of a thread that processes a subcell. The described way of processing subcell blocks is extremely important on GPU since GPU memory controller always operates with a relatively large block of memory (32*4b

for used cards). And the best memory bus usage efficiency can be achieved only if all values are used in calculations by a warp. The same limitation also becomes a problem for using the traditional Octree since every iteration require processing only 8 elements or 16bit of data. If the algorithm uses only 16 bit of data it means that it uses only 1.5% of the memory bus (for used NV GTX580) which is extremely inefficient.

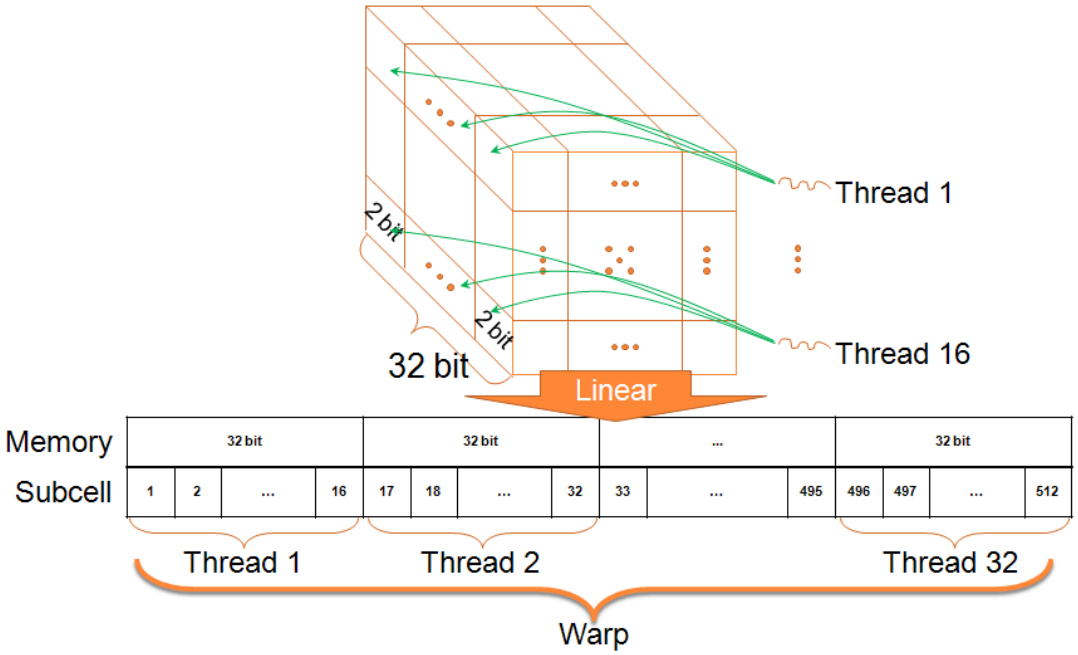

Figure V-9: Threads distribution during subcells editing

Another interesting implementation detail is the memory management. The OpenCL used in this work does not allow allocating and releasing memory from the GPU kernel code. (Actually, even traditional Windows memory system does not work efficiently in case of continuous allocation and releasing of small blocks so the described algorithms would be useful for CPU implementation). As a result, memory management

is implemented by storing a nodes pool, where each node has enough space for storing a 16x16x16 block of subcells, and an address stack (implemented as an array of nodes indexes and an index of a top element) of available blocks. Initially, the nodes pool is full of nodes that represent completely full subcells and the address stack stores references to all nodes. When the algorithm finds that a completely full cell is intersected by a swept volume and its subcells have to be further processed, it pops a top address from an address stack and associates an empty node with this cell.

The nodes releasing algorithm is a bit more interesting and complicated. The problem with nodes releasing is related to node values. After using a node for storing subcells values in an edited cell, it obviously has random values. But a newly allocated node has to be "clean" or has to have all "completely full" subcell values. The cleaning basically means that all subcell values are changed to "completely full" state and it is nothing more than writing some predefined values to a node memory. Although it may look like a simple and trivial operation, the decision of when to do the cleaning is not as trivial and significantly affects performance. There are two obvious ways to do cleaning: during node allocation (during cell editing operation) or during node releasing. Both of these ways have a significant problem: it is not known when they happen and they almost always happen in few threads of a warp. It brings two important problems. First, if only one thread in a warp needs to get or release a node, 31 other blocks have to wait until it works with a node. Second, only one thread has to clean an entire node which means that it has to issue 32 times more memory writing commands and use 1/32th of a memory bus than it is really needed. As result memory management works very slowly. The

developed solution is using a temporary list of nodes (Figure V-10) that have to be cleaned before returning to the nodes pool and centralizing cleaning of these nodes by all warp threads. As was mentioned before, nodes go from the nodes pool to the geometry model when a cell is intersected by a swept volume and there is a need to represent a cell with higher accuracy by subdividing it into subcells. There are two possible ways for a node to go back. First, a cell lies completely inside of a swept volume and it becomes completely empty in result. Second, it is detected that all subcells of a cell are empty and an entire cell can be marked as an empty cell. In both cases a node goes to a temporary cleaning storage. When an application is idling it can run the node cleaning algorithm that rewrites nodes values and return them back to a node pool. It may significantly improve memory management performance and allows the use of idle time for useful operations.

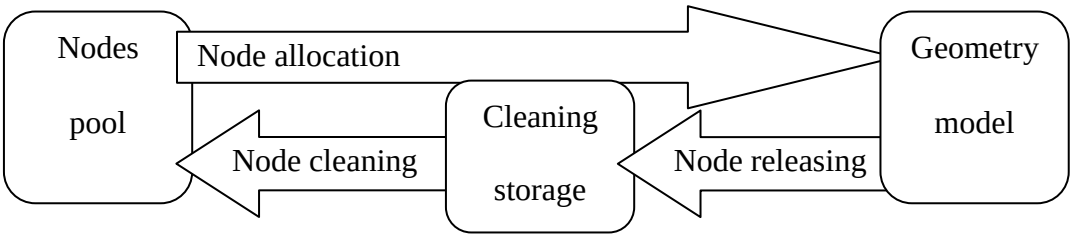

Figure V-10: Nodes memory management model

Irregularly sampled volume rendering algorithm

The geometry editing process is only part of all the geometry representation jobs. Another important part is data visualization, or geometry rendering. The rendering process is important from two points of view. From one side, showing geometry to a user

may be a goal of an application, for example, showing of a milling simulation result is one of main goals of a simulator. From the other side, even if an application does not have to produce any visual output, rendering still may be important for debugging purpose. This part describes rendering algorithms designed especially for the developed geometry representation and efficient highly parallel multi-GPU rendering.

As was mentioned earlier some geometry representations such the triangular mesh or the voxel model can be rendered directly but other model such as the height map has to be converted to another geometry representation for rendering. There are many rendering techniques that have been developed for various situations and geometry representations. For example, a ray tracing approach attempts to simulate a physical world and can produce a photorealistic image. However it requires a lot of computational resources and cannot be easily parallelized. On the opposite side, a ray casting approach can be easy parallelized but usually produces not physically realistic images. The developed in this work approach uses a mix of ray casting and direct rendering approaches for producing an image that is not photo realistic but provides even more useful information than a physically accurate pictures. The proposal for this research project contained description of a possible rendering technology for the proposed geometry data structure. Since during the research project there was made a decision to use the simplified version of a volume representation, the actually implemented renderer uses a simplified algorithm adopted for the simplified data structure. However it is important to describe the originally proposed approach since it may be implemented in future for more complicated geometry representation.

The originally proposed rendering algorithm works in two steps. First it iteratively generates a height map oriented as a screen by casting rays from each filled cell to a screen plane and subdividing the visible boundary cells to increase the resolution until the size of each cell becomes smaller than half of a pixel size. Then normals are calculated for each height map point for a correct lighting. There are two possible options for normal calculation: the first is to estimate normals directly from a height map which will produce reasonable results. The second option is to calculate normals based on analytical information about a surface which has to produce exact values for normals but requires additional calculations. In this case the algorithms will identify the closest surface that is represented analytically and use an analytically calculated normal at the closest surface point. The closest point is not always an actual ray intersection point; however, the maximum possible error cannot be greater than the pixel size. Therefore, it is possible to assume that a surface is continuous and the calculated normal approximates the actual normal to a high degree of accuracy. Figure V-11 shows the results of the two iterations used by rendering algorithm to generate a height map where red line shows actual surface and yellow line shows an approximated height map value at each pixel.

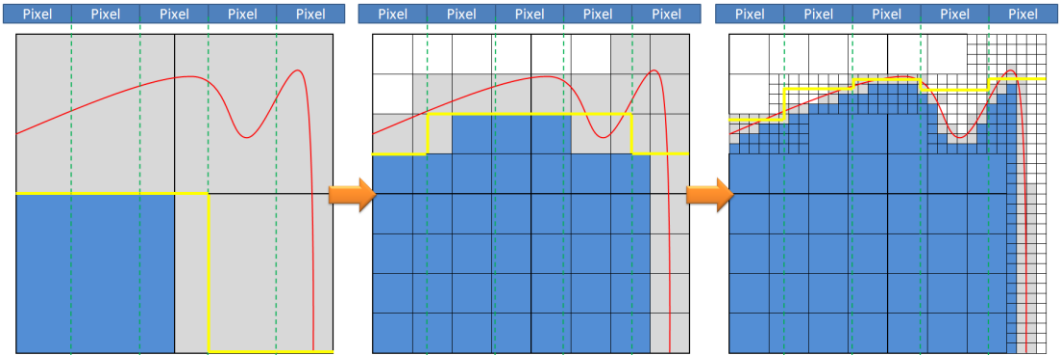

Figure V-11: Two height map generation iterations used for rendering

The Figure V-11demonstrates only an idea of an algorithm for generating a height map that can be used for true dynamically generated geometry models. Actually implemented geometry model has only 2 levels and use spherical cells in opposite to shown rectangular cells as shown on following figures that describe a rendering process.

The implemented rendering algorithm starts by creating a list of all boundary cells that are shown on Figure V-12 in yellow.

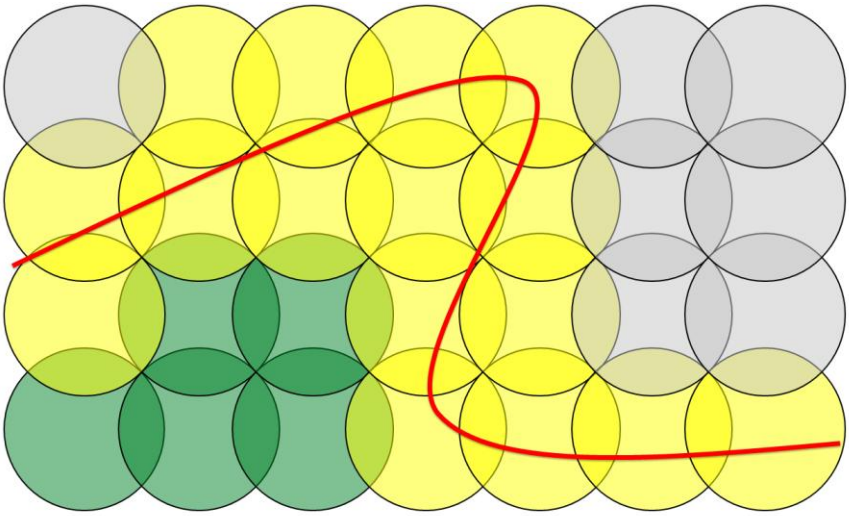

Figure V-12: Curve represented by spherical cells

Then it processes all boundary cells and creates a list of boundary subcells as shown on Figure V-13.

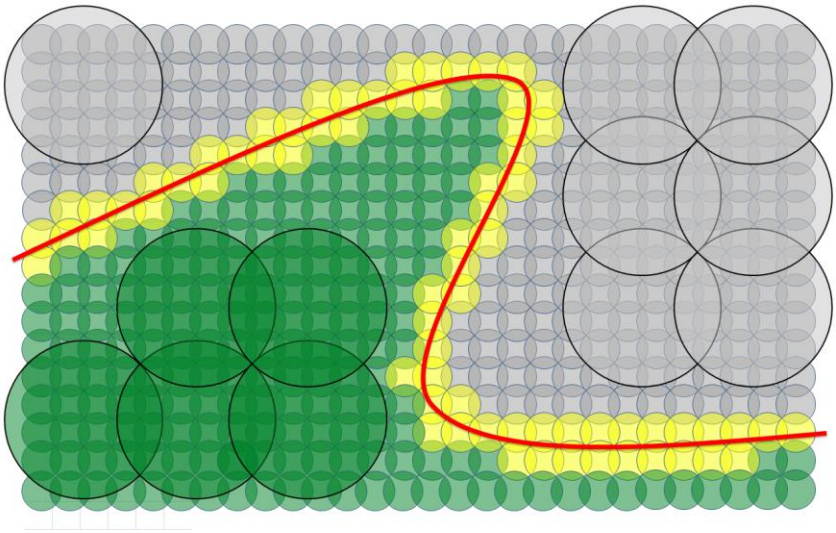

Figure V-13: Curve represented by spherical subcells

A list of boundary subcells is the main input for the next big step of the rendering algorithm. It is important to notice that these cells are completely independent and may actually be stored on different GPUs. The problem here is that multiple cells from different devices may affect the same pixel. As result there is a need for additional synchronization. Since synchronization reduces performance, the implemented algorithm is trying to do as much work as possible simultaneously on multiple GPUs and then synchronize results. One of the most important steps that it does in parallel is calculation of a height map by calculating distances from a rendering plane to the closest cell. However, as was mentioned above, each GPU has only part of the volume, and as a result each GPU calculates only distances to cells that are stored on this GPU.

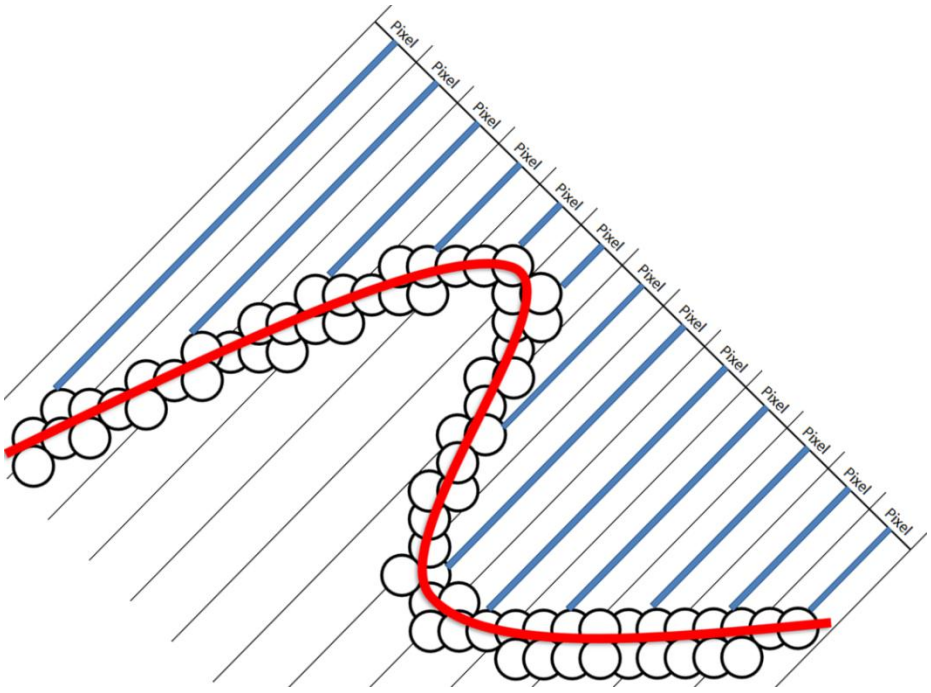

Figure V-14: Rays casted from each pixel on a screen plane

The current implementation does not actually cast rays from screen plane but casts them from each cell to a screen plane and stores the closest distance for each pixel as shown on Figure V-14. When all distances are calculated, they are downloaded to one GPU and combined there into a one complete real height map (before this step, GPUs had only parts of a height map although they were stored as a height map).

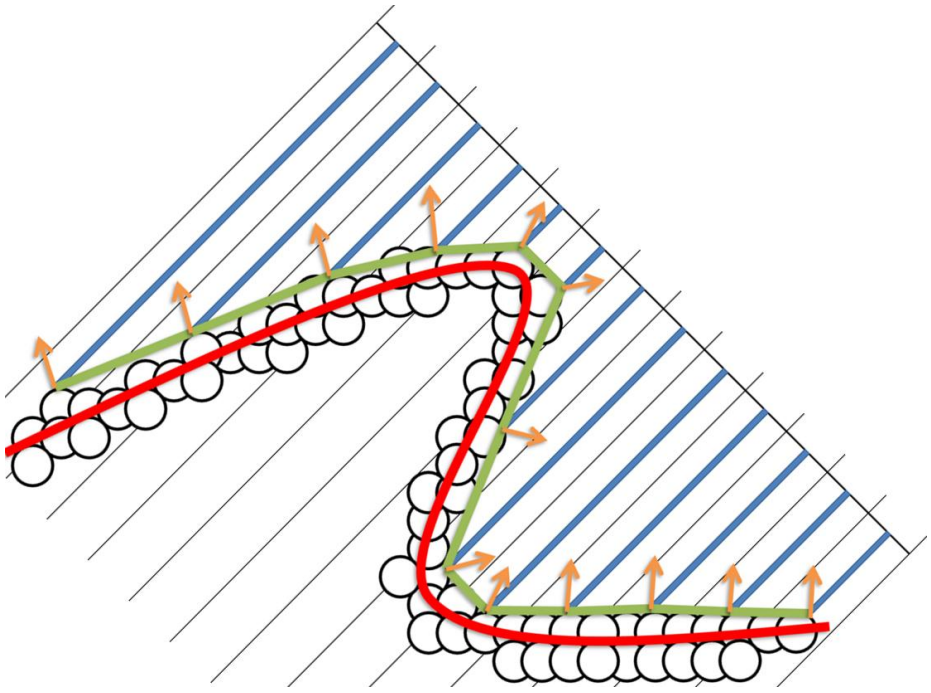

Figure V-15: Estimated surface and normals

The same GPU that combines all height maps also performs the last part of the rendering process. Calculated height map allows estimating a surface (shown in green on Figure V-15). But what is even more important, it allows estimating normals. The developed implementation uses expression (V-7), where $H_{x,y}$ is height map value at point (x, y), for estimating normal of a height map based on neighbor height values.

$$\begin{aligned} N_x &= \frac{\left[H_{(x+1,y)} - H_{(x-1,y)}\right]}{MAX_{UINT}} \\ N_y &= \frac{\left[H_{(x,y+1)} - H_{(x,y-1)}\right]}{MAX_{UINT}} \\ N_z &= -\left[\frac{2}{ViewportHeight} + \frac{2}{ViewportWidth}\right] \end{aligned} \tag{V-6}$$

When normals are estimated for each surface point associated with a screen pixel, a surface intensity is calculated as a dot product of a normal vector and light direction vector. An actual pixel value is calculated as a product of surface point intensity and a surface material color.

The complete list of steps performed during rendering process is shown by Algorithm V-3.

```
1   Collect a list of all boundary cells in parallel
2   Collect a list of all boundary subcells in parallel
3   For all subcells in parallel:
4   |   Calculate cell projection to a screen plane
5   |   For all pixels in projection area:
6   |   |   Calculate a distance between screen plane and cell surface
7   |   |   Update pixel value by a minimum between current value and calculated value
8   Combine height maps from multiple devices
9   For all pixels in parallel:
10  |   Estimate normal values
11  |   Calculate pixel color
```

Algorithm V-3: Rendering

The Figure V-16 demonstrates rendering results of the implemented rendering algorithm. It is similar to the original rendering algorithm but it has one significant limitation. It uses only single iteration, since the underlying data structure is static and limited to 2 levels. The implemented renderer cannot show perfect accuracy due to geometry model limitation but it already runs on 3 GPUs with almost linear performance improvement which is a very hard task that cannot be achieved even by multi-million computer games.

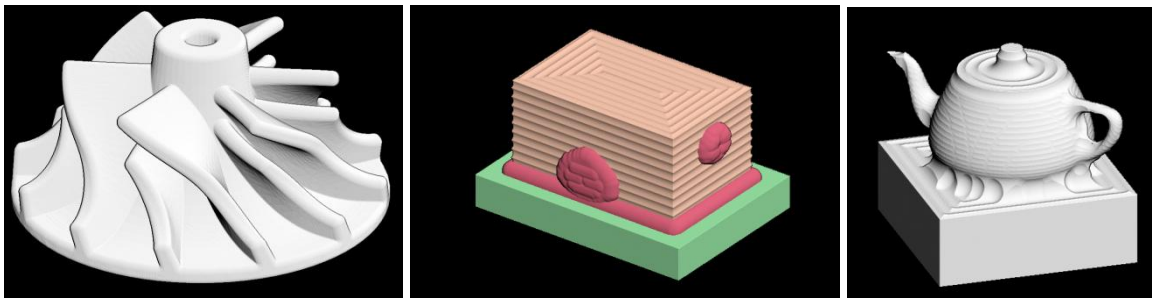

Figure V-16: Rendering results

It is interesting to notice that the selected method of normals reconstruction from a height map results in interesting visual effects. If one object stays in front of another object then it is not only rendered in foreground but there is also shown a dark border when it intersects deeper object. Figure V-17 demonstrates this effect. It is very easy to see which line is closer and which line is deeper.

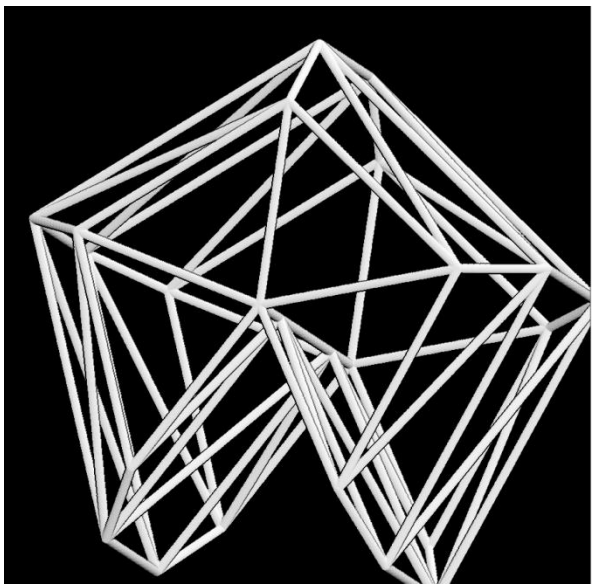

Figure V-17: Demonstration of dark borders around foreground objects

Accuracy analysis

The simulation of any process does not make sense if the simulation is not accurate enough. The key word in the previous sentence is “enough”, but there is no information about desired accuracy. It is obvious that perfect sub-atomic level simulation would be nice to have but would it really help in a machine shop from a practical point of view? It can be seen that sub-atomic level simulation would be quite slow. It would probably be at least a thousand times slower that actual machining and this level of performance already makes it useless. What is more interesting is that it is actually impossible to achieve sub-atomic precision level just because modern CNC machines cannot achieve this level of accuracy. Before discussing the accuracy of the developed simulator it is important to understand possible precision limits and practical requirements for machining simulation from an end user point of view.

Modern CNC controllers limit the input tool path accuracy to 0.002mm. It means that it does not make sense to simulate anything with input trajectory accuracy higher than 2μm because a machine does not know about this extra precision in any case. But 2μm is pure software limit that is not connected to physical world. During the machining process, the accuracy is affected by tool vibrations, external vibrations, thermal expansion, material deflection, etc. And many of these parameters cannot be measured because they depend on environment condition, tool properties, workpiece properties, etc. As result, 2μm precision can be achieved only in very well controller environment on expensive machines, tools and after good preparation. Most of real life machining provides more than an order of magnitude lower accuracy (20-50μm) that is still good

enough for most practical applications. It is easy to see that in most cases, simulation with precision higher than 20-50µm (2µm in very special cases) does not make sense at all since the actual accuracy is limited by machine capabilities.

Limits described in the previous paragraph are based on the machines limitations. This paragraph will discuss what makes sense from the end user point of view. But before going into this discussion it is important to describe use cases for machining simulation software. Most popular use cases include: collision detection, exceeding axis movement limits, exceeding tool load limits, overcuts detection and surface quality control. The collision detection has two components: collisions of machine parts (including tool and tool holder) with each other that and collisions between machine parts and workpiece. Collision detection between machine parts and exceeding axis limits actually do not require material removing simulation and are not discussed here. Now, when most popular use cases are listed, their simulation accuracy requirements can be discussed.

The collision detection process need to know if a machine part intersects workpiece material. Since it is not safe to have moving machine parts closer than few millimeters to material surface (for parts under 500mm long), it is safe to assume that 0.5mm accuracy of surface position is good enough for the collision detection purpose. Overcuts detection is a bit more complicated problem. It can be viewed as collision detection between tool and target geometry in case of large overcuts and it can be viewed as a bad finishing surface quality in case of small overcuts. For large overcuts scenario the same requirements as for collision detection can be used and it is safe to assume that 0.5mm accuracy is enough. Small overcuts and finishing surface quality control are two

most demanding use cases. Their requirements depend on the desired surface tolerance and generally it is possible to say that it is does not matter where surface is as far as it is possible to prove that it lies in tolerance limit. As an example of possible tolerance limits let use the ANSI B4.1 standard [63]. Figure V-18 shows tolerance limits for multiple grades defined in this standard. The milling process under normal conditions is capable of producing parts with tolerance grade in the range 10-13. For example, considering the best possible grade and a part with a size of 50mm the tolerance limit defined by the standard is ~0.1mm. And for a 500mm part which is a quite popular work envelope limit for modern 5-axis CNC milling machines, the tolerance limit is ~0.25mm.

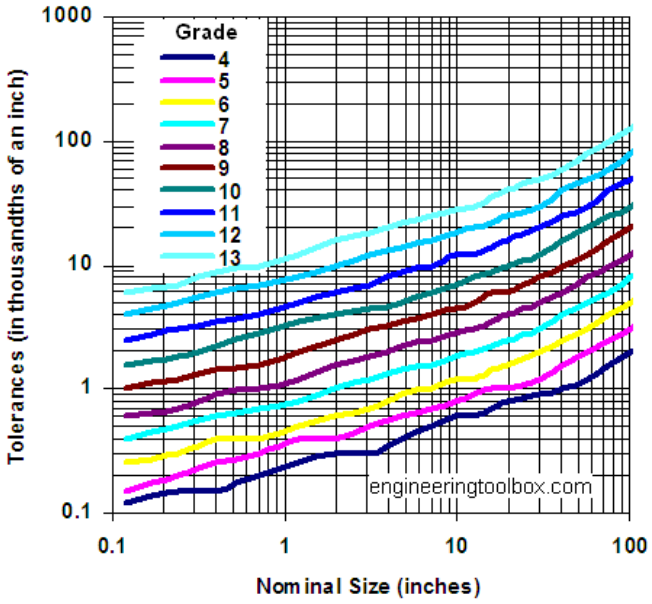

Figure V-18: Tolerances for multiple tolerance grades [64].

Now, when there are known accuracy requirements for popular milling simulation usage scenarios, it is possible to discuss capabilities of the developed simulation system and to see if it meets the requirements. The developed geometry representation does not

naturally represent surface but stores information about presence of a surface in each cell. As a result, surface position can be measured with precision limited to a small cells size and it is possible to say that geometry representation accuracy is equal to a size of the smallest cell. It is also important to mention that due to using spherical cells, linear cells size has to be multiplied by ~1.732. Considering resolution of 4096x4096x4096 for a workpiece with dimensions 50x50x50mm, it is easy to see that a cell size is ~0.021mm. For a larger workpiece (500x500x500mm) the resolution will be ~0.21mm.

It is easy to see that simulation with a resolution of 4096x4096x4096 meets requirements for all popular machining simulation use cases for parts with dimensions up to 500x500x500mm which is a common machining envelop size for modern 5-axis machines and the most accurate tolerance requirements for the ANSI B4.1 standard. It is also easy to see that for smaller parts such as 50x50x50mm a resolution can be reduced by 2 or even 4 times without significant problems from practical point of view. Performance benefits of resolution reduction will be described later. Although the developed system meets the precision requirements for popular use cases, its precision is quite close to this requirements and it is important to notice that it cannot be used for extra high precision simulation without modifications. In case of a need for highly accurate simulation, a possible way to do it is to implement the full version of the initially proposed geometry representation that can be dynamically generated. But as was mentioned earlier, even the already developed system is accurate enough.

Experimental 5-axis simulation results

The described data structure and algorithms were implemented during the research project. All low level highly parallel algorithms and data structures were implemented in C++ and OpenCL. High level algorithms and data management were implemented in Python. And a rendering was implemented as a mix of OpenGL with OpenCL based custom software renderer running on GPU. The developed system successfully uses a multiple GPUs (tested with 2 x GTX 580 + Quadro 6000) and provided good performance and scalability results which will be discussed later.

The set of input G-code files used for testing contains mainly programs generated by tool path planning solutions discussed in this work (both 3 and 5 axis) as well as few test programs from industrial partners.

The first part of the testing process is simulation of previously described 3-axis parts from chapter about 3-axis machining simulation and tool path planning.

Figure V-19: 3-axis model “Sculptures” (new 5-axis simulator on the right)

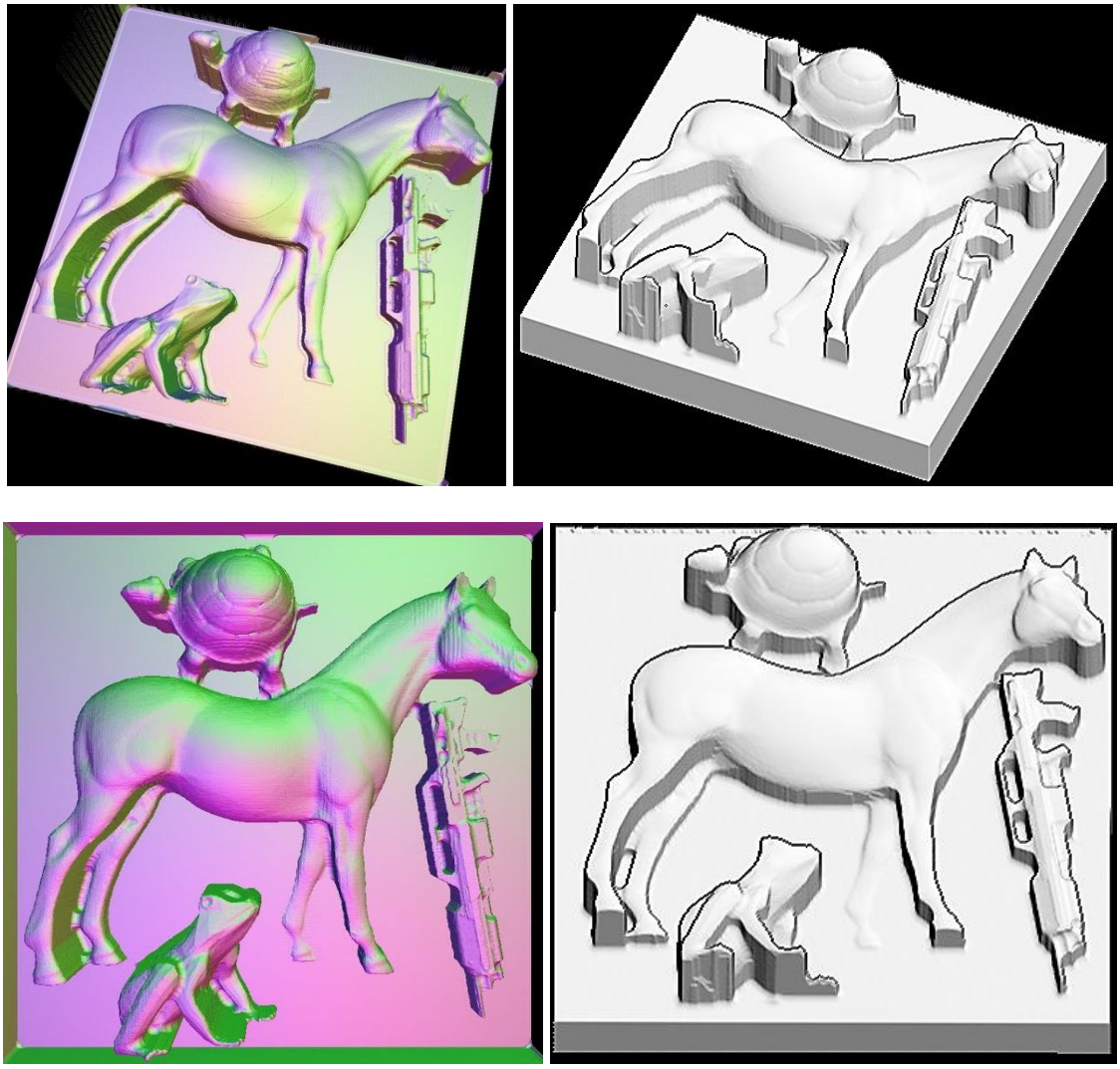

Figure V-20: 3-axis model “Zoo” (new 5-axis simulator on the right)

Figure V-19 and Figure V-20 demonstrate the results of the developed 5-axis simulator in comparison to the height map based 3-axis simulator from previous chapters. It is easy to notice that the produced results are very similar to the original 3-axis simulation results except color (easy adjustable) and projection type. The original 3-axis simulator uses perspective projection and the new 5-axis simulator uses orthogonal projection.

The next part of the testing process is the continuous simulation of 5-axis parts. Since an editing process is a continuous test pictures will demonstrate workpiece state at multiple time points during an editing process with a target geometry model at first image and actually milled part on the last image.

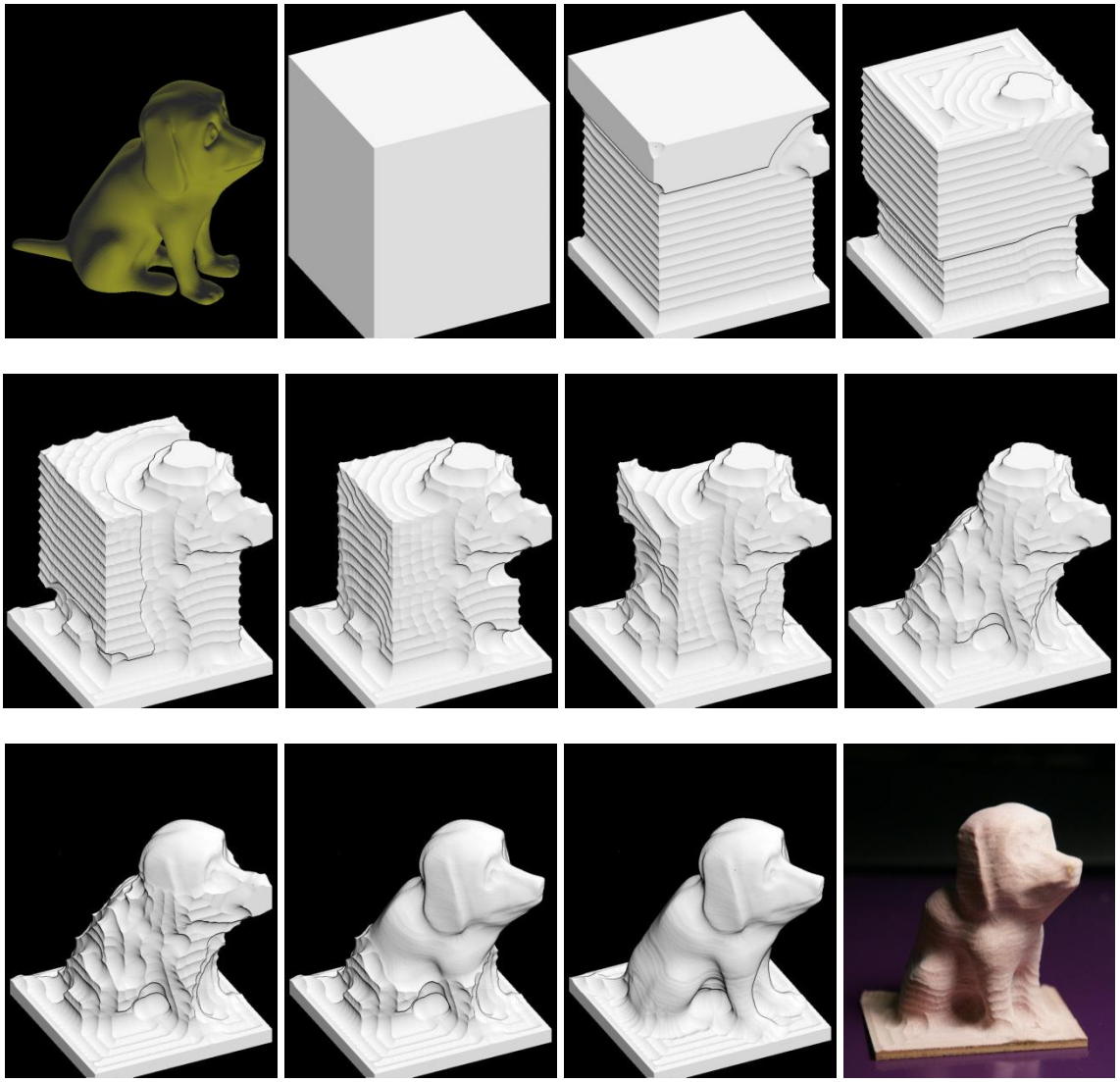

Figure V-21: 5-axis machining simulation process for model “Puppy”

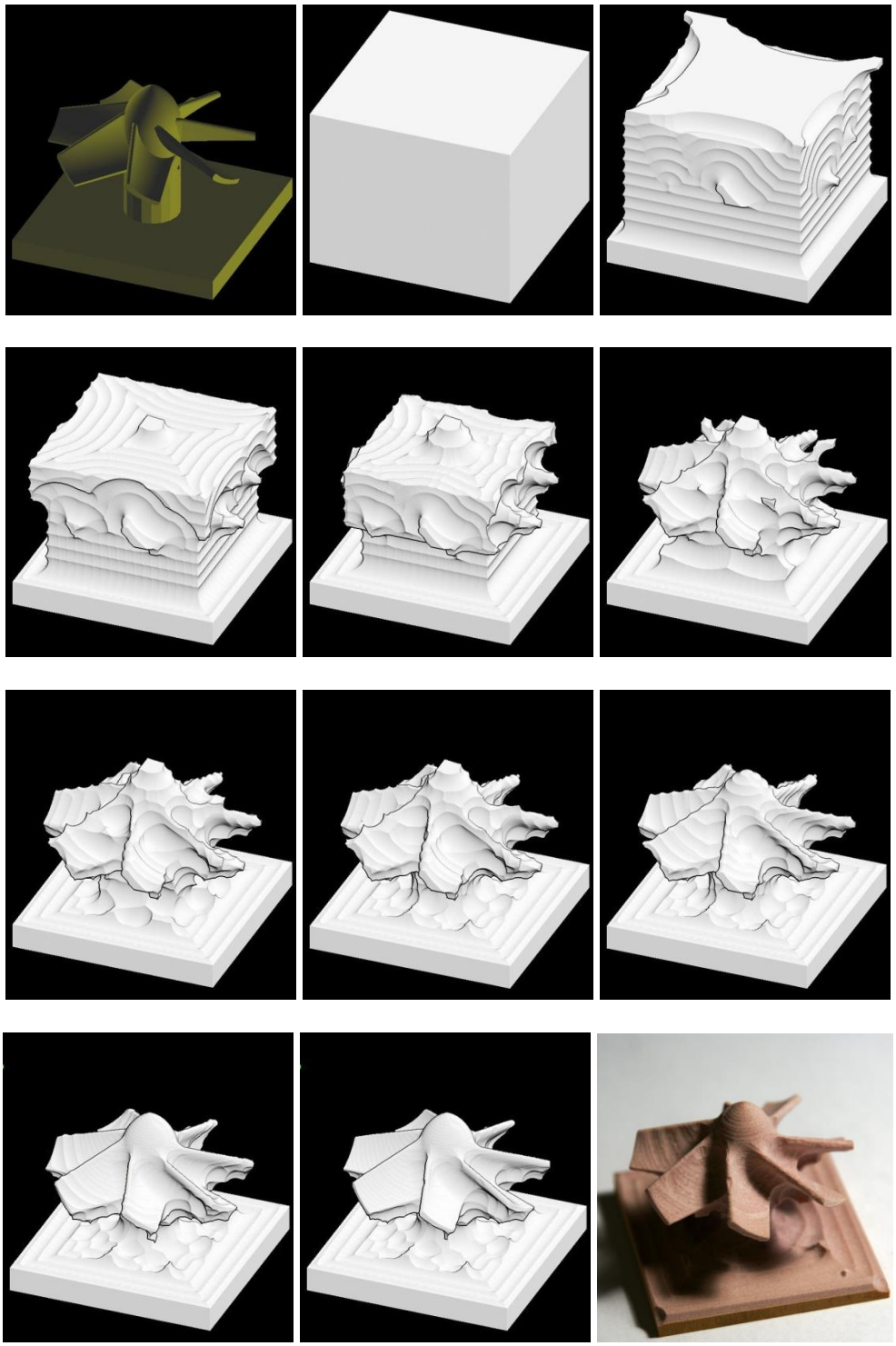

Figure V-22: 5-axis machining simulation process for model “Fan”

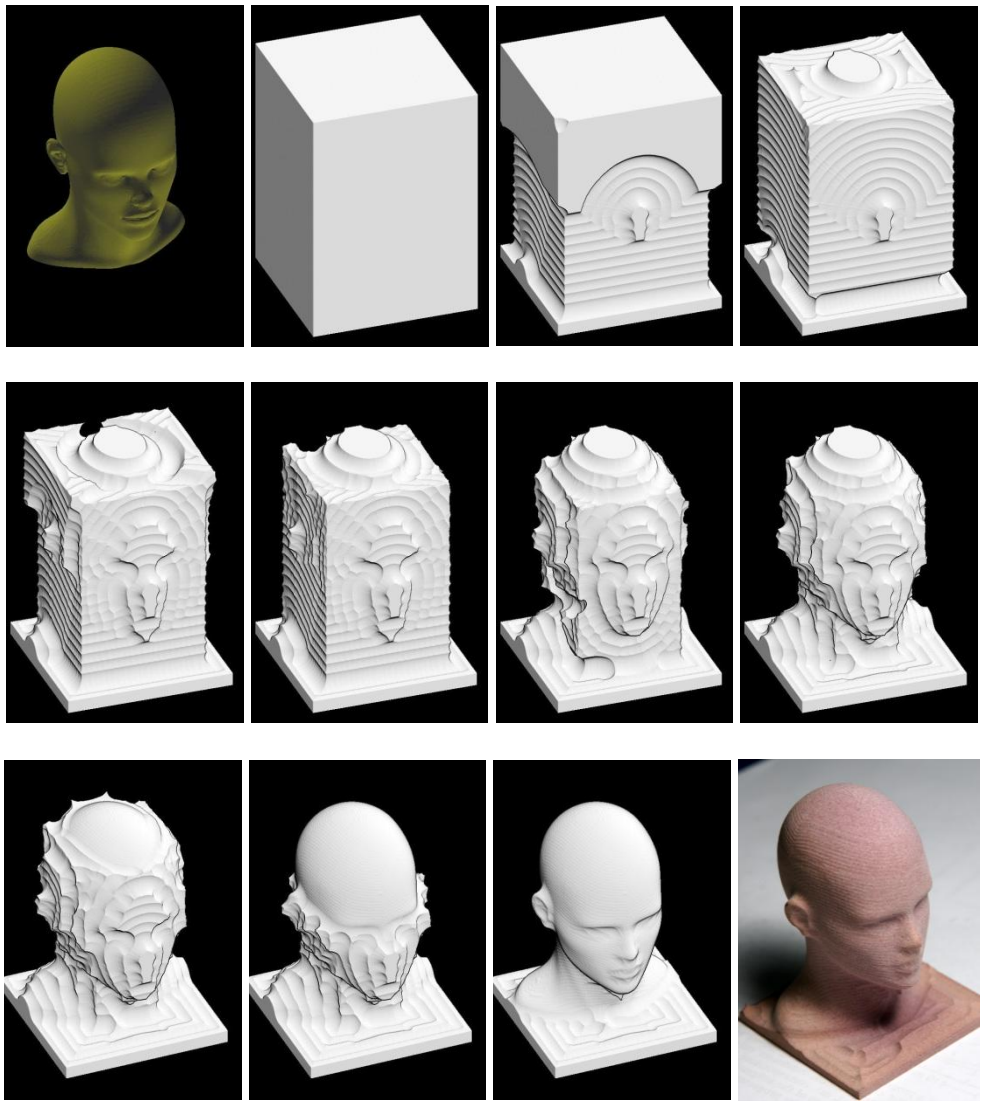

Figure V-23: 5-axis machining simulation process for model “Fan”

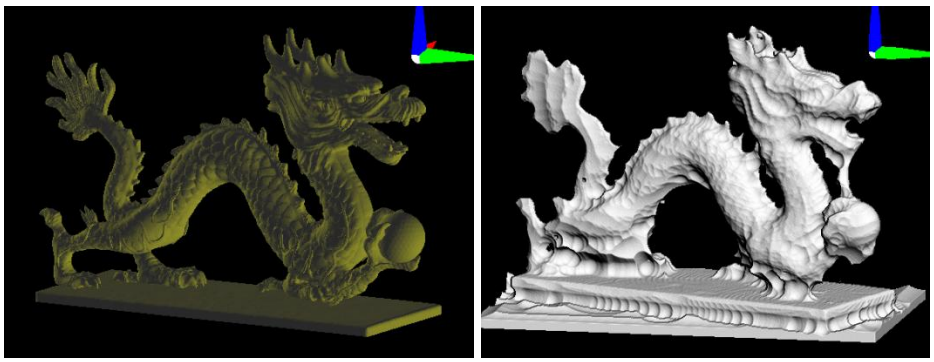

Figure V-24: Simulation result for model “Dragon”

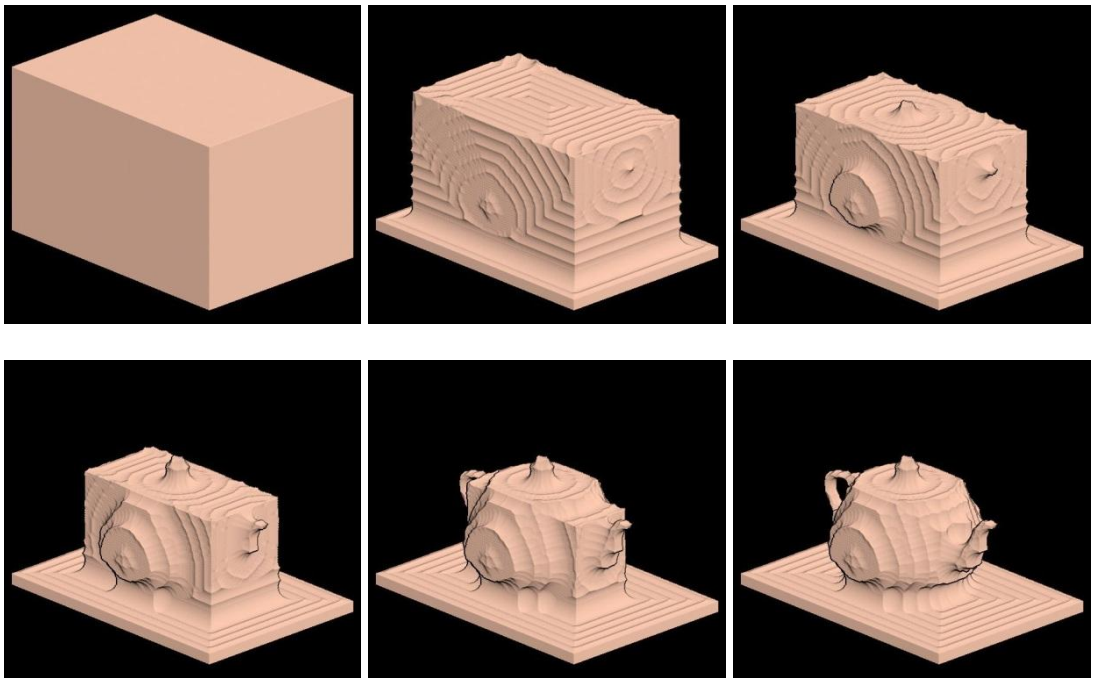

Figure V-25: Roughing process of the “Teapot” model

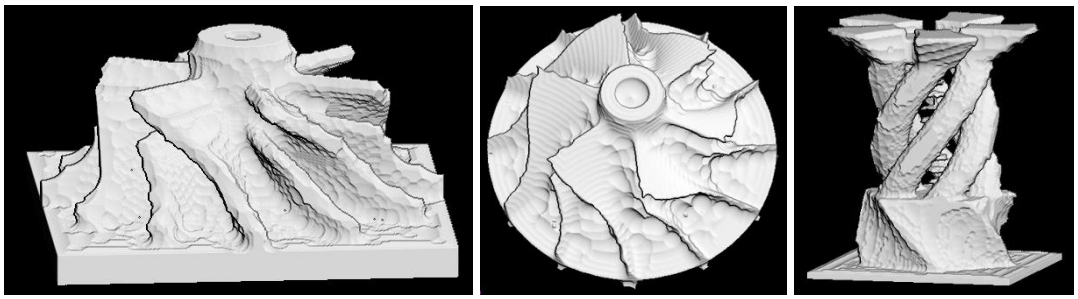

Figure V-26: Various simulation results

Figures above demonstrate that the developed 5-axis simulation system is capable producing accurate CNC milling simulation by using the newly developed geometry representation and parallel algorithms that can run on multiple GPUs. It is also easy to see the high quality of images produced by implemented rendering algorithms. The comparison of the simulator output to real machined parts also shows that simulated results accurately predict machined results.

Simulation performance analysis

The previous part demonstrated that the developed 5-axis simulator is capable of producing correct simulation results. This section will discuss performance measurements of the simulation and rendering algorithms as well as scalability issues.

First of all it is important to describe how performance will be measured since there are no known tests for CNC machining simulators at time of testing and by the author knowledge. Since there is no significant dependency between target shape and underlying algorithms behavior, material removing test is designed to be as simple and as general as possible. It simulates removing a layer of material from a cube workpiece as shown on Figure V-27. The rendering test will actually use the result of the material removing test and render the machined workpiece from multiple sides.

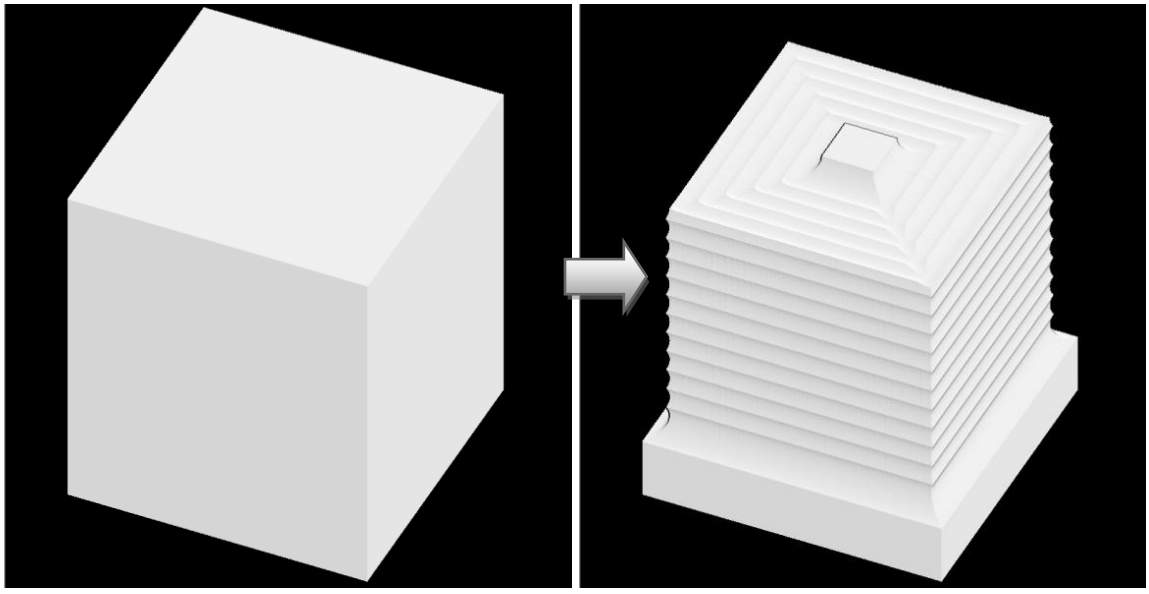

Figure V-27: Machining test setup

All performance measurements are performed with following default parameters:

- Resolution of 2048x2048x2048. For simplicity only one number will be written latter but it is always a cube of a material;
- A big cell contains 16x16x16 small cells.
- Step size is 64. The step size is a number of tool movements processed concurrently during each material removing simulation operation;
- Zoom level is 1X (as shown on Figure V-27);
- The test computing system includes 3 NVidia GPUs (Table V-3):
    - 2x GeForce GTX580
    - 1x Quadro 6000

Name	**CUDA cores**	**Clock frequency**	**IPC**	**SP GLOPS**
GeForce GTX580	512	1594 MHz	2	1632
Quadro 6000	448	1147 MHz	2	1027

Table V-3: GPUs parameters

The default configuration demonstrates performance results shown in Table V-4.

Simulation speed (mm/min, ms/mm)	24414, 0.04
Simulation speed (edits/s, ms/edit)	897, 1.11
Rendering speed (ms, fps)	60, 16.5

Table V-4: Base performance results

The difference between the two ways of measuring simulation speed is related to the fact that tool motions may have different length and as result remove significantly different amount of material. The first row represents the simulation speed measurement

technique normalized from distance point of view. Basically it shows how long trajectory can be simulated in a minute or how many milliseconds required for simulation of one millimeter of a tool path. Using mm/min units also allow direct comparison to a machine feed rate. For example simulation speed of ~25000 mm/min means that simulation can be done 5X times faster than machining at feed rate of 5000 mm/min. Another measurement way uses the actual number of tool movements called “edits” and useful in case when there are many short tool movements. The idea behind these performance measurement techniques is similar to measurement storage performance that can be done from bandwidth point of view or from number of input/output operations point of view.

It is also important to notice that the developed simulation is not a production grade software system that is precisely tuned and optimized. As result it is more important to measure not a pure simulation performance itself (although it is good enough even now) but how well it scales with respect to available computational performance, resolution, etc. Although the performance of current implementation can be significantly improved by optimization for desired hardware, scalability and parallelizability cannot be improved so easily, and they were the initial goal for the new geometry representation and algorithms design.

One of the most important properties of any simulator is accuracy. As was mentioned above, the data structure implemented in this work is static and as a result, accuracy is directly related to model resolution. At the same time resolution obviously affects a number of elements that have to be processed for editing simulation. In case of pure 3D discrete volume representation such as voxel model, the number of elements is

N^3 where N is resolution, which is extremely bad from computation time point of view. However for the developed geometry representation, a number of elements that have to be processed is:

$$T_1 * \left(\frac{N}{16}\right)^3 + T_2 * 16^3 * X = T_1 * \frac{N^3}{4096} + T_2 * X * 4096 \quad \text{(V-7)}$$

where X is a number of big cells containing material boundary and modified by a set of processed tool movements. T_1, T_2 time required to process big and small cells accordingly. It may look like the complexities are $O(N^3)$ in both cases and there is no benefit from using the developed geometry representation. And it is theoretically correct but in real use cases under memory size limitation N has values about ~2000. As a result, it is possible to assume that the first part of the (V-7) becomes negligible and only the second part represented by X affects simulation performance.

As was mentioned before, the X represents a subset of all big cells (so it is already bounded by $(N/16)^3$ value) that meat two conditions: modified by one or more tool movements and contain material boundary. It is actually very hard and almost impossible to estimate how many cells are affected by tool movements under an assumption that there are no limitations on tool movement geometry. But it is possible to assume that a number of modified cells is proportional to a surface area affected by tool motions and a surface area is completely independent from resolution. As result it is easy to see that X is proportional to a number of big cells required for containing a given surface area. In order to estimate X now, it is important to make one more assumption: big cells are small enough that a surface that they contain can be represented by a plane. With respect to this assumption, a big cell contains surface area equal to $(16/N)^2$ and X is equal to:

$$X = \frac{S}{\left(\frac{16}{N}\right)^2} = N^2 * \frac{S}{256} \tag{V-8}$$

Where, S is modified surface area. Now the (V-7) can be rewritten in the form:

$$T_1 * \frac{N^3}{4096} + T_2 * N^2 * 16 * S \tag{V-9}$$

Based on (V-9) it is possible to assume that at reasonably low values of N (such as few thousands) the machining simulation algorithm should show a quadratic dependency of simulation time and resolution. The experimental performance measurement shown on Figure V-28 has proved the assumption about quadratic simulation complexity. It is easy to see that the 2nd order approximation of processing time data perfectly describes measured results.

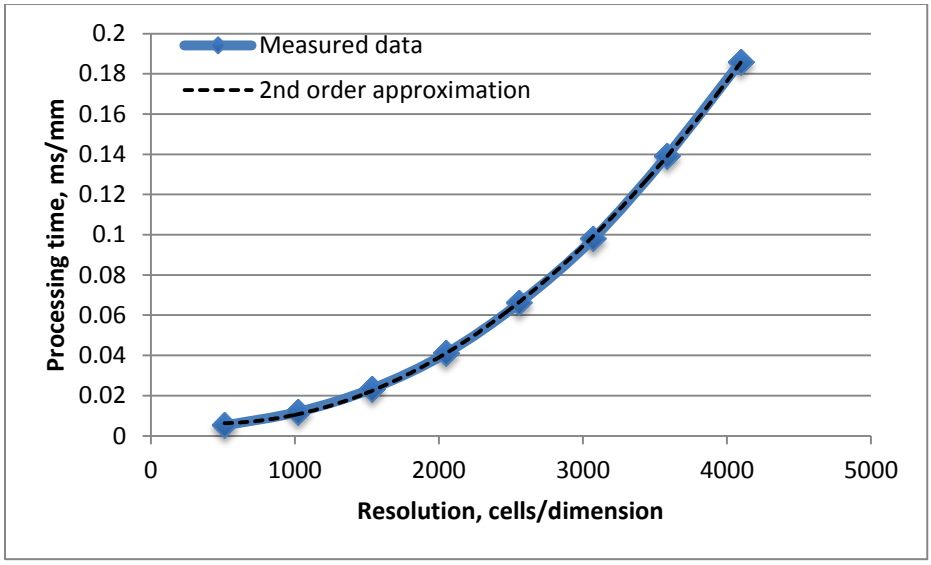

Figure V-28: Editing time vs. Resolution

As was shown above, the newly developed geometry representation has managed to reduce machining simulation complexity from cubic to quadratic. But this is only one of the important benefits that the new data model provides. Other extremely important

benefits are the parallelizability and scalability required for running developed algorithms on multiple highly parallel devices such as GPUs. From a theoretical point of view, the developed data model and parallel algorithms should scale really well since different parts of the volume can be processed completely independent. However real implementations always contain some overheads related to jobs scheduling, synchronization, load balancing, etc. As a result, real systems do not scale perfectly linear.

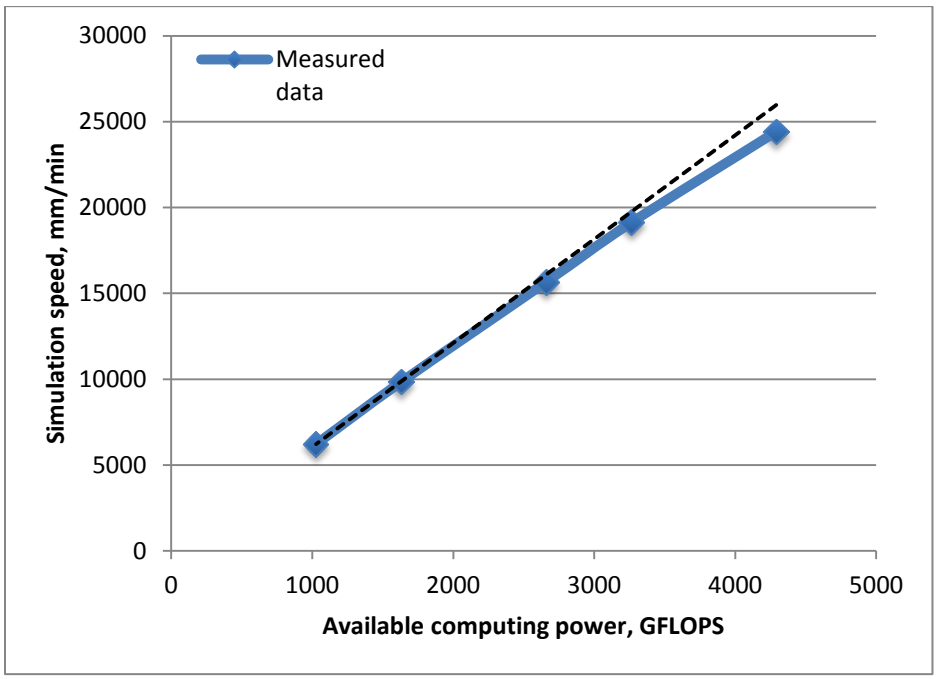

Figure V-29: Performance vs. Available computing power

The Figure V-29 demonstrates how the simulation performance of the developed 5-axis simulator scales with respect to available computational resources. There were 5 possible combinations of available GPUs used and the simulation speed of each was measured. The “Perfect scaling” line was constructed by linear scaling of the single

slowest card performance with respect to performance of each combination measured in single precision GFLOPS. It is easy to see that the actual measurement performance is very close to the theoretical limit. As Figure V-30 shows, all configurations (even with 3 different graphics cards) achieve more than 90% of theoretically possible performance that assumes perfect linear scaling.

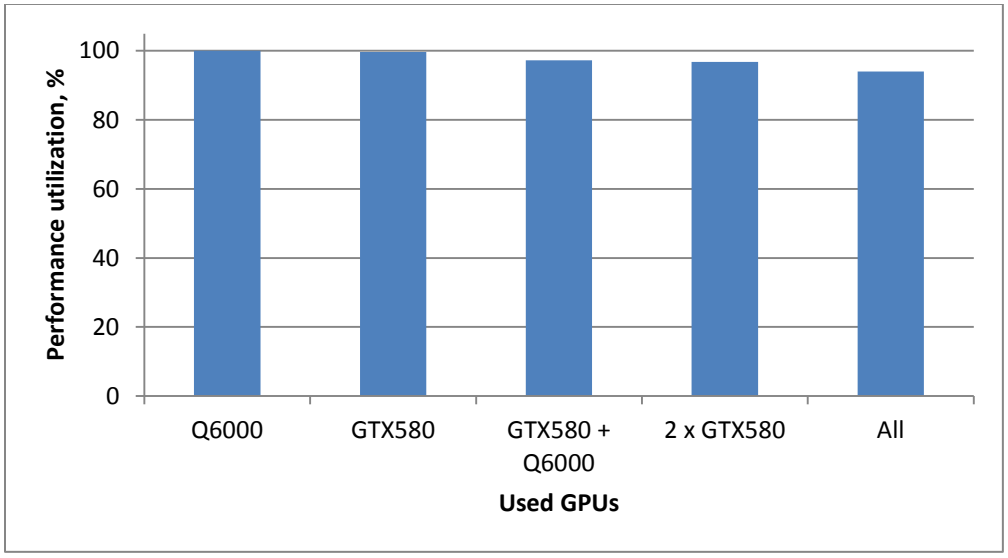

Figure V-30: Utilization of available computation power

There is an interesting fact: only adding more GPUs reduces efficiency. Increasing number of cores and frequency does show perfect linear scaling. It means that the developed system is bounded by available computing power, not by memory bandwidth which is extremely important for GPGPU approach.

The last part of the material removing algorithm testing is measuring dependency between simulation speed and a number of tool motions processed during single iteration (called step size). The step size affects performance in two ways. Too small step size does not allow hiding kernel launch overhead. And a too large step size results into high

algorithm branching that reduces GPU efficiency since multiple threads in a warp have to wait for each other.

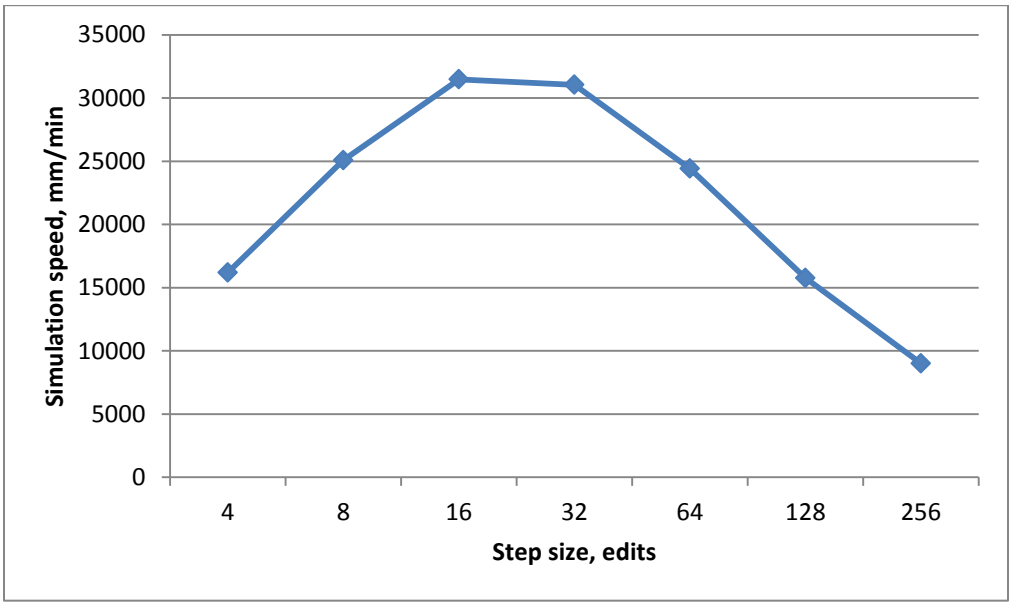

Figure V-31: Performance vs. Step size

The Figure V-31 demonstrates measured performance of the simulation algorithms for multiple step sizes. It shows the described above behavior with a peak performance that lies in a range from 16 to 32 edits per iteration. Although during real life continuous simulation a step size is not constant, measured data can be used for selection of the best step size if simulation of an entire tool path is requires and a user is interested only in a final result.

Performance measurement of the simulation algorithm has shown great scalability and parallelizability which can be explained by the fact that all volume cells can be processed completely independent. But good milling simulator also requires efficient rendering algorithm. However in the case of rendering, it may be a bit more complicated

to achieve the same level of scalability because results computed on all GPUs have to be combined and this process was not parallelized in current implementation.

As was done with editing algorithm, the first part of the rendering performance testing is measuring of the dependency between rendering speed and volume resolution shown on Figure V-32.

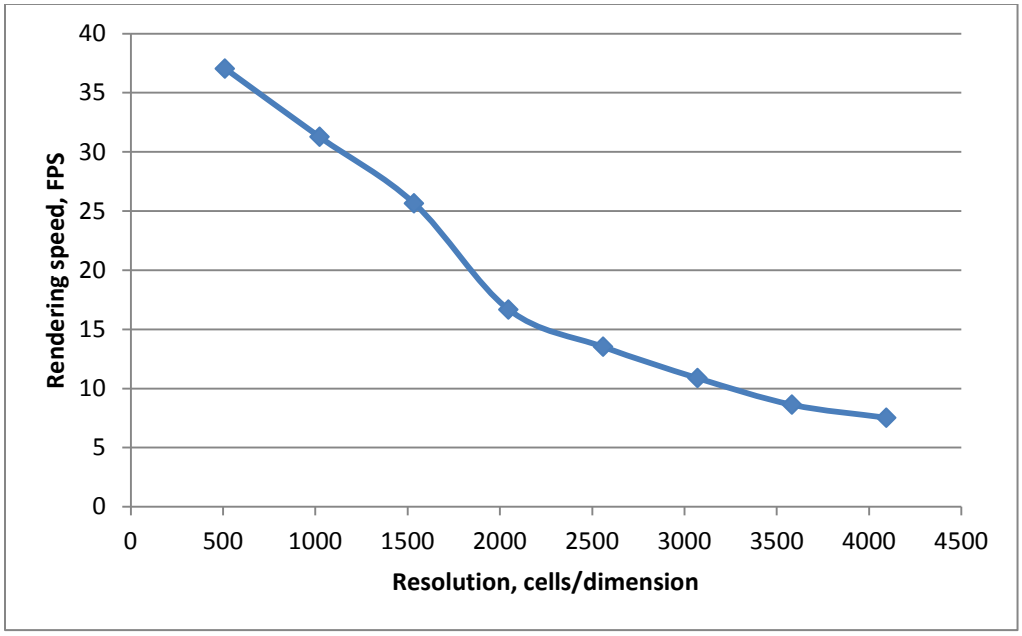

Figure V-32: Rendering speed vs. Resolution

The analytical analysis of the rendering algorithm cannot be done easily since the rendering algorithm heavily depends on actual rendering geometry and volume orientation. However, it is possible to do some non-accurate theoretical estimation. But even based on actually measured data, it is hard to find one mathematical dependency. It may be either two independent linear segments related to two independent bottlenecks. For example memory bandwidth limitation in for resolutions less than 2000 and computational power limitation for higher than 2000 resolution. It also may be a single

quadratic dependency with some random errors in measurements. In any case it is important to notice that for resolutions up to 3000 the developed algorithm provides high enough speed for well interactive work (>10FPS) with the simulator.

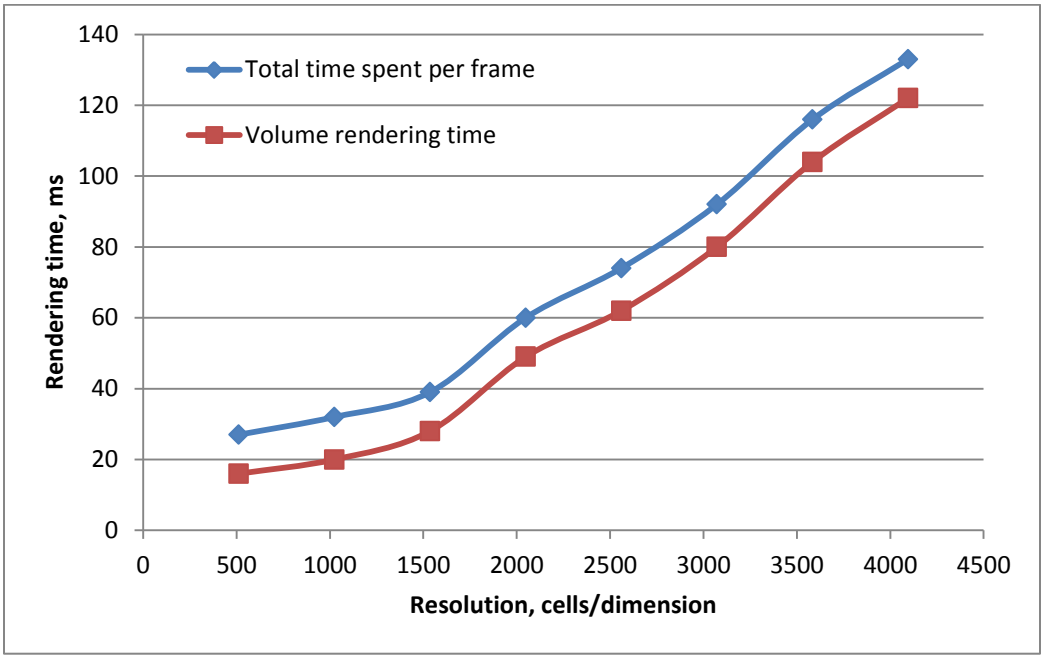

Figure V-33: Frame rendering time vs. Resolution

Another important aspect of the rendering process is the amount of time that the renderer spends on non-parallel work. This work includes mixing image components from multiple devices, drawing to a screen, job scheduling and other required operations. It can be calculated as a difference between time that each device spends concurrently with other devices and time required for rendering of an entire frame. As Figure V-33 shows, this difference is constant for all tested resolutions and it is equal ~12ms. Although this time is usually hard to parallelize, it is possible to convert it into delay between user input and rendering output and reduce GPUs idling. In this case a

calculation of the next frame has to be started before previous frame is visible. This approach will increase frame rate by improving hardware utilization.

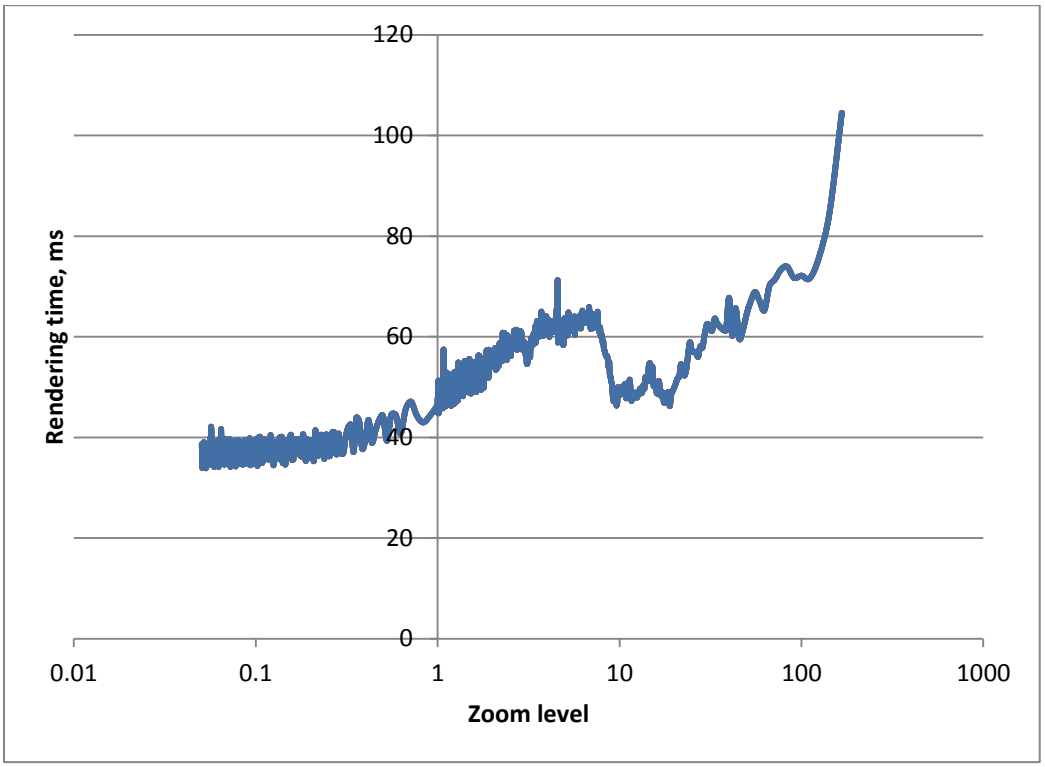

Figure V-34: Rendering time vs. Zoom level

In opposition to editing algorithms, the rendering performance depends not only on the geometry itself but also on a way how it is rendered and especially on scale or zoom level. Figure V-34 presents measured results for rendering time versus zoom level where zoom level equal 1.0 means that an entire volume is shown on a screen and it fills entire screen. Lower than 1.0 zoom levels mean that the image is zoomed out or scaled in a way that an image fills only a portion of a screen. Higher than 1.0 zoom levels mean that a volume is zoomed in and only a part of it is visible. It is noticeable that extremely high zoom levels (>100X) require significantly more time for rendering. It may be

explained easily because at very high zoom levels only few big cells are visible and there is not enough work for loading all available GPU cores. But except this extra high zoom levels, rendering performance fluctuates in the range of 50-150% relatively to a default zoom level which is acceptable from practical point of view.

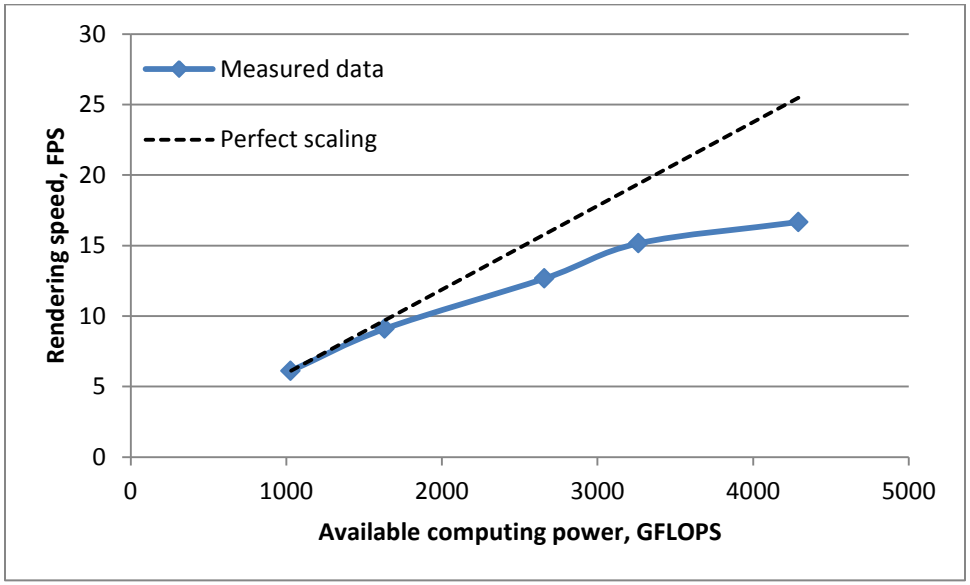

Figure V-35: Rendering speed vs. Available computing power

The last and probably one of the most interesting part of the rendering performance testing is the analysis of its scalability with multiple GPUs. Figure V-35 demonstrates rendering performance versus amount of computational resources available. As in case of editing performance testing, there were used 5 possible combinations of available GPUs and the “Perfect scaling” line demonstrates the best possible linear scaling. It may look like the rendering performance scales is much worse than the editing even for the same number of graphics cards. It actually makes sense since images generated by each GPU has to be mixed and displayed and this time is not parallelizable.

However, as was mentioned before, mixing and drawing time can be hidden by converting into output delay.

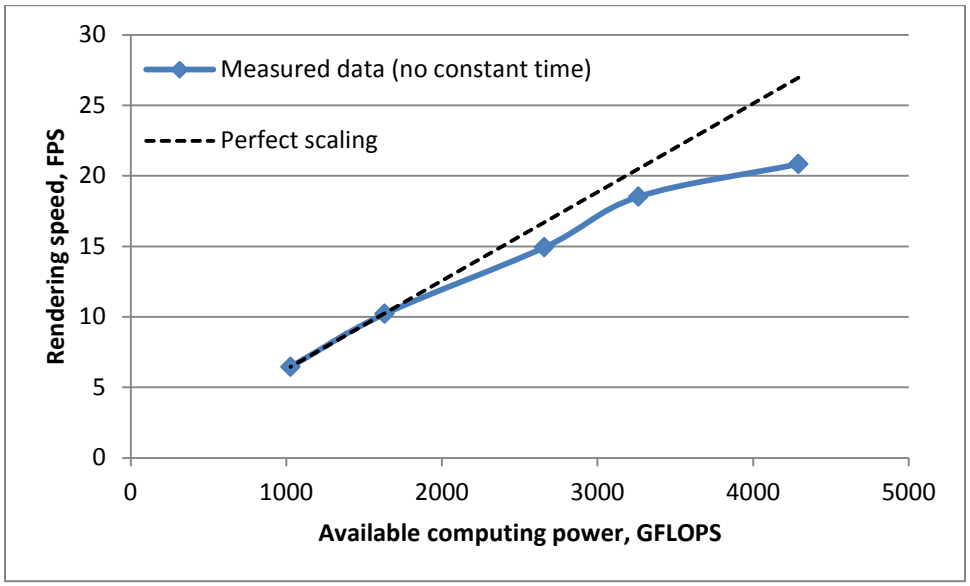

Figure V-36: Rendering speed vs. GFLOPS (w/o constant time)

Figure V-36 demonstrates how it would look if there is no constant non-parallelized time. Now it easy to see that increasing number of cores and frequency increases rendering performance linearly. This means that rendering algorithm is also limited by pure computational performance which is actually a good thing because it can be relatively easily improved with GPU processors and multiple GPUs. Although, as shown on Figure V-37 the efficiency of multi-GPU rendering configurations is lower than multi-GPU editing because results have to be combined, 75% of theoretically possible limit on 3 devices is still a very good result, especially for a non-optimized code that already provides real-time rendering.

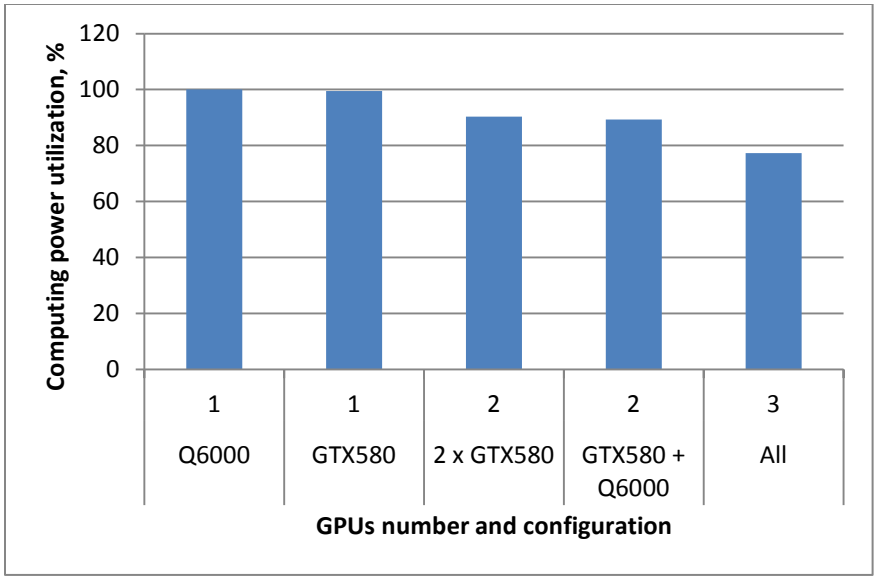

Figure V-37: Available computing power utilization

Discussion

This chapter has described the developed highly parallel geometry representation, appropriate data structure and parallel geometry processing and rendering algorithms. As proof of concept, the 5-axis milling simulator based on the described geometry represented was developed and tested by performing accuracy, performance and rendering benchmarks of the developed 5-axis milling simulator.

As was discussed earlier, in opposition to traditional analytical geometry representation, the new designed geometry representation is based on discretized geometry representation approach that allows solving some of the important issues of traditional geometry models. The most important benefit is ability to design highly parallel and scalable geometry processing algorithms because the geometry representation is naturally parallel. Another important benefit that comes from its discrete

nature is the simplicity of algorithms and absence of the requirement to describe all possible special cases and their combinations.

The mentioned ability to design highly parallel and scalable geometry processing algorithms was proved during the performance testing. It was shown that the developed data structure and algorithms may successfully run on highly parallel hardware such as GPU and also proved that the developed system has great scalability and shows almost linear performance improvement by using multiple GPUs.

The accuracy analysis has shown that the developed 5-axis milling simulator can be successfully used for most simulation jobs but extra high precision simulation requires significant accuracy improvement that can be implemented by using dynamic geometry generation.

VI. TOOL PATH PLANNING FOR 5-AXIS MACHINING

Tool path planning for multi-axis milling CNC machines is a complicated problem that requires knowledge of the material removing process, selecting multiple appropriate strategies and highly accurate calculations. Today in most cases knowledge and appropriate strategies selection are the responsibilities of a human engineer and calculations are performed by geometry processing engine. CAM software lies in between and allows interaction between human and computer. This approach can solve almost every problem that appears in modern manufacturing, but it requires two important components: a trained engineer and time that is actually quite high even for simple parts. Although these requirements can be easily resolved, especially for high volume production, they become extremely critical when there is a need to make a single or few parts. In the case of low volume production, time of an engineer may cost many times more than actual machining cost. As a result, today the low volume market is occupied by usually additive Rapid Prototyping technologies such as 3D printing which allow manufacturing of a part almost without machine-human interaction. However existing RP technologies cannot provide a set of cost, surface quality and available material properties found in traditional subtractive CNC machining. As a result there is an important need for a change in modern CNC milling manufacturing process that will bring traditional CNC milling in par with 3D printing technologies from time requirements point of view and allow using existing multi-axis milling machines efficiently for low-volume production or RP.

The key for this change is reducing the time required for tool path planning. This time includes two components: the time used by a computer for calculations and the time used by an engineer for selecting the right machining approach. Although these components look completely independent, they are parts of the same performance related problem. Time used by a computer for calculation obviously depends on performance of this computer and on ability to use available performance efficiently which is not so obvious. Time used for selection of right machining strategy depends on experience of an engineer and complexity of algorithms that may help with this decision or even select a right strategy automatically. It is important to notice that a complex automated algorithm may eventually replace an engineer completely, which is the target for fully automated manufacturing, and in this case a tool path planning part will include only computational part. However in order to do it, automated path planning algorithms should be good enough and the problem is that good algorithms almost always require a lot of computations. As a result it is possible to say that in order to solve the tool path planning problem, the computational performance problem has to be solved first and new automated path planning algorithm should be developed.

A solution for the computational problem, as was mentioned before, requires having enough computational performance and an ability to use available resources efficiently. At the time when further increasing of processors clock frequency is almost impossible, both requirements are pretty much identical and mean support for parallel processing and ability to use multiple cores, devices and even computers simultaneously. Although parallel processing itself is not a complicated idea, the parallelization of

existing geometry processing algorithms and data structures is not a trivial process. In order to simplify this process, there was proposed earlier in this work the fundamentally parallel geometry representation. The idea behind it is to move parallelization complexity from an algorithms design level to a data structure design level. As a result, every algorithm that uses the described geometry representation can be easily parallelized.

This chapter provides a methodology for designing parallel algorithms by reformulating path planning problems in a way that they can be described in terms of operations supported by the developed geometry representation. As a proof of concept this chapter will describe a complete and fully automated 5-axis tool trajectory planning system capable of machining almost any possible shape. First there will be presented a highly parallel GPGPU based volume offset calculation approach based on the developed data structure. Then there is be described the developed surface filling algorithm that is used as a foundation for two tool center trajectory planning algorithms. These two fully automated robust 5-axis tool path planning algorithms are used for path planning of roughing and finishing processes with ball end mills. All described algorithms follow the proposed methodology and can run on multi-GPU system. As a final part of the tool path planning system, a tool orientation selection approach based on a developed accessibility map calculation algorithm will be presented. At the end this chapter the results of experimental 5-axis machining will be demonstrated and the implementation of all developed algorithms that run on multi-GPU system will be discussed.

Parallel algorithms design methodology

Before discussing problem reformulation and algorithms design methodologies it is important to know what operations are provided by underlying data structure. The most flexible and powerful basic operation is the belonging test that can be performed for each cell. It uses two user provided expressions that determine if a sphere with a given position is completely inside or completely outside of a target shape. These expressions are calculated independently for each cell and their results are used for updating cell state based on predefined rules as shown by Algorithm VI-1. If a cell fails both tests it is assumed that a cell potentially has a boundary.

```
1  For each cell in parallel:
2  |  Calculate belonging expressions
3  |  |  Update cell state
```

Algorithm VI-1: Belonging test

The flexibility of the belonging test allows it to be used as a main component for designing many useful algorithms such as machining simulation volume offset calculation or contour offset path planning which will be described later. But what is more important is that any derived algorithm is always highly parallel.

```
1  For each cell in parallel:
2  |  For each tool movement:
3  |  |  If cell is completely inside of a tool movement swept volume:
4  |  |  |  Mark cell as empty
5  |  |  If cell is not completely inside or outside of a tool movement swept volume:
6  |  |  |  Mark cell as boundary
```

Algorithm VI-2: Belonging test for machining simulation

For example, the simulation algorithm that uses the belonging test is described by the Algorithm VI-2. It is easy to see that user defined expressions used only in steps 3 and 5 do not affect the loop on step 1. At the same time, this loop always can be parallelized since it process completely independent cells. If higher parallelizability is needed, loop on step 2 can be parallelized as well with additional synchronization required for updating cell state.

Another important base operation is the volume surface intersection calculation. It takes two independent volumes and outputs a set of points that contain volume boundaries in both volumes. Then it uses a post processing algorithm that converts a point cloud into a list of continuous curves. The idea behind the post-processing algorithm is to start with a random boundary point and to use a wave approach iteratively for connecting neighbor points. By calculating a center of each wave for all iterations it is possible to get a continuous curve that describes actual volume intersection curve. The described operations are shown by Algorithm VI-3.

```
1  Find all cells that have boundary states in both volumes
2  While there are non-processed cells:
3  |   Select a random cell
4  |   Initialize new intersection curve
5  |   While there are non-processed neighbors around selected cell:
6  |   |   Mark all neighbors as a current wave cells
7  |   |   Calculate center of the current wave
8  |   |   Append a wave center to a current intersection curve
```

Algorithm VI-3: Volume surface intersection

It is important to notice that only step 1 of the described algorithm can be easily parallelized but other steps are iterative and cannot be performed in parallel easily. However, this should not be a problem since they always process a reasonably small subset of all cells that represents a curve. There is also possible a situation when volume surface intersection a represented by a surface and not a curve. This special case can be detected by calculating a standard deviation of processing waves and should be processed separately but it is not considered in this work.

Two main operations described above are enough for implementing most path planning algorithms. However there were also developed some special algorithms for solving the tool orientation selection problem. These algorithms will be discussed later in this chapter.

Volume based parallel algorithms design methodology and limitations

As was mentioned before belonging test and volume intersection are main tools for working with the developed geometry representation. But solutions for most tool path planning problems should be reformulated in a way that allows expression of these solutions with available tools. For example a simple iso-planar [3-5] approach that uses intersection between a sequence of parallel planes and a part surface as contact point curves, can be easily implemented in a parallel fashion in two ways. First, intersection between part surface and planes can be represented as intersection between part volume and a sequence of parallelepipeds. Second, the belonging test can be applied where a target shape is actually a sequence of plains. Although both approaches do the same task,

they are quite different and use different tools. But they both have two important benefits. First, there is no need to care about special cases, singular points, discontinuities, etc. Second, both approaches can be implemented in a highly parallel way and run on highly parallel hardware.

The most important concept is to reformulate operations with surfaces by operations with volumes that can be represented by independent operations with volume's cells. This reformulation guaranties that a new algorithm can be easily parallelized. It also makes algorithms simpler since there is no need to handle special cases anymore. Although reformulation of algorithms in volumetric fashion is usually not too complicated, this approach requires caution due to some limitations of the underlying discrete geometry representation.

The first important and probably the most dangerous limitation is related to the volume boundary position. It is important to accept the fact that an actual surface position is never perfectly known. The reason for it is a fact that a surface is represented by cells that have very little information about what happens in them. Precisely each cell stores only 2 bit of information that represent 3 states and only 2 of 3 states are guaranteed. If cell has a completely empty state, it is guaranteed that it does not have any material inside and vice versa for a completely full cell. But if a cell does not hold any of these states, there is no guarantee that it actually contains a surface. In most cases and for most applications it is safe to assume that such cell actually contains a surface. However even if cell does contain a volume surface there is no way to know where a surface lies inside of a cell. In most cases, especially for roughing planning application when removing few

tens of microns of material more or less does not really matter, the precision provided by a cells size itself (since surface positioning error is limited by cell dimensions) is enough for valid tool path planning process. But for finishing and especially high precision finishing path planning additional tool path corrections may be needed.

The second limitation is related to the derivatives calculation. It is important to eliminate using derivatives or assume that their accuracy is not perfect. Since the underlying geometry representation has a discrete nature, derivatives calculation cannot produce perfectly accurate results in many cases. However approximate derivatives values can be calculated and used if they are needed. For example, surface normals used in the rendering process for lightning calculations are actually estimated from a discrete geometry representation in runtime and still provide good enough precision for rendering accurate images.

Offset volume calculation

Despite the described limitations, many complex geometrical problems can be easily solved by following the described approach. One of these tasks is the offset surface finding problem. The offset surface is defined as a surface at equal distance from an original surface (Figure VI-1). It is often used in tool path planning process as a surface where a tool center may move freely without producing overcuts. By replacing tool contact point trajectory planning with tool center trajectory planning it is possible to eliminate a complicated gouge prevention process and make tool path planning algorithms simpler.

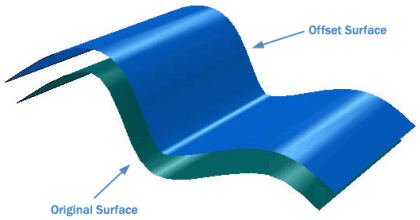

Figure VI-1: Offset surface [65]

Although the offset surface makes path planning algorithms simpler, finding an offset surface is not a trivial problem for analytical geometry representations. Most common problems of this process are special cases such as holes and self-intersections [66] as shown Figure VI-2. The developed offset surface finding approach eliminates the self-intersection problem completely and allows using models with holes that are smaller than offset distance. It is important to notice that the developed approach uses triangular meshes as an input geometry representation but similar algorithms can be implemented for other data structures. The reason for selecting the triangular mesh format is the weak support of this format in modern CAM software and its popularity in RP industry.

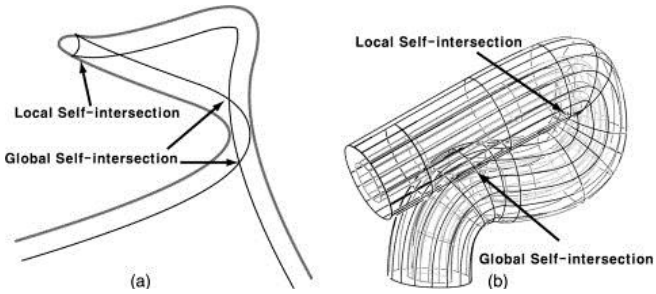

Figure VI-2: Offset surface self-intersections [66]

The main idea behind the developed surface offset algorithm is working with volumes and not with surfaces, so it is more correctly to describe it as the “offset

volume" algorithm. Here the offset volume represents a volume that contains all points that are closer than an offset distance to initial surface. At the same time, it is easy to see that a boundary surface of the offset volume contains a target offset surface and an offset surface calculation can be replaced by offset volume calculation. In 2D case an offset curve calculation can be replaced by offset area calculation as shown on Figure VI-3.

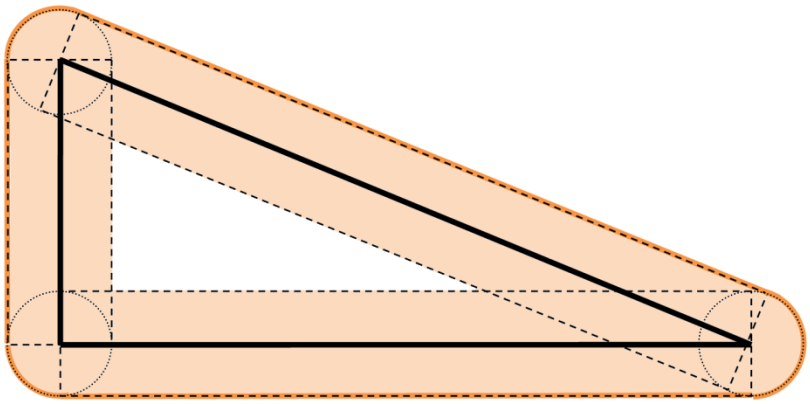

Figure VI-3: 2D offset surface decomposition

In order to construct an offset volume efficiently, it can be represented as a composition of primitives associated original surface elements. For 2d case (Figure VI-3) every point is associated with a circle and every line is associated with a rectangle. For 3d model and triangular geometry representation there is a similar association list:

- Vertex – Sphere
- Edge – Cylinder
- Face – Prism

As a result a triangular mesh may be converted in a list of volumetric primitives that can be composed together and represent an offset volume. Then every cell of geometry model can be tested against this list of volumetric primitives and marked as a

part of an offset volume if it passes belonging test with one of these primitives. The offset volume calculation algorithm that combines all these steps is shown by Algorithm VI-4.

```
1   For all vertexes in input model in parallel:
2   |   Add appropriate sphere to primitives list
3   For all edges in input model in parallel:
4   |   Add appropriate cylinder to primitives list
5   For all faces in input model in parallel:
6   |   Add appropriate prism to primitives list
7   For all cells in geometry model in parallel:
8   |   For all primitives in list:
9   |   |   If cell belongs to primitive:
10  |   |   |   Mark cell as an offset volume cell
```

Algorithm VI-4: Volume offset calculation

Loops 1, 3, 5 of the described algorithms are completely independent and can be easily parallelized. Loop 7 is actually a part of the belonging test described before and can be easily parallelized as well since all cells are always completely independent in the developed geometry model. Even loop 8 can be parallelized with an additional synchronization required for the cell updating process. It is obvious that the selected approach can be parallelized in many ways but the implemented version is parallelized only in step 7. Everything else is done sequentially, and there are few reasons for this. First, with a high enough number of cells (which happens almost always for high resolution models), there is no real need for higher level of parallelization. Second, steps 1-6 do not take too much time in any case. And finally, serial processing of primitives for each cell allows stopping when a cell changes state first time and it saves a significant amount of calculations.

For testing the developed offset volume algorithm implementation there were selected 4 test models (their properties are shown in Table VI-1) and performed offset volume calculations for multiple offset distance values and geometry model resolution equal to 2048x2048x2048. All tests were performed with 3 GPUs: 2x GTX580 and Quadro6000.

Model name	Vertices number	Edges number	Faces number
Turbine	10897	32691	21794
Teapot	28922	86280	57360
Candle holder	18998	57008	38000
Head	115147	345429	230286

Table VI-1: Test models properties for offset volume calculation

The Table VI-2 demonstrates performance results measured during testing process.

Model	Offset value	Time (s)
Turbine	1	43.441
	3	43.26
	5	40.383
	7	39.835
	10	40.387
Teapot	1	99.542
	4	102.253
	7	105.862
Candle holder	1	72.669
	4	72.319
	7	69.803
Head	1	0
	4	386.024
	7	393.356

Table VI-2: Offset volume calculation performance results

It is noticeable that the offset value itself almost does not affect calculation time. At the same time the offset volume calculation time almost linearly depends on

complexity of a geometry model. The Figure VI-4 demonstrates the offset volume calculation performance in faces/second for all tried models and it is easy to see that calculation speed is almost constant for all of them.

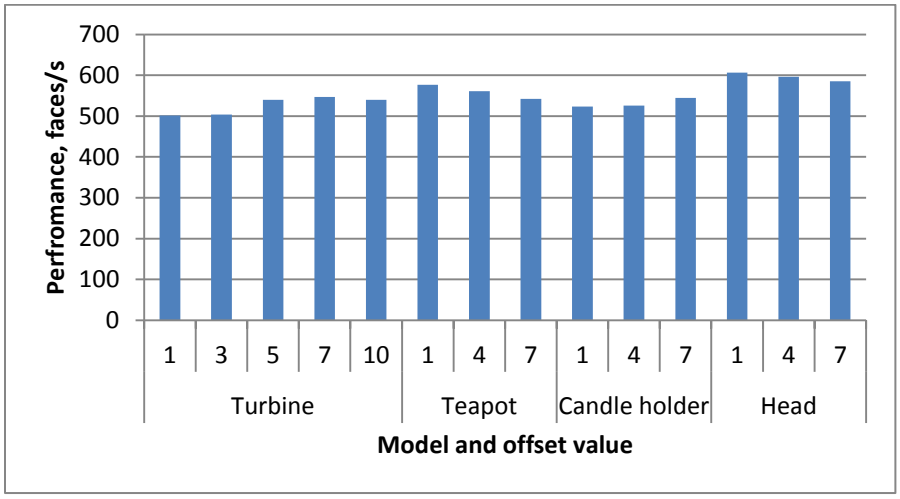

Figure VI-4: Offset volume generation performance

Pictures below demonstrate offset volume testing results for all test models.

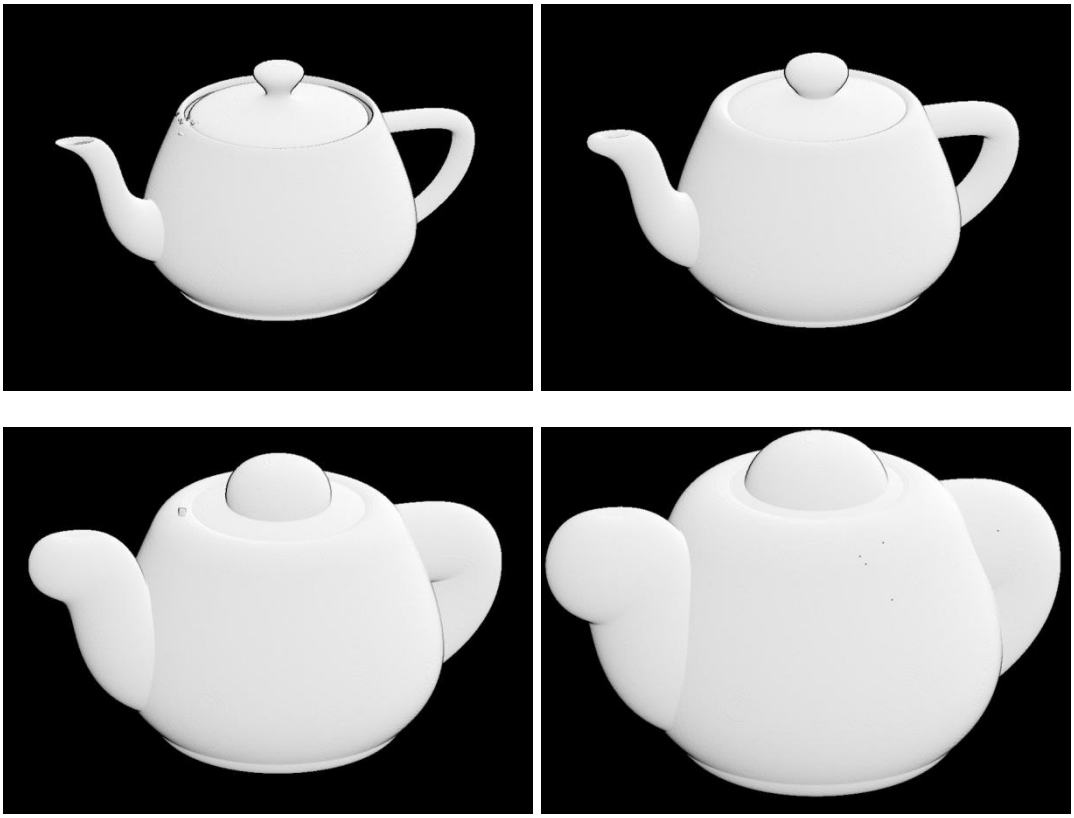

Figure VI-5: “Teapot” volume offset

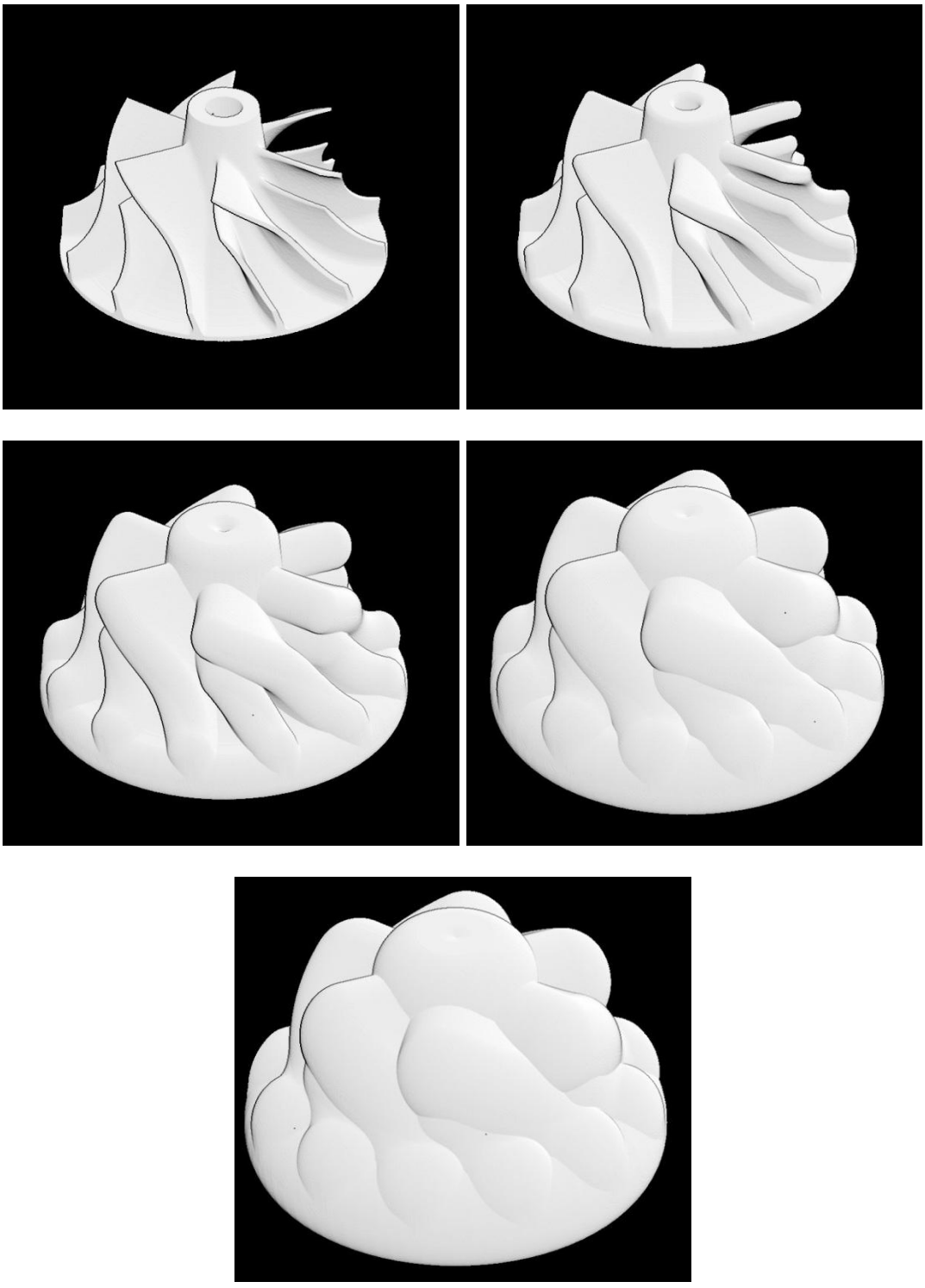

Figure VI-6: “Turbine” volume offset

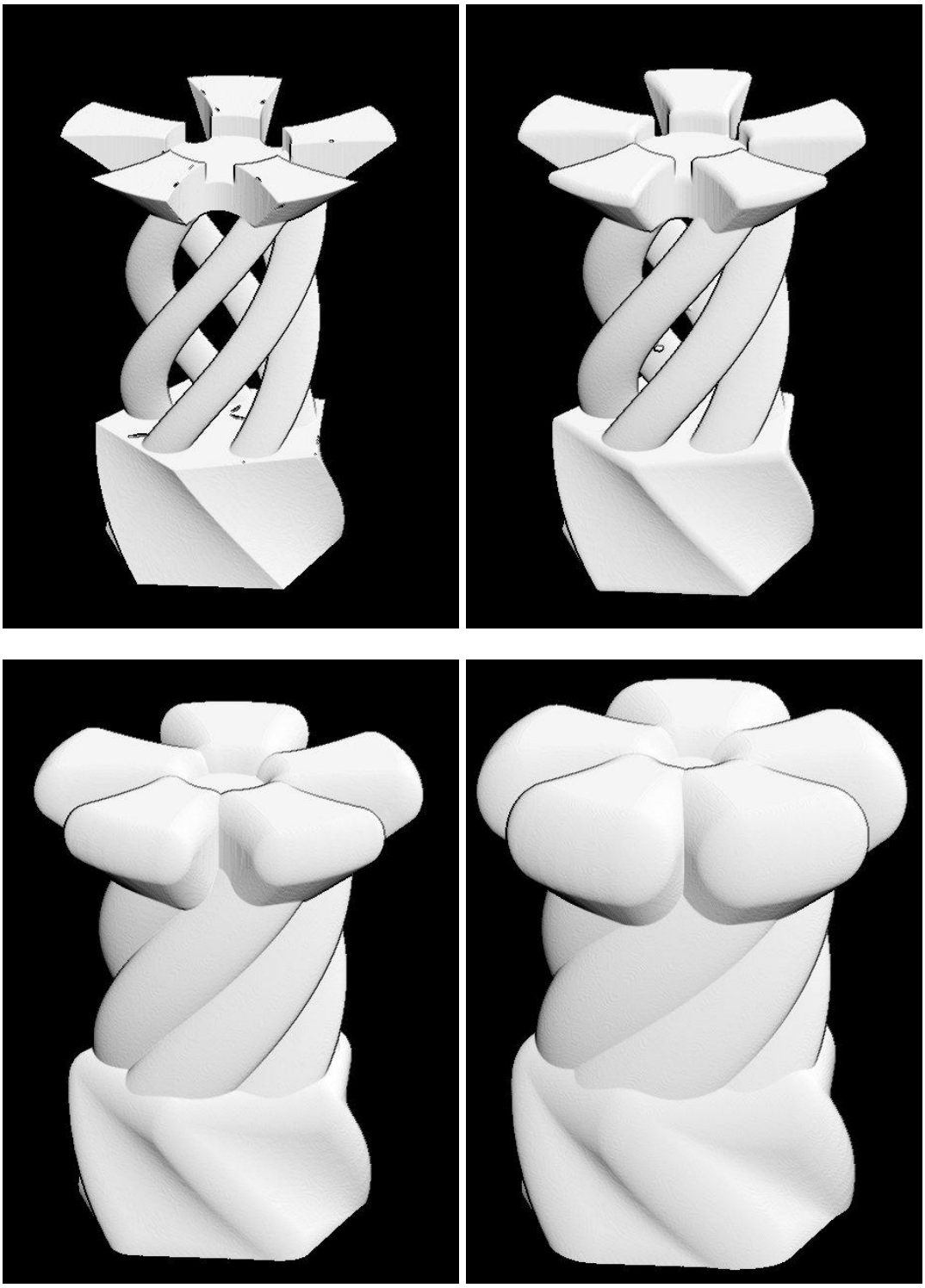

Figure VI-7: “Candle holder” offset volume

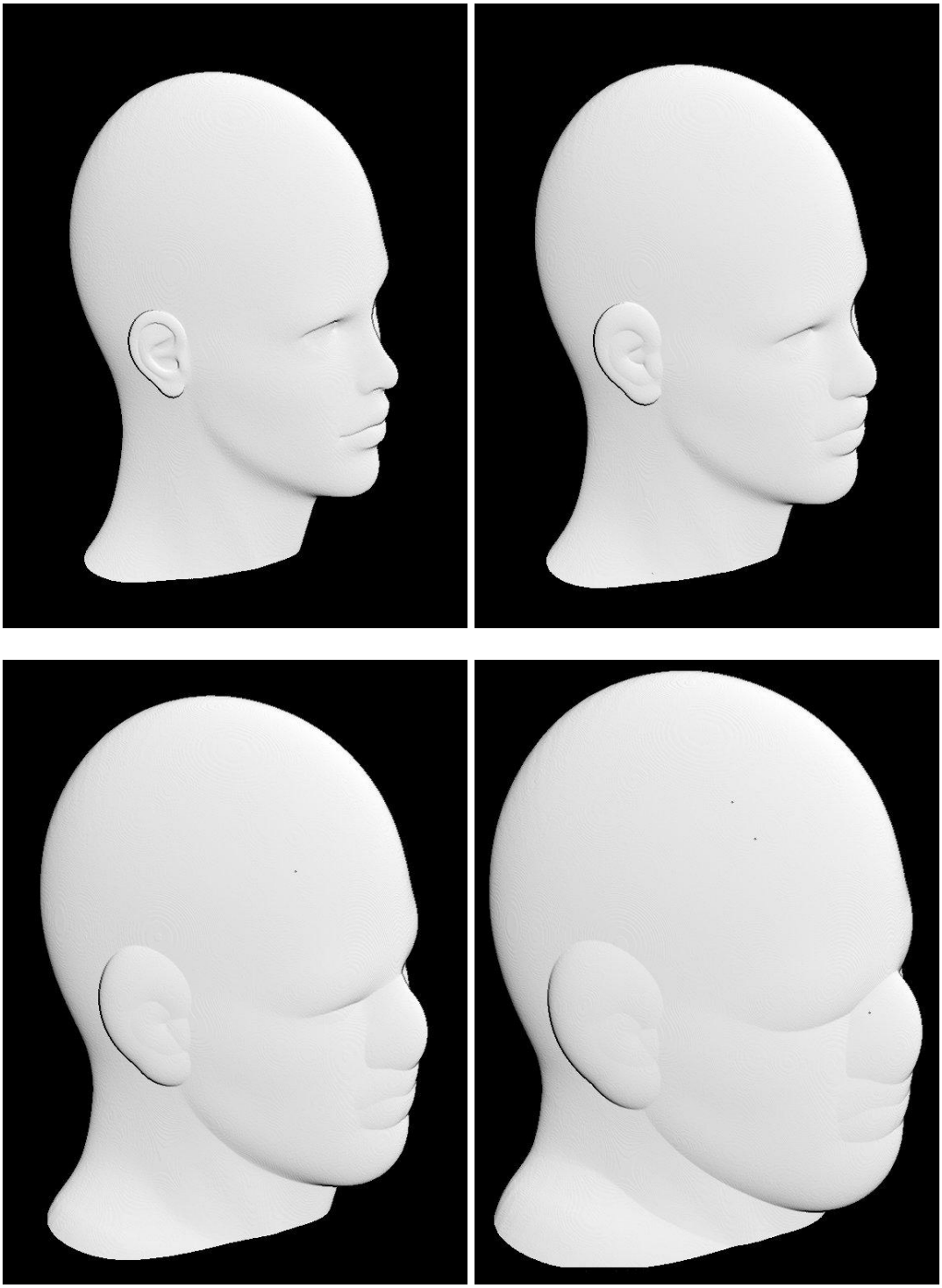

Figure VI-8: “Head” offset volume.

Surface filling algorithm based on 3D contour offset approach

The example of the offset volume calculation algorithm has shown that it is possible to use the described earlier methodology and geometry representation for solving computational geometry problems. This part will talk about problems that are more closely related to tool path planning process itself.

First of all it is important to notice that modern CAM systems support a large variety of tool path planning strategies (such as iso-parallel, spiral, contour offset, etc.) that produce efficient tool paths for a variety of different situations. And although there are so many possible options for tool path planning, these solutions are usually quite specialized and do not work well as a true general purpose solution for any possible situation. This limitation requires the presence of an engineer that select a sequence of appropriate strategies with appropriate parameters and it has to be eliminated in order to create a fully automated path planning system. One of possible ways for resolving this problem is creating a system that can make decisions like an engineer and select the best sequence automatically. However such a system should be quite smart and it should support all known strategies in order to replace a human. It is obvious that the development of such system will require a significant amount of time and it will be quite useless before it is finished since there is no sense to use a program that can generate only a portion of a tool path. The solution for this problem is development of a robust tool path planning strategy that can take any possible geometry and produce a tool path for machining it. It is obviously not possible to make this strategy optimal and efficient for all cases but its goal is different. With such a strategy, development of a fully automated

tool path planning system will be much easier and useful because even if the developed system cannot generate a complete tool path, it can always use the generalized robust strategy for making a part. The robust strategy in this case becomes the foundation for a fully automated tool path planning system. Such strategy was designed by following the described methodology and implemented in this work. Before discussing the details, it is important to notice that the developed version is designed especially for ball-end mills but it can be improved for supporting other cutter types.

The idea behind the developed robust path planning strategy is generalizing the 2D contour offset strategy often used in modern CAM software to 3 dimensions. Although 2D and 3D versions are conceptually similar (in fact a 2D version is a special case of a 3D algorithm), there are some important differences related to where and how they generate a tool path. Traditional contour offset approach calculates a tool path on a plane which is orthogonal to a tool direction. It iteratively offsets a contour and uses offset curves as tool path components. Usually a sequence of parallel planes is used for removing most of volume during a roughing process. The 3D version does perform very similar steps but does not require using a planar surface (although it can use a plane and in this case it becomes a 2D contour offset approach). It uses any possible user selected surface called “Target surface”. The problem here is an additional dimension. As a result, offsetting a contour creates a tube like shape that cannot be used for path planning (Figure VI-9b). As a solution for this problem, an additional step is required – calculation of the intersection between a tube and a target surface (Figure VI-9c). By calculating the intersection, it generates a curve that lies on a constant distance from an original contour

and can be used for further path planning. The important property of the contour offset approach is preserved – the distance between path components is constant in most cases and always bounded. This property allows controlling a scallop height of the machined surface by controlling distance between path components.

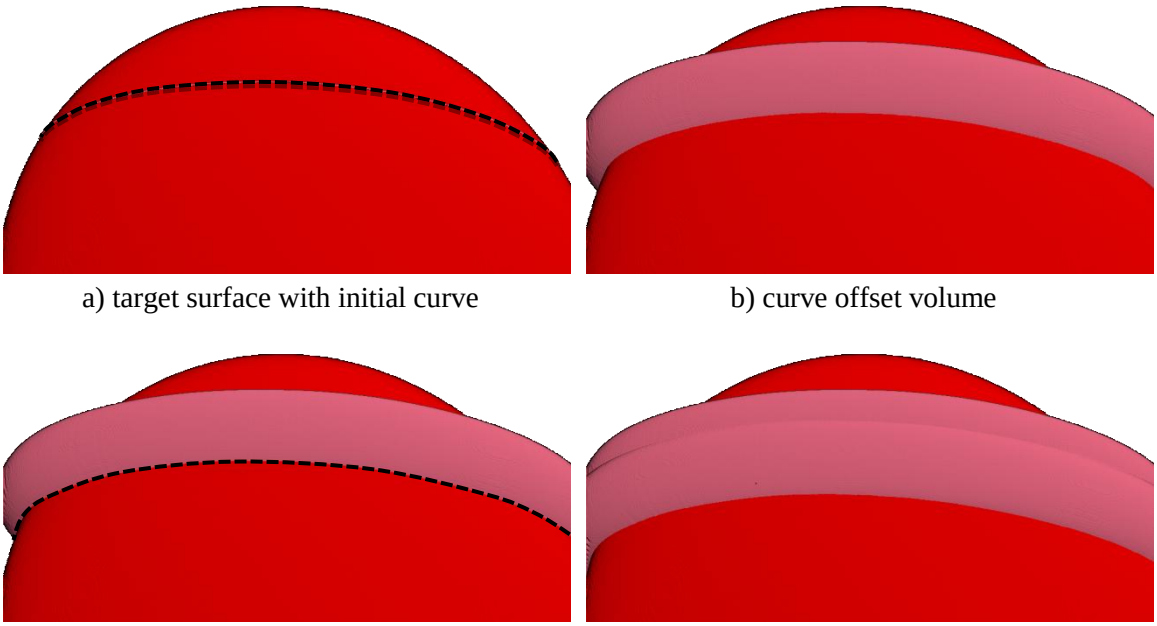

a) target surface with initial curve b) curve offset volume

c) intersection curve d) offset volume of an intersection curve

Figure VI-9: Curve offsetting

Iterative performing of the contour offset algorithm until an entire surface (or a surface part) is covered (Figure VI-10) generates a sequence of curves that completely fill a target surface and that are further than the offset distance to each other. The developed implementation determines that an entire surface is processed if it is not possible to calculate intersection between curve offset volume and a target volume. It is also important to notice that curve offset volume combines all offset volumes calculated

during previous iteration, so if a part of a target surface is already processed it will not be processed again.

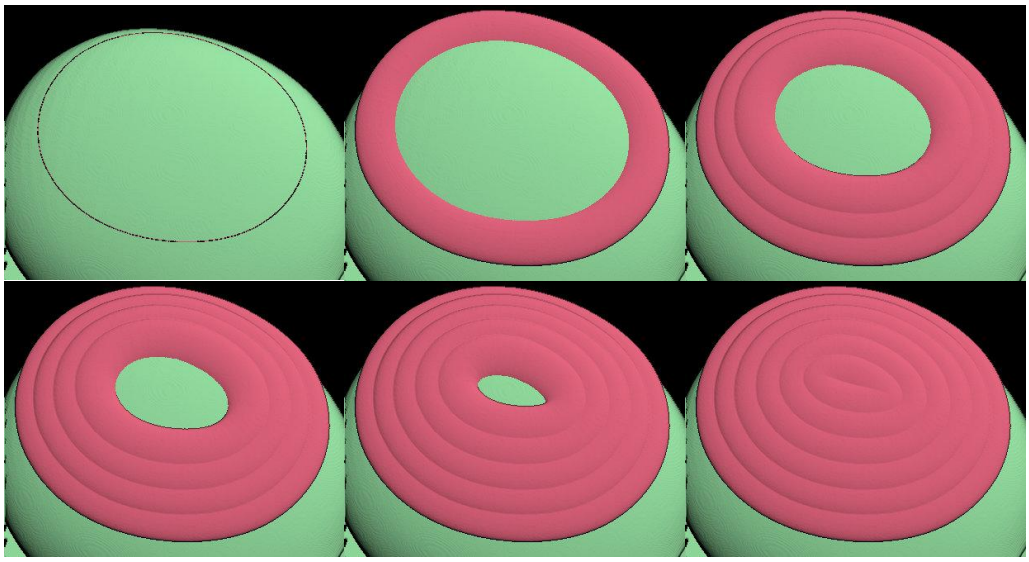

Figure VI-10: Iterative surface area filling

Before describing the complete surface filling algorithms it is important to talk about the third component used in this process – restriction volume. Boundary conditions and also any required restrictions are represented as a restriction volume that contains areas where tool movements are not desired or dangerous. For example, during roughing path planning for ball end tool, restriction volume includes a part offset volume with an offset value equal to a tool radius. By not allowing path planning in areas that are too close to a part surface, it predicts overcuts because a tool center will never come closer than a tool radius and a tool surface will never intersect a part surface as a result. A restriction volume also limits filling algorithm in a way that only a desired part of a surface is processed even if an entire surface is not processed yet. This is useful for protecting fixtures from accidental machining. For example, Figure VI-11 demonstrates

the restriction volume for the “Head” model that contains two parts: offset volume of the model with offset distance equal the tool radius and a box volume in the bottom for protecting fixtures.

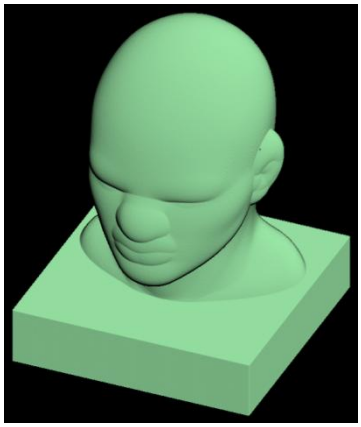

Figure VI-11: Restriction volume for the “Head” model

The entire surface filling process is described by Algorithm VI-5.

```
1  Current curve = Initial curve
2  Do:
3  |   Offset current curve
4  |   Calculate Intersection curve between Target surface and Offset volume
5  |   If intersection curve exists:
6  |   |   Save intersection curve as a tool path component
7  |   |   Current curve = Intersection curve
8  Until: Intersection curve does not exist
```

Algorithm VI-5: Surface filling

The most important property of the developed surface filling algorithm is parallelizability. Since it is based on volume offset (curve offset algorithm, which is actually used, is a special case of volume offset algorithm described earlier) and volume

intersection algorithms which are both parallel, the entire surface filling algorithm becomes naturally parallel and all algorithms that use it are also naturally parallel.

Robust tool trajectory generation for 5-axis machines

The described 3D contour offset algorithm is used both for the roughing and the finishing tool path planning by using different target surfaces. In case of finishing a model offset volume surface is used as s target surface. An offset value in this case is equal a tool radius. And a contour offset value controls path step and it is selected based on a desired scallop height. As it was mentioned before, limiting tool center movements to an offset surface prevents overcuts by a ball part of a tool. For the finishing path generation, an initial curve can be selected in many ways but the current implementation uses an intersection between a horizontal plane and a top of an offset model.

The Figure VI-12 demonstrates an example of the surface filling process used for a finishing tool path generation and Algorithm VI-6 demonstrates required algorithm steps. Intersection curves calculated during this process are used as tool center trajectory curves in a finishing tool path.

1	Calculate intersection curve between part offset volume and horizontal plane
2	Apply the Surface filling algorithm starting with the intersection curve (Algorithm VI-5)
3	Generate a finishing tool path by combining all generated curves

Algorithm VI-6: Finishing tool path generation

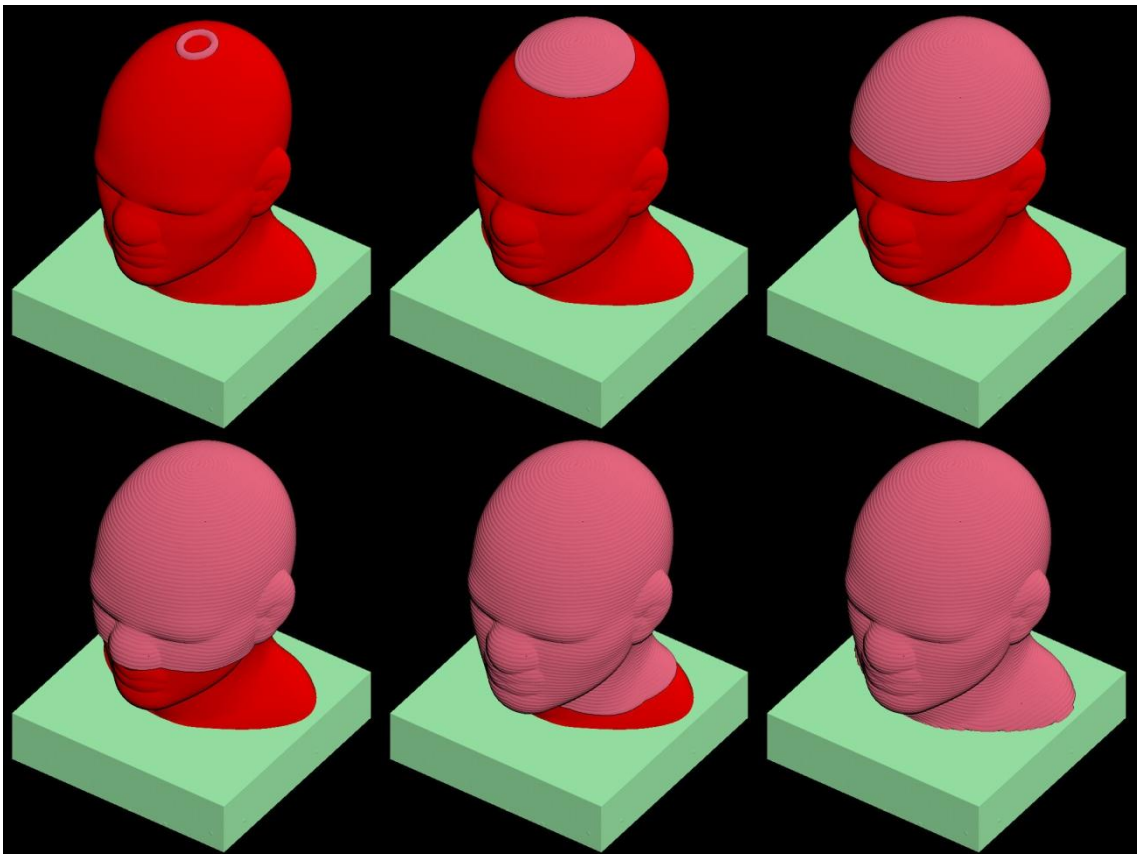

Figure VI-12: Surface filling for finishing tool path generation

The roughing tool path generation process is a bit more complicated than the finishing process because it has to process a volume, not a surface. There are three main differences. First, it uses iterative approach and generates a tool path that removes material layer by layer until it reaches a part surface. Second, a target surface for roughing process is a workpiece material surface itself. Similarly to the finishing process, it uses surface filling algorithm for generating a set of curves on a material surface that are used as tool center trajectory curves. And finally, roughing algorithm selects initial curves differently. The current implementation uses the intersection between a workpiece and a model offset volume for selecting an initial curve. After the intersection is

calculated, the longest intersection curve is selected (Figure VI-13) and the surface filling algorithm is used. This process repeats until all intersection curves are processed and it is not possible to find a curve that lies outside of a safety zone. All roughing path planning steps are demonstrated by Algorithm VI-7.

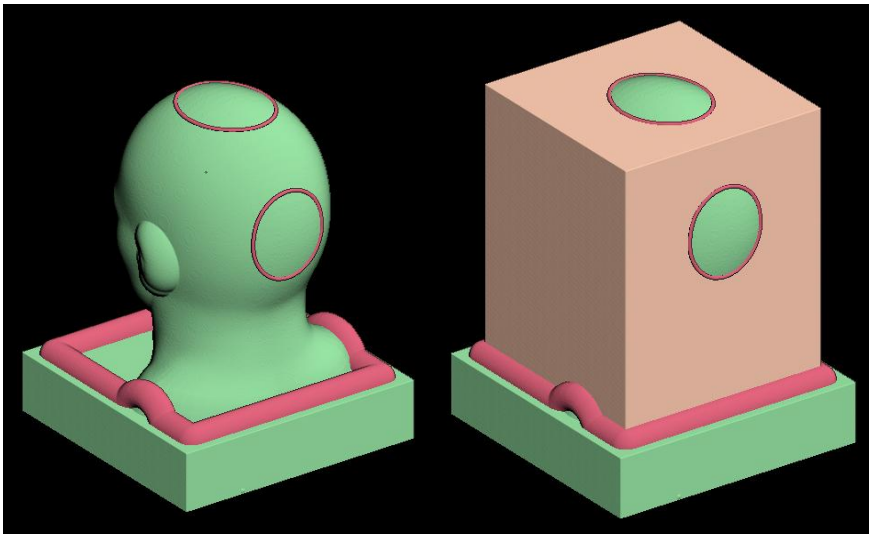

Figure VI-13: Initial curve selection for roughing process

```
1  Calculate part and fixtures offset volume (Algorithm VI-4)
2  Do:
3  |  Calculate intersection curves between workpiece and part offset volumes
4  |  While non-processed intersection available:
5  |  |  Select the longest intersection curve
6  |  |  Apply the Surface filling algorithm starting with the selected curve
7  |  |  Generate a roughing tool path for a layer by combining all generated curves
8  Until intersection curves exist
9  Generate a roughing tool path by combining all layers
```

Algorithm VI-7: Roughing path planning

The Figure VI-14 demonstrates workpiece geometry after removing each layer of material during a roughing process with a tool path generated by the described roughing algorithm. It is also easy to see exact tool trajectory on the first few layers.

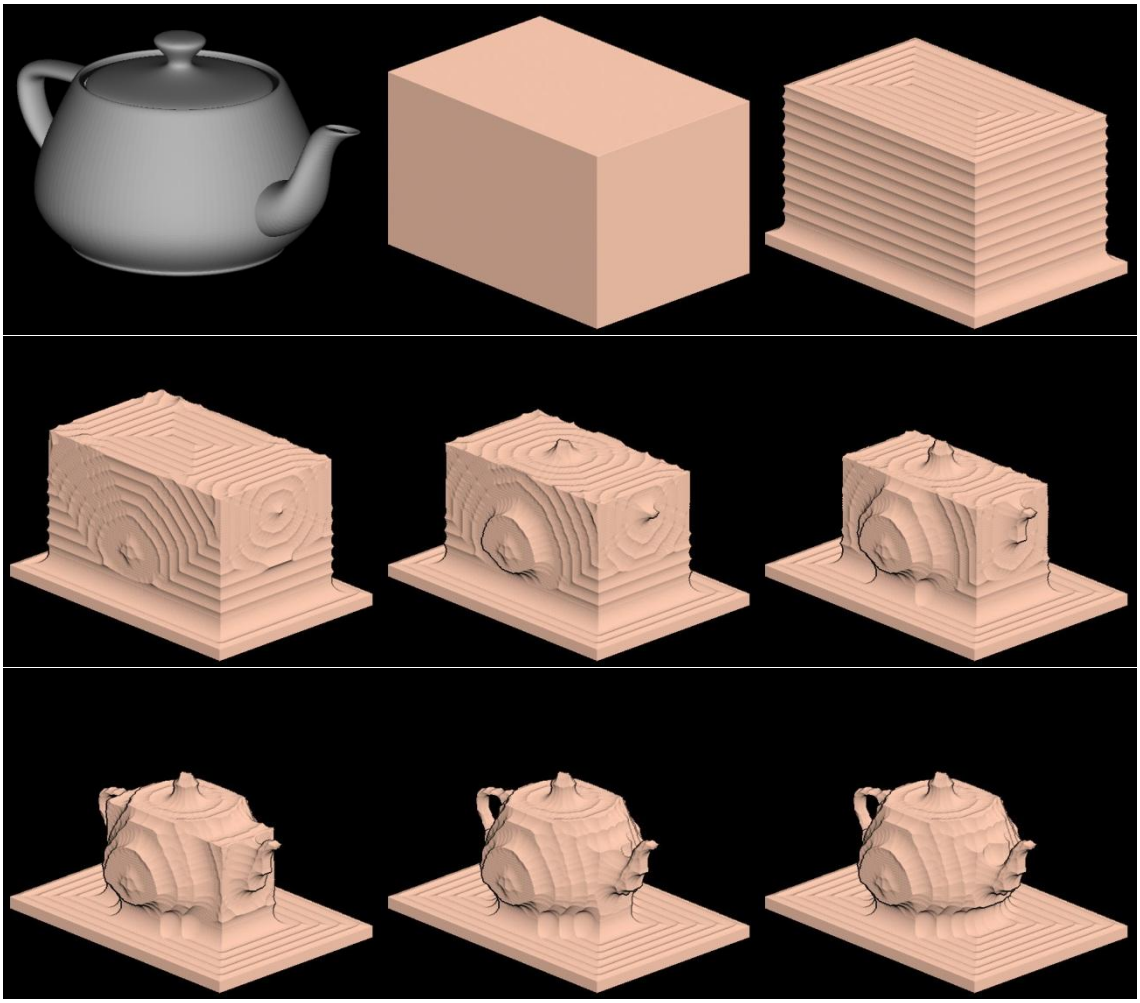

Figure VI-14: Layer by layer material removing during a roughing process.

The described finishing and roughing tool path planning approaches have some important properties that should be mentioned. First of all, these algorithms follow the developed methodology and mainly perform volume offset, volumes intersection and

surface filling operations. Since all these operations are naturally parallel, all developed tool path planning algorithms hold this property. The second important property is robustness. In context of this work, robustness means an ability to generate a valid tool path for any given geometry. It is easy to see that both algorithms just perform a set of steps without knowledge about geometry itself so they are geometry agnostic and can be applied to any possible part. It is also easy to see that both algorithms stop to work only when they process an entire surface or volume since it is part of existing conditions.

These properties make the described algorithms great candidates for a foundation of a completely automated tool path planning platform because even if an optimal algorithm for geometry is not known, these algorithms can always generate a tool path. However it is important to remember that in most cases they do not provide an optimal result, and that they should be used as a last resort.

Orientation selection

The previous part described algorithms that are capable of generating a tool center trajectory that results in machining of a desired geometry. But a tool center trajectory is only a part of a tool path for 5-axis machines since there is a need for a valid tool orientation at each point. This work makes an important assumption: tool orientation can be calculated independently after calculation of a tool trajectory. Although this assumption does not always work and probably does not allow generating an optimal tool path for all possible scenarios, it works in most cases and significantly simplifies a tool path planning process by decomposing it into two independent process of trajectory and

orientation planning. It is also important to notice that in spite of the assumption made, the implemented tool path planning system generates orientation for each layer of a roughing path planning process and as result orientation planning on each layer actually does affect trajectory planning on a next layer. For example if some volume cannot be removed on a layer because it is not possible to select a collision free orientation for a tool path, it may become possible on future layers because there are less constraints due to removed volume.

Before discussing a tool orientation selection process, it is important to mention that it heavily depends on a concept of accessibility map that represents all collision- and gouge-free orientations for a given tool center position (cutter contact point can be used as well with minor changes but it is not discussed in this work). An accessibility map is stored as a bitmap where each pixel represents two rotary axis coordinates and has a value of 0 if this is a valid orientation or value 1 if this orientation results into collision as shown on Figure VI-15. A description of a highly parallel efficient algorithm for accessibility map calculation will be provided later in this work. Although this algorithm does not include a prediction of machine components collisions, there is an assumption that it is possible to calculate an accessibility map with a high enough resolution in a reasonably short time for any given point.

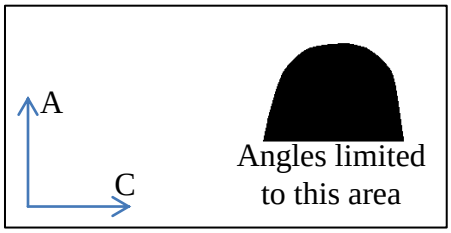

Figure VI-15: Accessibility map example

It is also important to describe the desired orientation properties used in this work. Since there are infinite possible tool orientations, selection of tool orientation can be viewed as an optimization process with constraints represented by accessibility maps (machine dynamics constraints are not considered directly in this work) and a selected optimization criteria that represent desired orientation properties. In this work a smooth orientation change is selected as a target tool orientation property. The idea behind this is to be as continuous as possible, and to use as low speed rotary axis movements as possible. This can be described as true 5-axis machining which usually happens during machining complex true 5-axis parts. There was an assumption that solving a tool orientation problem for this scenario will allow solving orientation problems for simpler 3+2 axis cases by adding more constraints.

The developed orientation selection system uses an assumption that orientation selection happens after tool trajectory planning and 3 of 5 axis values are already known for each tool path point, so there is a need to find only 2 more axis values. An orientation of each tool trajectory point can be described as a 2D point in orientation space and orientation for all tool path points can be described as a set of 2D points. Considering the fact that orientation change physically means a continuous rotary axis movement, tool orientation change during following a tool trajectory should be continuous and can be described as moving a point on a 2D curve. Movement of a 2D point brings a 3rd dimension that can represent either a time or a distance from the beginning of tool center trajectory. There is obviously no difference from a mathematical point of view between point movement on 2D curve and a curve in 3D space but the last one is better from a

constraints visualization point of view. Since every tool center point has a different accessibility map, an orientation selection process can be viewing as construction of a 3d curve that goes through a stack of accessibility maps (Figure VI-16).

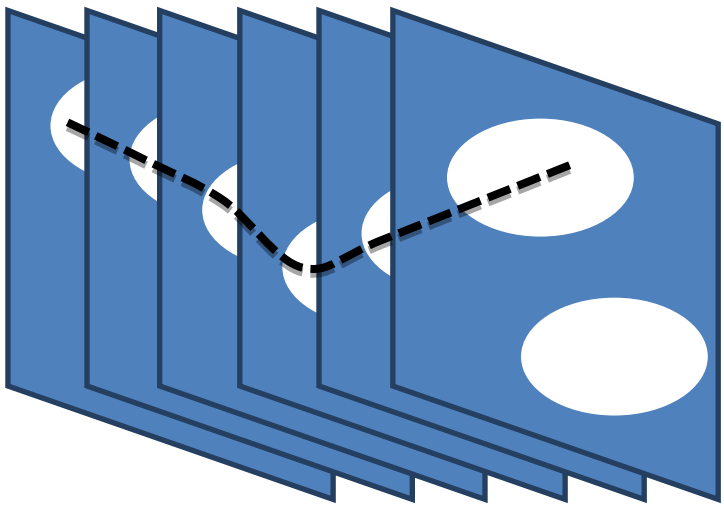

Figure VI-16: 3D curve going through a stack of bitmaps

The implemented version of the orientation selection algorithm actually works by constructing a curve through a stack of accessibility map. It uses a two stage process: first, it selects an optimal accessibility space topology; second, it generates an initial curve, by selecting points that lie as far as possible from borders, and iteratively optimize a curve shape for making it smooth.

The first step is needed for reducing the number of tool retractions due to impossibility of continuous orientation change (these retractions will be called “jumps”). Jumps happen when a tool center position can be accessible only from orientations that cannot accessed by continuous rotary axis movement from a position that was selected

for a previous tool center position. In this case a tool is retracted, orientation is changed and a tool center is moved to the next tool center position.

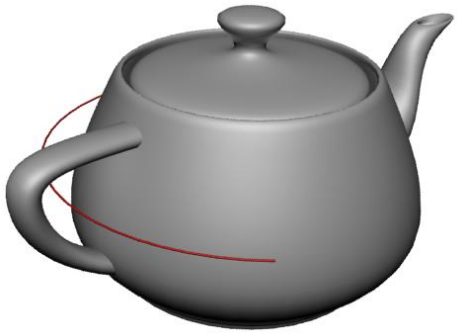

Figure VI-17: Example of a tool trajectory that requires a tool retraction

For example, as shown on Figure VI-17, if a tool center follows the showed trajectory, earlier or later it will not be able to continue without a jump. It is important to notice that the last point where tool can go without a jump depends on a tool movement direction as shown on Figure VI-18.

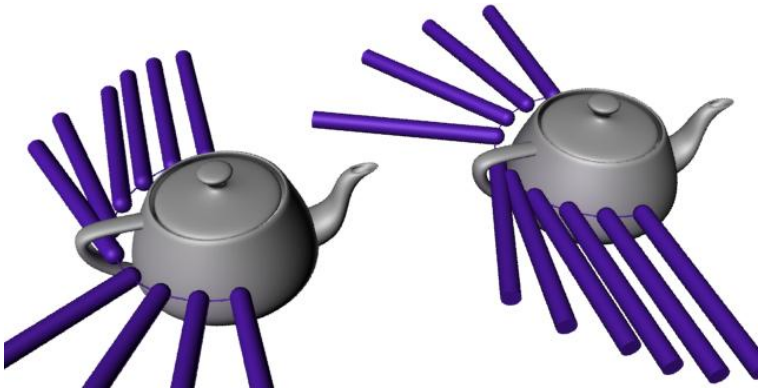

Figure VI-18: Dependency of a jump point on tool movement direction

The shown example is a simple case when only one jump is done and required. But, even with this example, it is already possible to notice that this situation is a

limitation of the earlier assumption about the independency of a tool trajectory planning process and orientation selection. It is easy to see that an entire surface of the demonstrated teapot can be processed without any jumps if a different tool trajectory is selected. However in many situations jumps are not avoidable at all. In these cases a tool path planning algorithm can try to minimize a number of jumps because tool retractions increase total machining time and also may decrease a tool life by increasing a number of tool load changes. For example, in situation shown on Figure VI-19 there are 2 possible ways for selection a tool orientation if a tool follows a straight line trajectory as shown on Figure VI-20.

Figure VI-19: A scenario with a complicated tool space topology

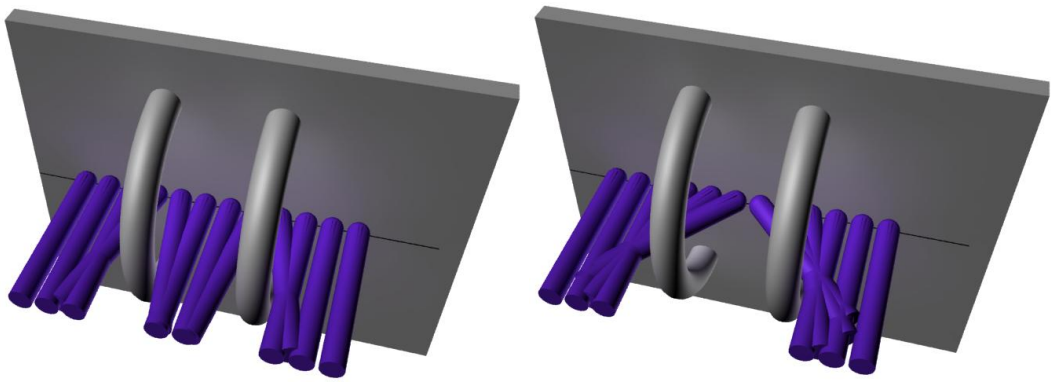

Figure VI-20: Two possible ways of orientation selection

It is easy to see that the left way requires two jumps and the right one requires only one jump and it probably should be selected. In order to understand how the right way can be selected it is important to look on an accessibility space that shows all valid tool orientations. For a 5-axis machine with 2 rotary axises, an accessibility space has 3 dimensions (2 axis + time). But in order to simplify explanation and visualization an assumption is made that there is only 1 rotary axis (around and axis that lies in a wall plane perpendicular to a tool path line on Figure VI-20) and an accessibility space has 2 dimensions (accessibility map accordingly has only 1 dimension in this case). In this case an accessibility space for the described situation looks similar to Figure VI-21 where a center line represents a tool orientation along a wall normal and grey area represents valid orientations.

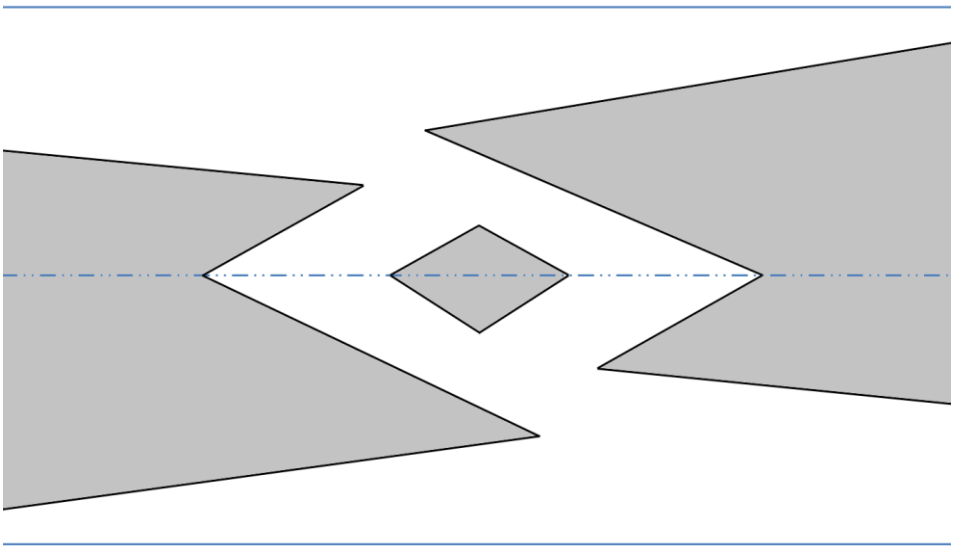

Figure VI-21: Accessibility space

The Figure VI-22 provides an explanation of a construction process for the accessibility map shown on Figure VI-21. The top part of it demonstrates a top view on a

target part. The accessibility space is located in the bottom and divided into 5 zones accordingly to a possible combination of orientations in each zone. Approximations of accessible zones are marked by blue rectangles. Finally, considering the fact that a tool moves continuously, black lines represent corrected accessibility area borders.

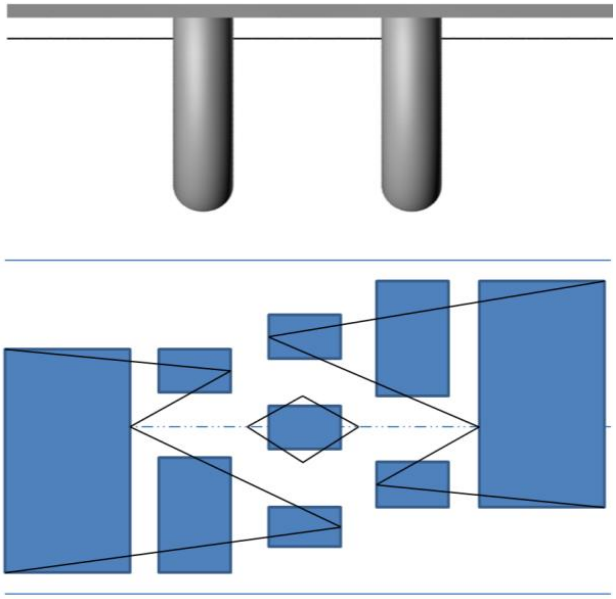

Figure VI-22: Explanation of an accessibility map construction process

Before the explanation of the optimization process, it is impossible to explain how a jump looks in accessibility map space. Considering that a jump always happens for exactly the same tool center orientation, it means that it always happens in a vertical slice of the accessibility space. As a result it can be viewed as a rapid movement from one accessibility zone to another (

Figure VI-23). Where an accessibility zone is a part of the accessibility space for a given tool center position that includes all points that can be accessible by continuous orientation change. It is important to notice that accessibility zone always has the same number of dimension as an entire accessibility space.

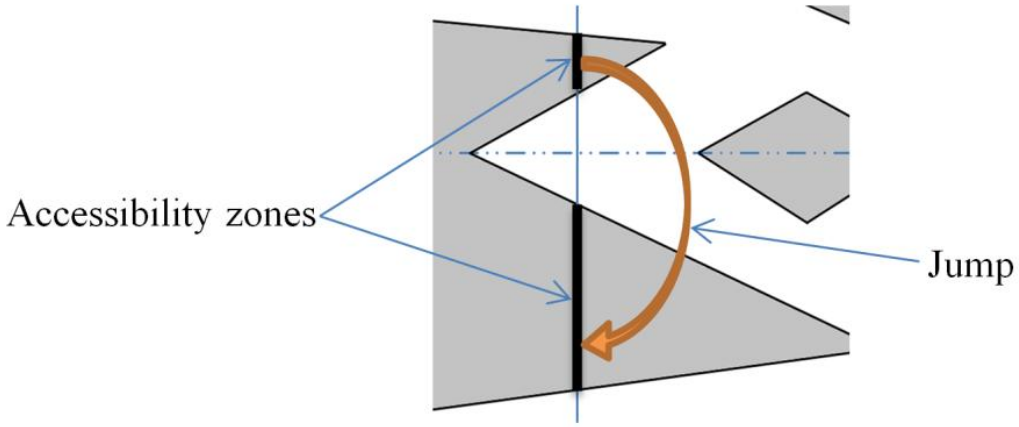

Figure VI-23: “Jump” concept explanation

The developed topology optimization approach is based on the idea of representation of an accessibility space as a graph of connected accessibility zones and searching for a shortest path. It is easy to see that an accessibility space can be discretized by slicing it into a sequence of accessibility map (the developed implementation actually works in an opposite way, it generate a sequence of accessibility map and constructs an accessibility space from them). Each accessibility map will have a set of accessibility

zones that can be connected based on possibility of moving from one zone to another as shown on

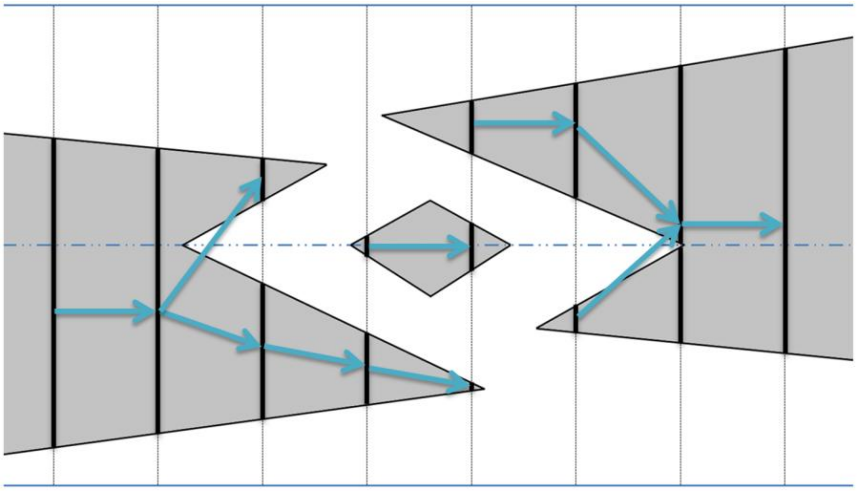

Figure VI-24. Two accessibility zones can be connected only if they intersection is not empty. From a machining point of view it means that a tool can move from one tool center position to another without changing a tool orientation.

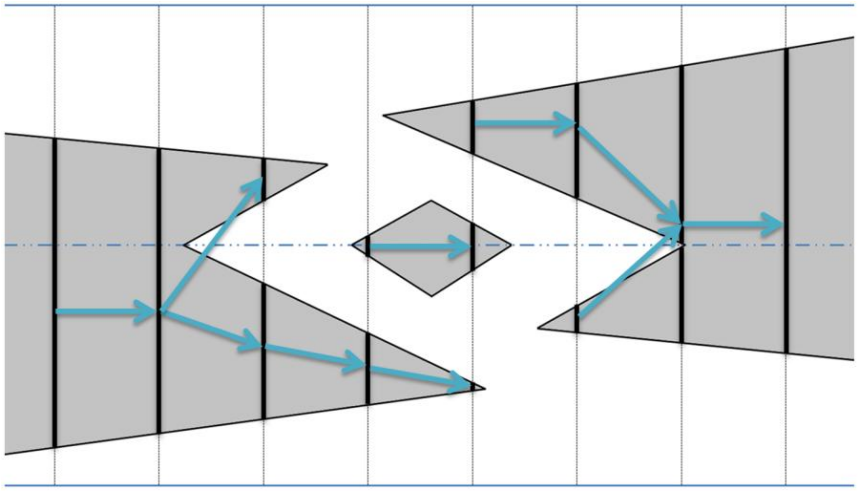

Figure VI-24: Accessibility space slicing and connection

It is easy to see that accessibility zones can be viewed as nodes of a graph that represent an accessibility space topology. However, it is not possible to find a path from

beginning to end in such a graph without some additional improvements that represent jumps. As was mentioned before, a jump is a movement from one accessibility zone to another in a slice. This movement can be represented as an edge in a graph but a number of edges will be equal to a square of accessibility zones number in each slice. The developed version uses a slightly different approach and introduces a “Jump” node connected to each accessibility zone of each slice that has more than one accessibility zone. It allows using less edges and better visualization. The Figure VI-25 demonstrates a graph constructed for the accessibility space shown on Figure VI-24 based on the described rules. Edges that have the gold color represent the shortest path in the graph. This path contains a sequence of accessibility zones and jumps that have to be used for selecting a part of an accessibility space that contains an orientation curve with the lowest possible number of jumps.

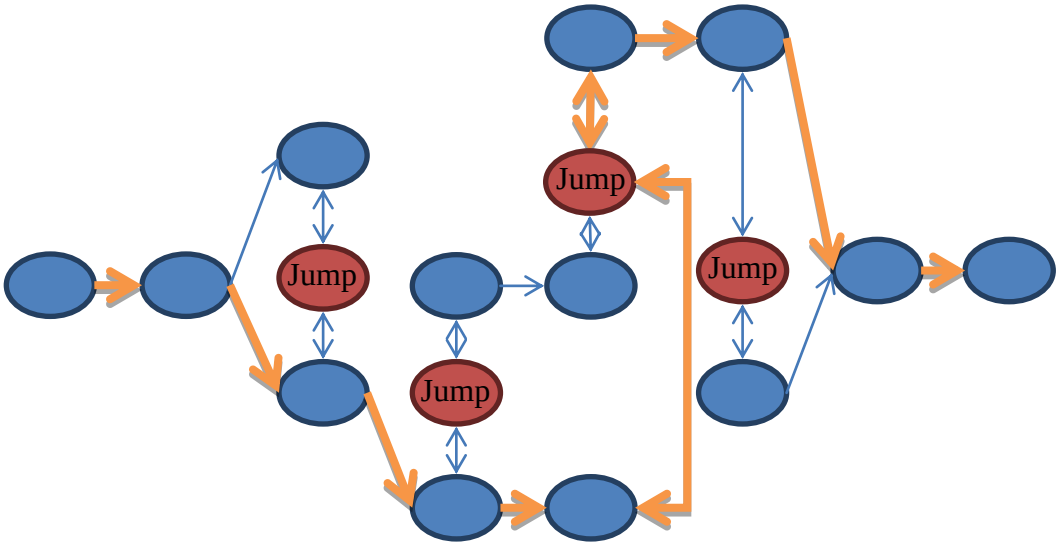

Figure VI-25: Graph representation of an accessibility space

The developed implementation of the discussed algorithm uses the "NetworkX" Python library for managing a graph structure and searching for the shortest path in a graph ("Dijkstra's algorithm with Fibonacci heap" [67] with O(E+V*logV) complexity) and implements the graph construction process described by the Algorithm VI-8.

```
1   Calculate accessibility map (AS slices) for each tool center point (Algorithm VI-11)
2   For all accessibility maps:
3   |   Find all accessibility zones (AZ)
4   For all accessibility zone:
5   |   Add a node to a graph
6   |   For all accessibility zones on a previous slice:
7   |   |   If intersection between AZ on current layer and previous layer exist:
8   |   |   |   Add an edge
9   For each slice:
10  If there are more than one accessibility zone:
11  |   Add "Jump" node and edges from this node to all AZ in this slice
```

Algorithm VI-8: Accessibility graph construction

It is important to note that the developed version of the described algorithm actually works with 3D accessibility space in opposite to the described 2D case. Although a number of dimensions is different, it implements conceptually the same ideas of representing an accessibility space as a graph and search for the shortest path. An example of a real life accessibility space graph is shown on Figure VI-26 (node values represent a number of an accessibility zone in a slice).

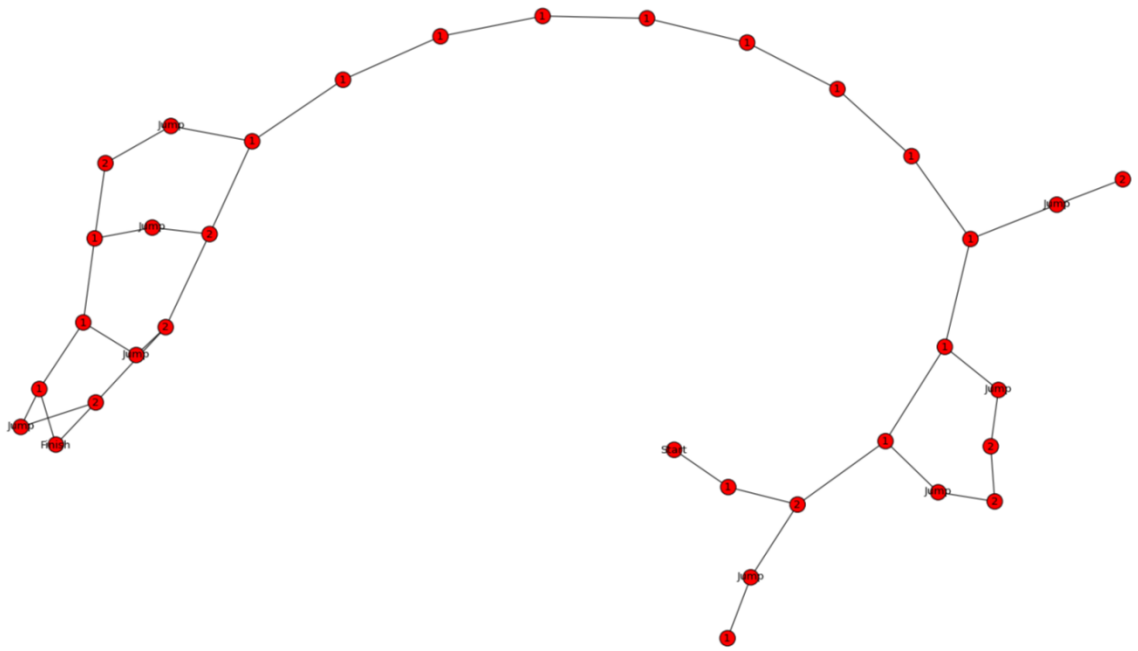

Figure VI-26: Real life example of an accessibility map graph

The next step in the orientation planning process is the construction of an orientation curve in a selected part of the accessibility space. Before the construction of an actual curve, an accessibility space should be reduced by using only accessibility zones represented by the shortest path in a graph. At this point a tool path is also divided into a sequence of segments corresponding to segments of nodes in the shortest path. Since there are jumps between these regions, tool orientation at ends of these segments can be selected independently and it does not make sense to optimize them together. As a result it is possible to reduce a length of a curve that has to be optimized at once. The curve construction process has two main parts: construction of an initial curve and iterative optimization.

Generally, an initial curve can be selected randomly if a stable optimization algorithm is used but, as with any other optimization techniques, a good initial guess results in much faster convergence. The developed accessibility curve construction system generates a curve from points that lie as far as possible from border of accessibility zones. The developed implementation uses the "Distance transform" algorithm [68] (with $O(N^2)$ complexity) implemented in OpenCV library in order to find these points. The distance transform algorithm calculates an approximate distance to the closes zero pixel of a given bitmap. As a result, a pixel with the maximum distance value represents the furthest point from an accessibility zone boundary. As a result, an initial curve is constructed by applying a distance transform to all accessibility maps and using points with maximum distance values. Although the described way guarantees that all accessibility curve points lie inside accessibility zones, there is no guarantee that an entire curve lies in accessible area because some curve segments between initial points may lie in non-accessible areas. A solution for this problem is the developed implementation is applying Boolean "And" operations between all neighbor accessibility maps before construction of an accessibility space graph. Although it reduces an accessibility space and can result into impossibility of a tool path construction, this situation is not likely. However if Boolean "And" produces an empty map, this will mean that it is dangerous to machine this area since a tool will be very close to a part. As a result, it will be treated as an inaccessible area and the tool path planning algorithm will try to machine it later when more material is removed and the area may become accessible.

The complete process of preparing of an accessibility space and an initial curve construction is described by Algorithm VI-9.

```
1  Calculate the shortest path in an accessibility space graph
2  Remove all accessibility zones that are not part of the shortest path
3  For all accessibility zones:
4  |  Apply a distance transform
5  |  Find a point with maximum distance value
6  |  Add found point to an initial curve
```

Algorithm VI-9: Initial accessibility curve construction

After generating an initial curve, the last part of the accessibility curve construction is an iterative optimization. The implemented optimization approach is quite simple and tries to smooth a curve as much as possible while staying in accessible area. For simplicity of an algorithm explanation, there is an assumption that an accessibility curve has only 2 dimensions. The actual system works with 3 dimensional curves since it is designed for 5-axis machines, but it uses conceptually the same algorithm.

A 2D curve can be represented by 1D array of floats (as it is done in a height map, Figure VI-27) under assumption that all curve points are evenly spaced, which is correct since they are located on accessibility space slices in the developed system. Before continuing the optimization part it is possible to note that although the idea of slicing an accessibility space is a good way to deal with it, selecting equal space between slices in some cases is inefficient and bring a lot of problems. It is possible to recommend that dynamic accessibility space subdivision with non-constant slices density is a better approach that may save a significant amount of memory. But the actually implemented

orientation system uses constant distance between slices and all following explanation will be done based on this fact.

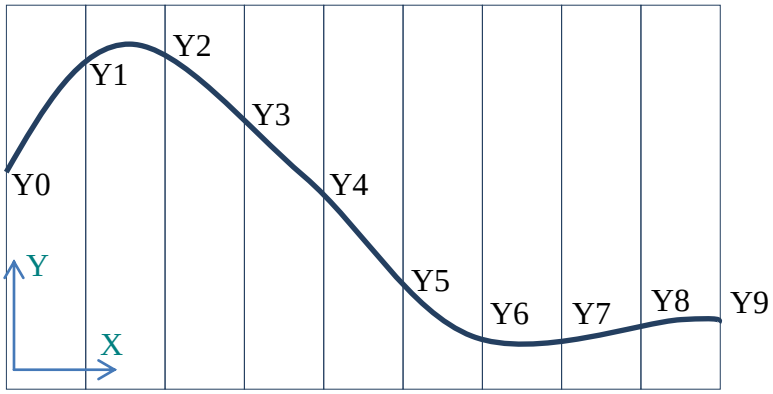

Figure VI-27: Curve representation

The first step of optimization iteration is calculation of a gradient by using the formula (VI-1).

$$\nabla y_i = k\frac{(y_{i-1} + y_{i+1})}{2} \quad \text{(VI-1)}$$

Where "y_i" is a coordinate of ith point and "k" is a damping coefficient used for prevention oscillation. The used value for the "k" is 0.9. After calculating gradients for each point (except first and last points which are always locked at their initial positions), a new point position is calculated:

$$\nabla\tilde{y}_i = y_i + \nabla y_i \quad \text{(VI-2)}$$

If the new position lies inside accessible zone, a point position is updated by a newly calculated value. However if a new position is not a valid orientation, a point is not moved. The developed orientation curve optimization system performs described iterations continuously during a given time that is based on a curve length. Using a time

limit as a single stopping condition was selected for simplification of the development process and better control over optimization time.

```
1  Calculate an initial accessibility curve
2  While time limit is not reached:
3  |  For each point in a curve:
4  |  |  Calculate gradient
5  |  |  Calculate next position
6  |  |  If next position is in accessible zone:
7  |  |  |  Update point position
```

Algorithm VI-10: Accessibility curve optimization

The Algorithm VI-10 demonstrates steps performed during an accessibility curve optimization process.

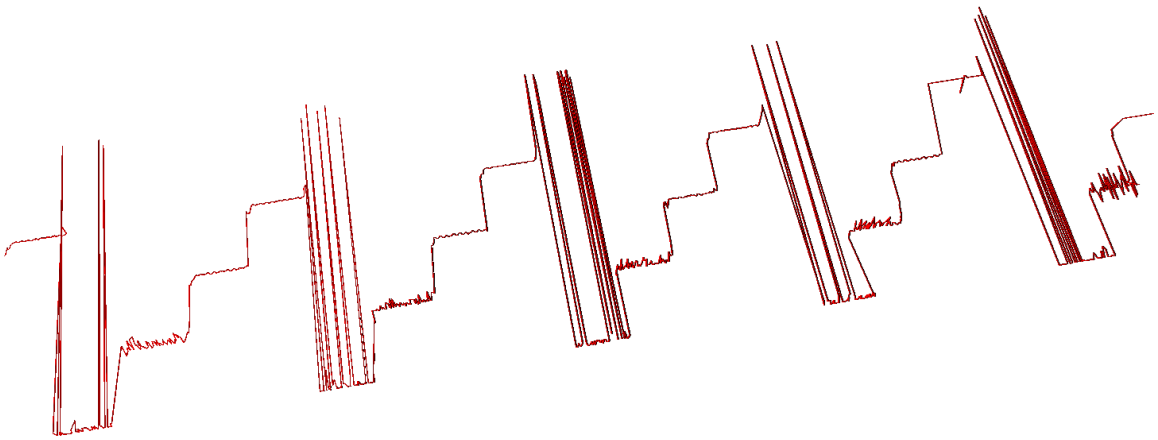

Figure VI-28: 3D curve optimization example

The Figure VI-28 demonstrates an example of a real 3 dimensional accessibility curve optimization. It is important to remember that this curve has 3 dimensions and is calculated for 5-axis machine with a continuous C axis, so it is normal to see rapid movements from one end to another. These movements are just a visualization of the continuous axis rotation and going from 359 to 0 degrees.

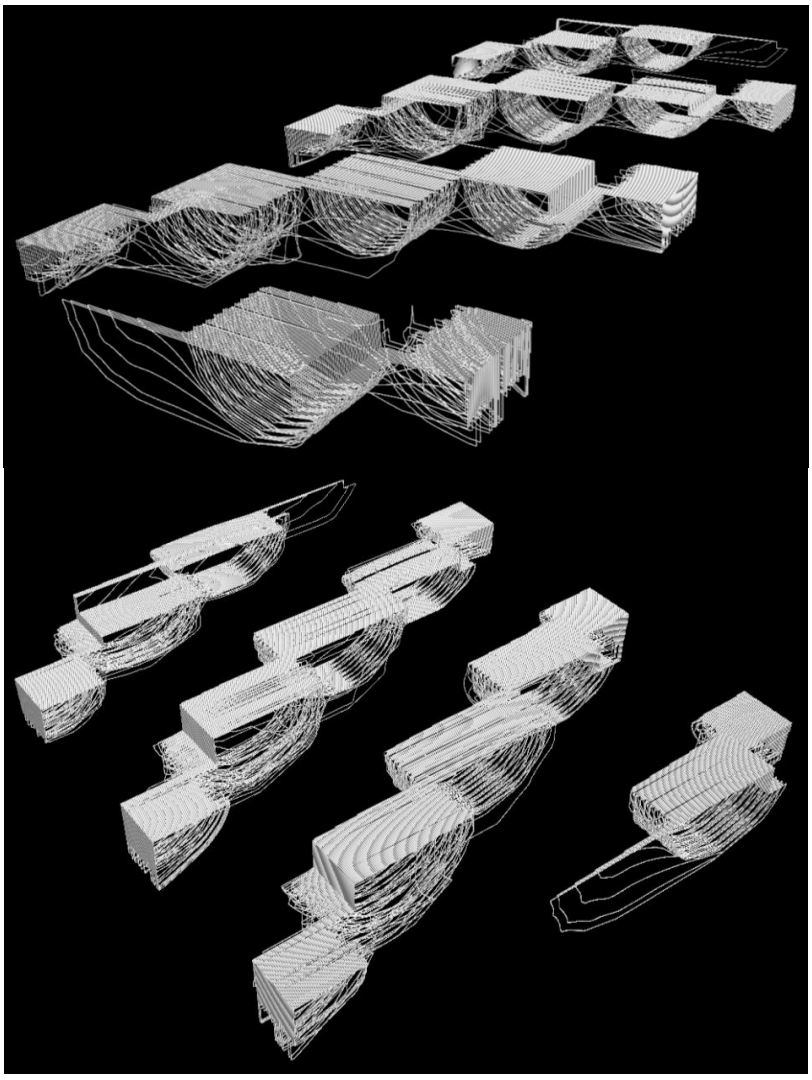

Figure VI-29: Accessibility space (views from multiple camera positions)

The Figure VI-29 demonstrates an example of a 3D accessibility space. On the picture, borders between accessible and non-accessible areas for each accessibility zone are represented by tubes. This accessibility space is calculated for the first few segments of a roughing path that process a cube of material. A real world example of an accessibility curve constructed in accessibility space is shown on Figure VI-30 - Figure VI-32.

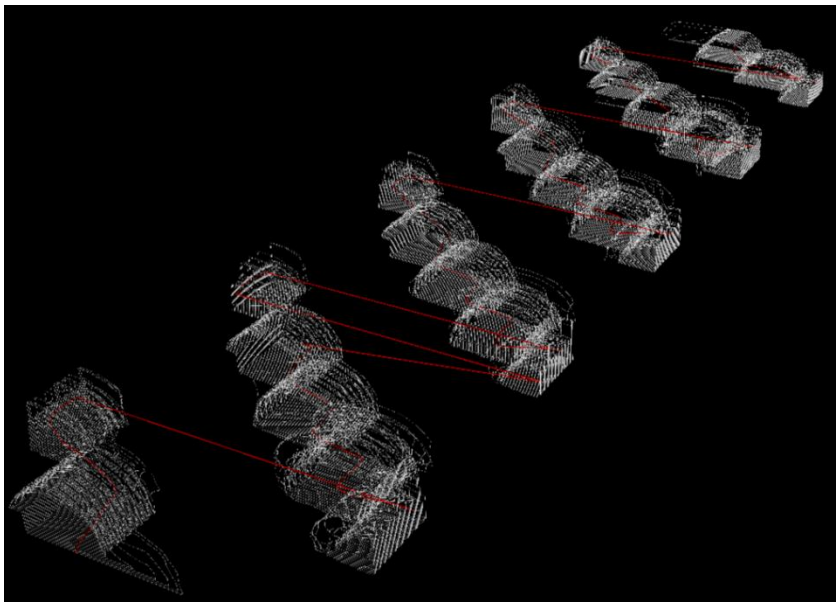

Figure VI-30: Accessibility curve going through accessibility space, view 1

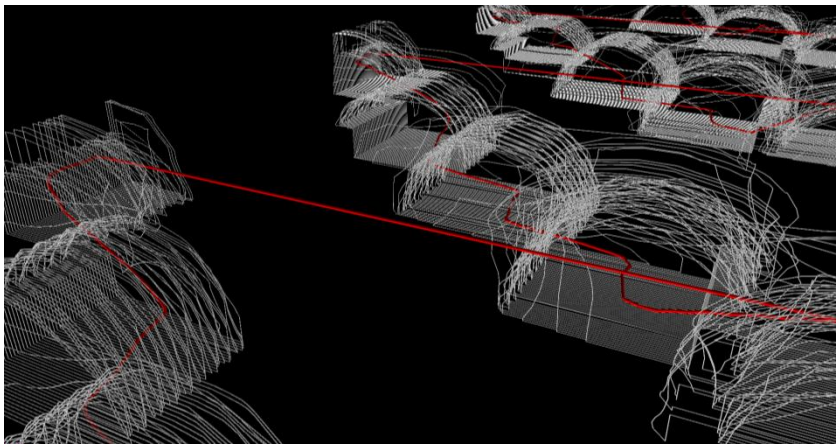

Figure VI-31: Accessibility curve going through accessibility space, view 2

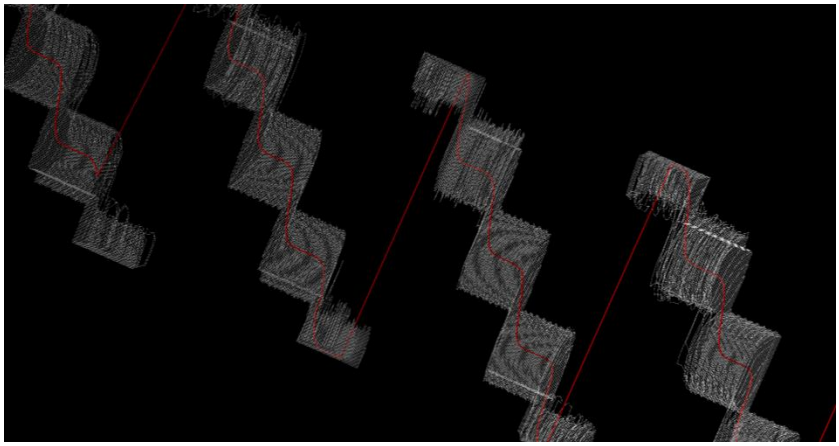

Figure VI-32: Accessibility curve going through accessibility space, view 3

Accessibility map generation

It was mentioned above that all orientation selection algorithms are based on an assumption that there is a known accessibility map. This part describes an algorithm developed for computing accessibility map for a given point and a given tool/holder combination. Most of research project related to orientation selection [69, 70] are based on a concept of accessibility (or visibility) cone [71]. The problem with this approach is the simplification of an accessibility map by a cone or a set of cones. Although it is often a good enough approach that saves a lot of memory and computational resources, it does not provide an accurate representation of a real accessibility map.

The developed approach is based on the completely opposite idea of using inaccessibility cones calculated for each geometry model element independently. Considering the fact that the developed geometry representation uses a set of spherical cells for representing a volume, it is possible to say that a valid orientation is an orientation that does not result in a collision with any of cells. So if it is possible to find

all orientations that result into collision for each cell, all collision prone orientations will be described by a union of collision prone orientations of each cell and all collision free orientation will be described by a complement of that union. Independence of cells and their collision prone orientation also allows calculation of these orientations in parallel which is an important property for this work. An interesting part here is the calculation of inaccessible orientations for a spherical cell and a give tool and tool holder combinations. It is easy to see that for a fixed tool center position and a given spherical cell, a tool may come to a cell as close as possible until their surfaces touch each other as shown on Figure VI-33. It is also possible to calculate the angle between a tool orientation and a vector from tool center to a sphere center.

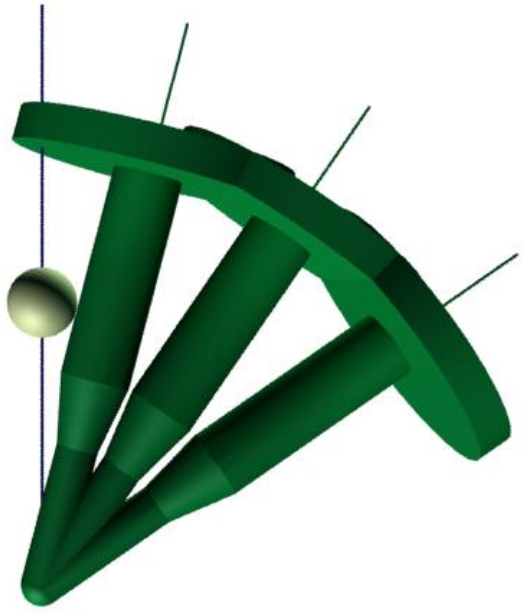

Figure VI-33: Touching a cell surface by a tool surface

It is also obvious that a tool may touch a sphere from many different sides as shown on Figure VI-34 but an angle between tool direction and a vector to a sphere center is constant in all cases.

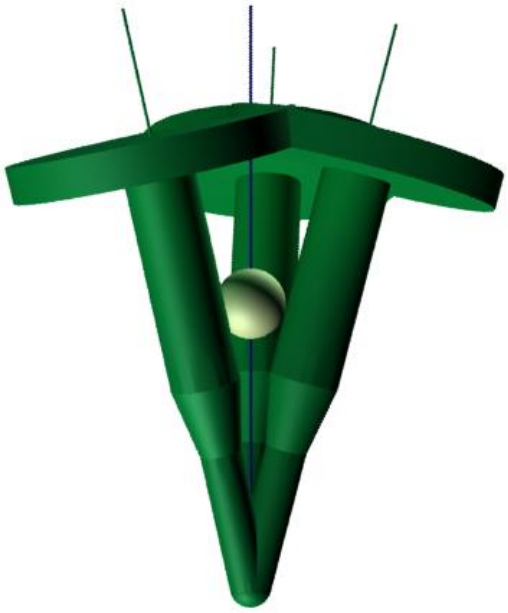

Figure VI-34: Touching a sphere from multiple sides

By looking on all possible tool orientations when a tool center is fixed and tool touches a sphere as shown on Figure VI-35, it is possible to see that the tool direction vectors make a cone around the vector to a sphere center.

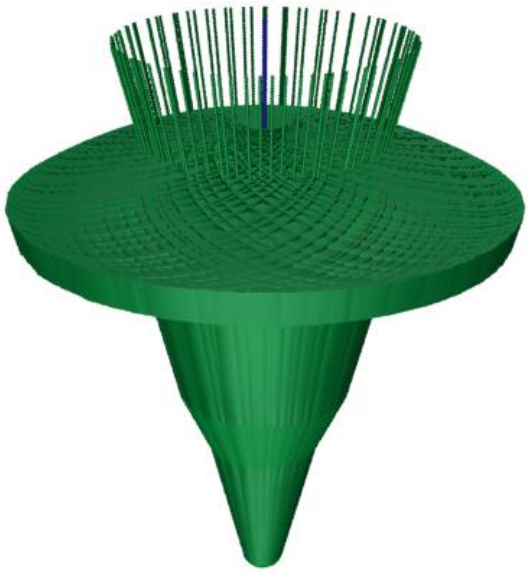

Figure VI-35: All tool orientation when a tool touches a sphere

This cone is called an inaccessibility cone since all tool directions that lie inside of this cone result into a collision. If given the tool center, the sphere center and the tool geometry, the angle between the cone center line and the cone surface can be calculated. Since a cone center line is a vector between a tool center and a sphere center, and a cone top is a tool center, this angle completely determines an inaccessibility cone. Since an Inaccessibility Cone Angle (ICA) is a single dimension value, there is no need to consider 3D space and an explanation can be done in 2D by using a 2D tool model shown on Figure VI-36.

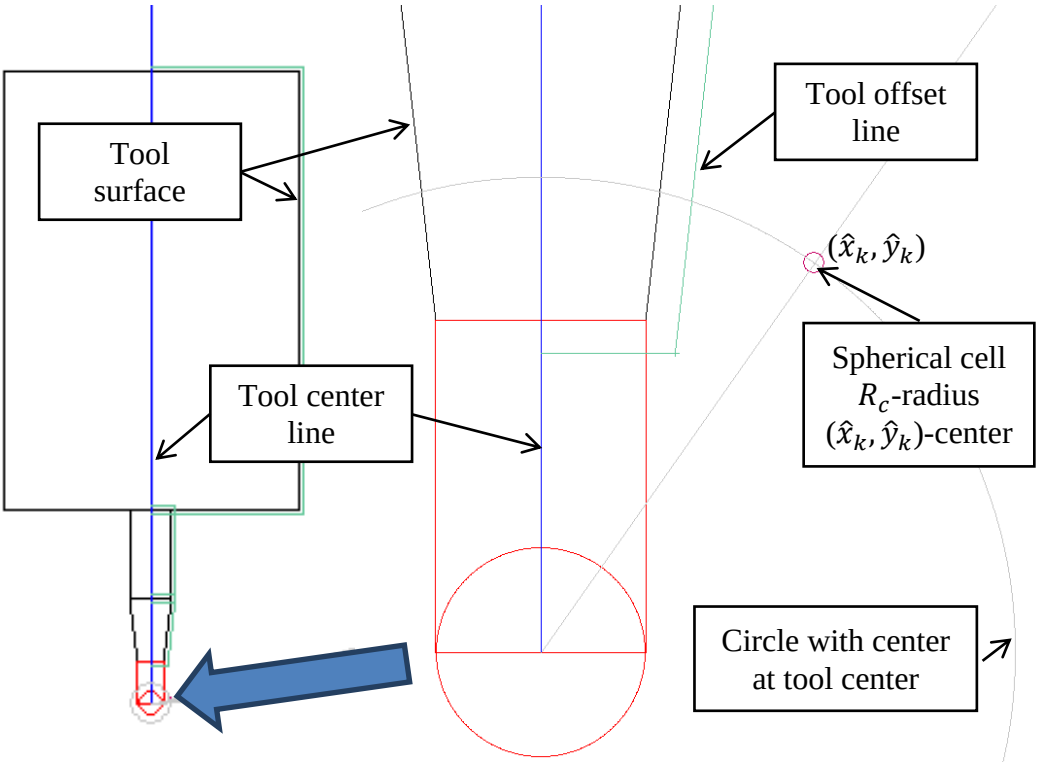

Figure VI-36: 2D tool model

An ICA has two components related to a spherical cell itself and tool geometry as shown on Figure VI-37. The spherical part of an ICA is needed since a cell is actually a sphere, rather than a point. So this part represents an angle between a cell center and a cell tangent.

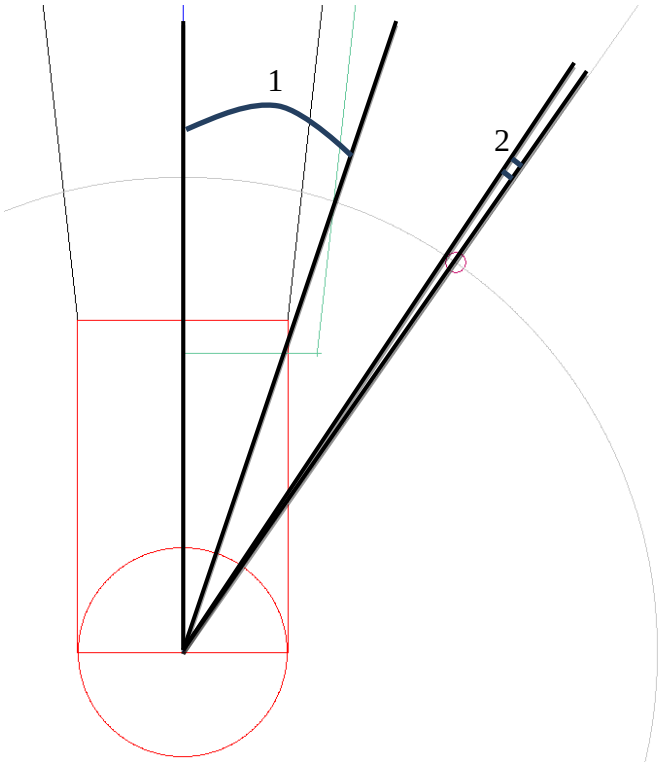

Figure VI-37: Inaccessibility cone angle components

The second component can be easily calculated by formula:

$$\sin^{-1}\frac{R_c}{\sqrt{\hat{x}_k{}^2+\hat{y}_k{}^2}}$$

Where $(\hat{x}_k, \hat{y}_k)$ – k-th cell center and R_c – cell radius.

The first part, which is related to a tool and tool holder geometry, is a bit more complicated. It is also important to mention here that for safety reasons, a tool surface offset is used instead of a tool surface itself. It allows controlling the gap between material and a moving tool during a machining process by changing surface offset value.

Calculation of the first ICA components is a bit more complicated. It is defined as an angle between a tool center line and a vector to a sphere center when a sphere center

lies on a border of a tool. Here an assumption should be made that the developed approach does not support a situation when a tool has complex shape that allows so that it is possible to have a material between tool surface and a tool centerline. Considering this assumption and the fact that a tool model has many components, the first ICA components can be found as a maximum angle between tool center line and a vector to an intersection between tool offset components and a circle with a center at tool center and radius equal to a distance to a sphere center. This can be calculated with formula:

$$\cos^{-1} \max_{p=0..Q} \vec{n} \cdot \frac{\overrightarrow{t_p}}{|\overrightarrow{t_p}|}$$

Where $\overrightarrow{t_p}$ −vector to p-th intersection between tool surface offset components and a circle around tool center that intersects a cell center and $\vec{n}$ – tool center line. As a result the ICA for a k-the cell can be defined as:

$$\gamma_k = \sin^{-1} \frac{R_c}{\sqrt{\hat{x}_k{}^2 + \hat{y}_k{}^2}} + \cos^{-1} \max_{p=0..Q} \vec{n} \cdot \frac{\overrightarrow{t_p}}{|\overrightarrow{t_p}|}$$

Now, when ICA can be calculated, it is possible to write a complete mathematical definition of an accessibility map. It can be represented as a matrix of Boolean values with resolution (n, m):

$$A = \begin{bmatrix} a_{1,1} & \cdots & a_{1,n} \\ \vdots & \ddots & \vdots \\ a_{m,1} & \cdots & a_{m,n} \end{bmatrix}$$

Where each matrix element with coordinates (i, j) represent a tool orientation defined by angles:

$$\theta_j = j\frac{180}{n}, \varphi_i = i\frac{360}{m}$$

All matrix elements can be calculated as:

$$a_{i,j} = \bigcap_{k=1}^{N} \left(\delta_{i,j,k} > \gamma_k\right)$$

Here the γ_k is an ICA defined earlier and $\delta_{i,j,k}$ is an angle between a tool orientation vector associated with a matrix element and a vector to a k-th cell center. This vector is defined by following formulas:

$$\delta_{i,j,k} = \cos^{-1} \frac{\overrightarrow{V_{i,j}} \cdot \overrightarrow{C_k}}{\left|\overrightarrow{C_k}\right|}$$

$$\overrightarrow{C_k} = (x_k, y_k, z_k)$$

$$\overrightarrow{V_{i,j}} = \overrightarrow{\left(\sin\theta_j \cos\varphi_i, \sin\theta_j \sin\varphi_i, \cos\theta_j\right)},$$

$$\delta_{i,j,k} = \cos^{-1} \frac{x_k \sin j\frac{\pi}{n} \cos i\frac{2\pi}{m} + y_k \sin j\frac{\pi}{n} \sin i\frac{2\pi}{m} + z_k \cos j\frac{\pi}{n}}{\sqrt{{x_k}^2 + {y_k}^2 + {z_k}^2}}$$

From a computational point of view, the implemented version uses OpenCL and runs all calculations on multiple GPUs by following the Algorithm VI-11. It calculated all ICA in parallel first and then calculates all accessibility map elements in parallel as well. Calculation of a single AM with resolution 256x512 takes approximately 20-40ms.

```
1  For all cells in parallel:
2  |  Calculate ICA
3  For accessibility map element in parallel:
4  |  For all cells in parallel:
5  |  |  Calculate angle between represented direction and cell center
6  |  |  If calculated angle is less than ICA:
7  |  |  |  Mark map element as inaccessible
```

Algorithm VI-11: Accessibility map calculation

The developed accessibility map calculation approach has shown great parallelizability and scalability as well as a quite good performance. In opposition to the other accessibility map calculation techniques mentioned earlier, it does not use any simplifications of an accessibility space and produces very accurate accessibility maps. However since there are no simplifications used, it uses significantly more memory for the storing accessibility map.

Another important property of the developed algorithm is an ability to use a complete tool and tool holder geometry representation without any simplifications. It allows considering all parts of a tool and holder and using orientations that are safe but not defined as safe for other methods due to simplified tool geometry representation.

High level tool path planning control algorithm

The previous parts have described all components required for creation of a complete robust tool path planning strategy that can produce a valid result. But it is important to show a high level algorithm that brings all components together into a path planning system. This algorithm is shown by the Algorithm VI-12.

```
1   Offset target geometry and fixtures volumes for roughing tool (Algorithm VI-4)
2   Do:
3   |   Generate roughing tool path for layer (Algorithm VI-7)
4   |   Generate accessibility map for each point (Algorithm VI-11)
5   |   Optimize accessibility space (Algorithm VI-8)
6   |   Construct initial accessibility curve (Algorithm VI-9)
7   |   Optimize accessibility curve (Algorithm VI-10)
8   |   Simulate generated tool path (Algorithm V-1 & Algorithm V-2)
9   While generated tool path length is greater than zero
10  Offset target geometry and fixtures volumes for finishing tool (Algorithm VI-4)
11  Generate finishing tool path (Algorithm VI-6)
12  Perform steps 4-7 for the finish tool path
```

Algorithm VI-12: High level control algorithm

Experimental 5-axis milling results

All described tool trajectory and orientation planning algorithms were implemented in Python, C++ and OpenCL languages during the research project. The developed system was tested on a computer with 3 GPUs and showed great parallelizability and scalability very similar to performance result showed in the previous chapter describing 5-axis milling simulator. This chapter will not provide additional

performance details for three reasons. First, both the simulation and the low level part of the path planning system use exactly the same implementation of the geometry representation and processing core. As a result, they have exactly the same level of parallelizability shown in the previous chapter and there is no need to show the same results. Second, high level path planning algorithms heavily depend on input geometry from the amount of calculations point of view. It means that all performance testing results will be valid only for test geometry models. And finally, the developed version uses a lot of reasonably slow Python code that can be much faster if it is rewritten in C++. In spite everything mentioned above, it takes about 10-20 minutes to generate a complete tool path for all tested models, so it can be stated that after performance tuning and code improvement it will take less than 10 minutes for generating a valid tool path for any given model.

In order to validate developed methodology and algorithms, the developed path planning system was used for generation G-code programs for multiple parts. These G-code programs were tested in both virtual and real environments on the developed 5-axis machining simulator and Okuma MU500VA 5-axis milling machine.

The process of converting of a tool path into a G-code program is done by the post-processor software. Commercial CAM systems usually include a generalized post-processor that can be configured for a particular CNC controller but they require using a special tool path description language. Since converting a tool path into a post-processor language is more complicated (due to the lack of documentation) than converting it into the G-code format itself, there was developed a simplified post-processor designed for

the used Okuma machine. It converts tool motions in the developed software format directly to G1 commands and use some simple program optimization such as combining collinear motions or removing constant components in order to reduce size of an output program.

The following pictures demonstrate simulation and machining results for various test models and materials.

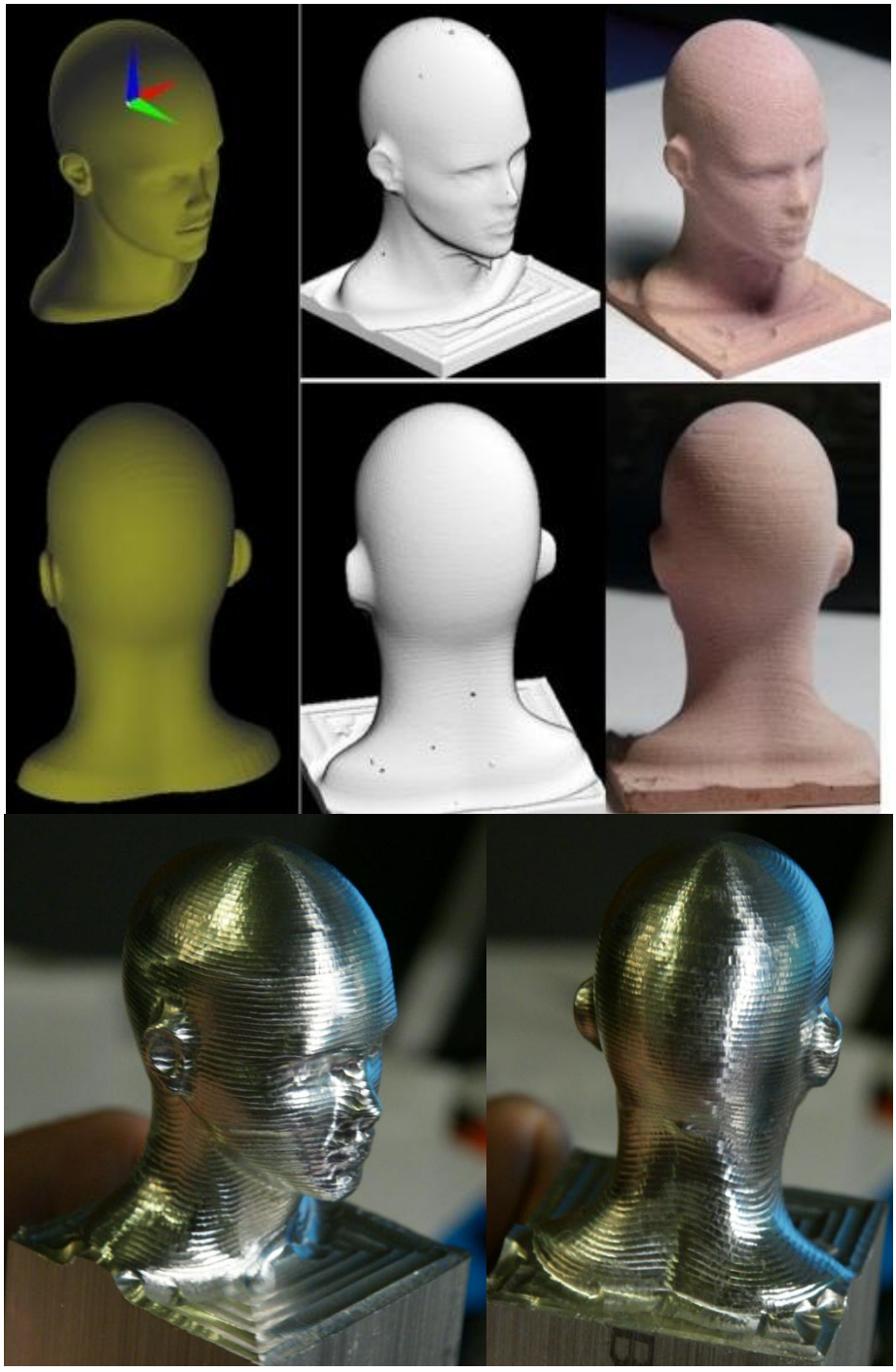

(15 minutes planning type; 3 hours machining time)

Figure VI-38: Test model “Head”

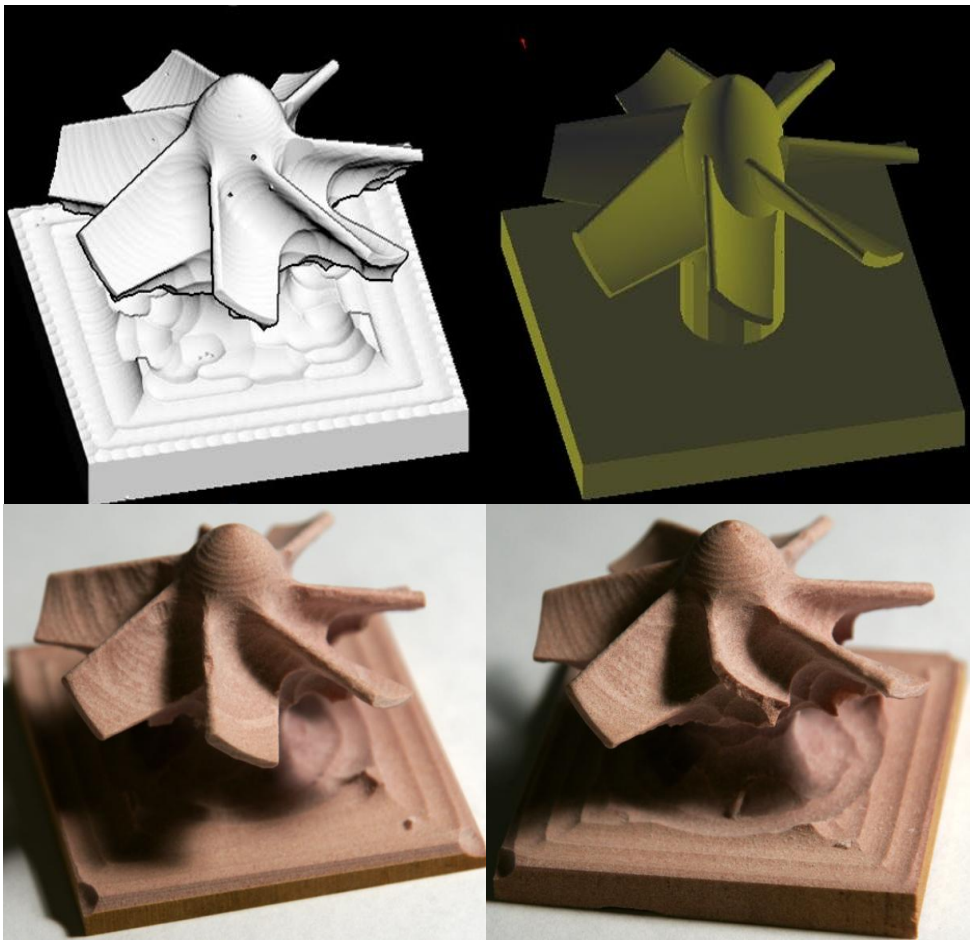

(15 minutes planning type; 1.5 hours machining time)

Figure VI-39: Test model “Fan”

(10 minutes planning type; 1.5 hours machining time)

Figure VI-40: Test model “Puppy”

Discussion

This chapter has described the developed design methodology for a highly parallel algorithm and a set of tool path planning algorithms developed by following the methodology. These algorithms include a solution for common computational geometry problems, such as offset surface calculation or volume surface intersections and a set of robust algorithm for multi-axis tool path planning used in CNC milling. Following the design methodology and using the developed highly parallel geometry representation have resulted in high parallelizability and scalability of these algorithms. As a result, they can efficiently run on multi-GPU systems with more than a thousand cores.

The developed path planning algorithms were combined in an automatic path planning system capable of producing a valid G-code program for 5-axis CNC milling machine with a very little guidance from a user. The developed path planning system was tested in both a virtual and a real environment by generating G-code programs a running them in the developed simulator and on a real machine.

The experimental results have proved that GPGPU approach can be used for acceleration and automation of the tool path planning process for CNC milling machines. Although the developed system often generates not the most efficient tool path, it can be used as a foundation for a fully automated tool path planning system since it already provides a set of very robust path planning algorithms that can generate a valid tool path for almost any possible input geometry.

Although the developed system demonstrated good results, it is important to remember that the implemented version of all path planning and accessibility map

generation algorithms is limited to the ball-end cutter only. It is also important that remember that if a tool center point lies in inaccessible area, the developed path planning system will just skip it and will not try to machine as close as possible. As a result, there may be areas where material is not removed at all even if it was possible to remove almost all material. And the most important limitation is the fact that the described path planning algorithms were designed as robust and they do not provide the most efficient tool path.

VII. CONCLUSIONS AND RECOMMENDATIONS

The first part of this work formulated the methodology for selection of a right geometry representation and a data structure suitable for parallel processing on GPU. Then the methodology was used for designing the 3-axis CNC milling simulation and path planning algorithms accelerated with the GPGPU technology. The developed algorithms were validated by performing 3-axis simulation and experimental machining. The experimental results showed the importance of a highly parallel design and demonstrate almost an order of magnitude difference between CPU and GPU performance results.

The second part of this work generalized the developed methodology for supporting multi-GPU systems and developed a completely new geometry representation for designing algorithms capable of performing 5-axis CNC tool path planning and simulation. Then the developed algorithms were verified by developing a fully automated 5-axis tool path planning system capable of producing valid G-code programs for any geometry. Finally the developed system was used for the generation of test programs that were tested in both virtual and real environments by running them in the developed 5-axis CNC milling simulator and on a real 5-axis CNC milling machine.

The experimental results produced in this work proved that highly parallel computing hardware (such as widely available and used in this work multi-GPU computing system) and appropriate highly parallel algorithms can significantly expand limits of modern tool path planning systems. The performance of parallel computing

allows implementing algorithms that were not considered before due to computational requirements. And as a result, it allows further manufacturing automation that may create completely automated manufacturing systems.

Although developed in this work algorithms and systems were successfully tested and demonstrated good results, it is important to remember that there were made some important assumptions and the developed solutions have many limitations. The most important assumption made in this work is that it is possible to generate a good tool path based just on geometric constraints without considering physical limitations. It is true in most cases, but it will not work for machining some material such as titanium and there will be a need to integrate physical limitations into a tool path planning process. Other assumptions were made about optimization of a tool path. For example, it is assumed that a tool orientation change should be as smooth as possible. Although it makes sense sometime, it may be more appropriate to use a constant tool orientation with few rapid changes. Some other limitations are more related to implementation of the developed ideas and algorithms. For example, the developed path planning and accessibility map generation algorithms are designed for the ball-end tool but it is possible to modify them in order to support some other tool types such as flat-end or conic-end.

Considering the good results, it is possible to recommend continuing this research project since there are still many areas that can be significantly improved. One of the most important aspects from a practical point of view is the implementation of an accessibility map algorithm that allows prediction collisions between machine components. This improvement would make the machining process significantly safer

and allow using the full range of machine motions. The next important part is the development of an expandable tool path planning system based on current robust path planning algorithms. In this case, expandable means an ability to use multiple implemented tool path planning strategies (that also have to be implemented in future) and select them based on a part geometry analysis (feature detection and part subdivision will be needed for this functional). Finally, it will be possible to create a tree of possible solutions and at that point it would make sense to run a developed path planning system on a cluster or cloud where each node processes an independent list of strategies used for tool path planning. Development of all described features will eventually make it possible to replace a human engineer completely and significantly reduce manufacturing the time and cost as a result.

REFERENCES

[1] Centrifuge Brand Marketing Research, 2010, "Machine Tool Professionals, Outlook on CNC Machine Investments," .

[2] Smith, K., Wang, A., and Fujino, L., 2012, "Through the Looking Glass: Trend Tracking for ISSCC 2012," IEEE Solid-State Circuits Magazine, **4**(1) pp. 4 - 20.

[3] BOBROW, J., 1985, "NC Machine Tool Path Generation from CSG Part Representations" Computer-Aided Design, **17**(2) pp. 69 - 76.

[4] HWANG, J., 1992, "Interference-Free Tool-Path Generation in the NC Machining of Parametric Compound Surfaces," Computer-Aided Design, **24**(12) pp. 667 - 676.

[5] LI, S., and JERARD, R., 1994, "5-Axis Machining of Sculptured Surfaces with a Flat-End Cutter," Computer-Aided Design, **26**(3) pp. 165 - 178.

[6] LONEY, G., and OZSOY, T., 1987, "NC Machining of Free Form Surfaces," Computer-Aided Design, **19**(2) pp. 85 - 90.

[7] Suresh K, Y. D., 1994, "Constant Scallop Height Machining of Free Form Surfaces," Journal of Engineering for Industry, **9**pp. 116-253.

[8] Rong-Shine Lin, Y. K., 1996, "Efficient Tool-Path Planning for Machining Free-Form Surfaces," Transactions of the ASME, **118**(1) pp. 20-28.

[9] Lasemi, A., Xue, D., and Gu, P., 2010, "Recent Development in CNC Machining of Freeform Surfaces: A State-of-the-Art Review," Computer-Aided Design, **42**(7) pp. 641 - 654.

[10] Lee, Y. -., and Ji, H., 1997, "Surface Interrogation and Machining Strip Evaluation for 5-Axis CNC Die and Mold Machining," International Journal of Production Research, **35**(1) pp. 225 - 252.

[11] Lauwers, B., Kiswanto, G., Kruth, J. -., 2003, "Development of a Five-Axis Milling Tool Path Generation Algorithm Based on Faceted Models," CIRP Annals - Manufacturing Technology, **52**(1) pp. 85-88.

[12] Giri, V., Bezbaruah, D., Bubna, P., 2005, "Selection of Master Cutter Paths in Sculptured Surface Machining by Employing Curvature Principle," International Journal of Machine Tools and Manufacture, **45**(10) pp. 1202-1209.

[13] Han, Z., and Yang, D. C. H., 1999, "Iso-Phote Based Tool-Path Generation for Machining Free-Form Surfaces," Journal of Manufacturing Science and Engineering, **121**(4) pp. 656.

[14] Ding, S., Mannan, M. A., Poo, A. N., 2003, "Adaptive Iso-Planar Tool Path Generation for Machining of Free-Form Surfaces," Computer-Aided Design, **35**(2) pp. 141-153.

[15] Yang, D. C. H., and Han, Z., 1999, "Interference Detection and Optimal Tool Selection in 3-Axis NC Machining of Free-Form Surfaces," Computer-Aided Design, **31**(5) pp. 303-315.

[16] Choi, B. K., Kim, D. H., and Jerard, R. B., 1997, "C-Space Approach to Tool-Path Generation for Die and Mould Machining," Computer-Aided Design, **29**(9) pp. 657-669.

[17] Morishige, K., Kase, K., and Takeuchi, Y., 1997, "Collision-Free Tool Path Generation using 2-Dimensional C-Space for 5-Axis Control Machining," The International Journal of Advanced Manufacturing Technology, **13**(6) pp. 393 - 400.

[18] Yang, D. C. H., Chuang, J. J., Han, Z., 2003, "Boundary-Conformed Toolpath Generation for Trimmed Free-Form Surfaces Via Coons Reparametrization," Journal of Materials Processing Technology, **138**(1-3) pp. 138-144.

[19] Yang, D. C. H., Chuang, J. -., and OuLee, T. H., 2003, "Boundary-Conformed Toolpath Generation for Trimmed Free-Form Surfaces," Computer-Aided Design, **35**(2) pp. 127-139.

[20] Sun, W., Bradley, C., Zhang, Y. F., 2001, "Cloud Data Modelling Employing a Unified, Non-Redundant Triangular Mesh," Computer-Aided Design, **33**(2) pp. 183-193.

[21] Ren, Y., Yau, H. T., and Lee, Y., 2004, "Clean-Up Tool Path Generation by Contraction Tool Method for Machining Complex Polyhedral Models," Computers in Industry, **54**(1) pp. 17-33.

[22] Yuan-Shin, L., 1997, "Admissible Tool Orientation Control of Gouging Avoidance for 5-Axis Complex Surface Machining," Computer-Aided Design, **29**(7) pp. 507-521.

[23] Warkentin, A., Ismail, F., and Bedi, S., 2000, "Multi-Point Tool Positioning Strategy for 5-Axis Mashining of Sculptured Surfaces," Computer Aided Geometric Design, **17**(1) pp. 83-100.

[24] Gray, P. J., Ismail, F., and Bedi, S., 2004, "Graphics-Assisted Rolling Ball Method for 5-Axis Surface Machining," Computer-Aided Design, **36**(7) pp. 653-663.

[25] Gray, P., Bedi, S., and Ismail, F., 2003, "Rolling Ball Method for 5-Axis Surface Machining," Computer-Aided Design, **35**(4) pp. 347-357.

[26] Fan, J., and Ball, A., 2008, "Quadric Method for Cutter Orientation in Five-Axis Sculptured Surface Machining," International Journal of Machine Tools and Manufacture, **48**(7-8) pp. 788-801.

[27] Morishige, K., Takeuchi, Y., and Kase, K., 1999, "Tool Path Generation using C-Space for 5-Axis Control Machining," Journal of Manufacturing Science and Engineering, **121**(1) pp. 144.

[28] Balasubramaniam, M., Joshi, Y., Engels, D., 2001, "Tool Selection in Three-Axis Rough Machining," International Journal of Production Research, **39**(18) pp. 4215 - 4238.

[29] Jensen, C. G., Red, W. E., and Pi, J., 2002, "Tool Selection for Five-Axis Curvature Matched Machining," Computer-Aided Design, **34**(3) pp. 251-266.

[30] Tukora, B., and Szalay, T., 2011, "Real-Time Determination of Cutting Force Coefficients without Cutting Geometry Restriction," International Journal of Machine Tools and Manufacture, .

[31] Hsieh, H., and Chu, C., 2011, "Particle Swarm Optimisation (PSO)-Based Tool Path Planning for 5-Axis Flank Milling Accelerated by Graphics Processing Unit (GPU)," International Journal of Computer Integrated Manufacturing, **24**(7) pp. 676 - 687.

[32] Li, J. G., Ding, J., Gao, D., 2010, "Quadtree-Array-Based Workpiece Geometric Representation on Three-Axis Milling Process Simulation," The International Journal of Advanced Manufacturing Technology, .

[33] Wang, C. C. L., Leung, Y., and Chen, Y., 2010, "Solid Modeling of Polyhedral Objects by Layered Depth-Normal Images on the GPU," Computer-Aided Design, **42**(6) pp. 535 - 544.

[34] "NEF: A Mesher Based on OpenCascade C.A.D. Software," **2012**(11/28/2012) from: http://www.ann.jussieu.fr/perronnet/mit/mit.html

[35] Wikipedia contributors, "Title="Constructive Solid Geometry" Invalid=""/>," **2012**.

[36] "Clingman D., Kendall S., Mesdaghi S. Practical Java Game Programming / Scene Graph Visibility Culling," **2012**(11/28/2012) from: http://flylib.com/books/en/2.124.1.130/1/

[37] Bertok, P., Takata, S., Matsushima, K., 1983, "A System for Monitoring the Machining Operation by Referring to a Predicted Cutting Torque Pattern," CIRP Annals - Manufacturing Technology, **32**(1) pp. 439 - 444.

[38] Van Hook, T., 1986, "Real-Time Shaded NC Milling Display," ACM SIGGRAPH Computer Graphics, **20**(4) pp. 15 - 20.

[39] Hsu, P. -., and Yang, W. -., 1993, "Realtime 3D Simulation of 3-Axis Milling using Isometric Projection," Computer-Aided Design, **25**(4) pp. 215-224.

[40] Roth, D., Ismail, F., and Bedi, S., 2003, "Mechanistic Modelling of the Milling Process using an Adaptive Depth Buffer," Computer-Aided Design, **35**(14) pp. 1287 - 1303.

[41] Jang, D., Kim, K., and Jung, J., 2000, "Voxel-Based Virtual Multi-Axis Machining," The International Journal of Advanced Manufacturing Technology, **16**(10) pp. 709 - 713.

[42] Cohen-Or, D., and Kaufman, A., 1997, "3D Line Voxelization and Connectivity Control," IEEE Computer Graphics and Applications, **17**(6) pp. 80 - 87.

[43] Wang, W. p., and Wang, K. k., 1986, "Geometric Modeling for Swept Volume of Moving Solids," IEEE Computer Graphics and Applications, **6**(12) pp. 8 - 17.

[44] Bohez, E. L. J., Minh, N. T. H., Kiatsrithanakorn, B., 2003, "The Stencil Buffer Sweep Plane Algorithm for 5-Axis CNC Tool Path Verification," Computer-Aided Design, **35**(12) pp. 1129 - 1142.

[45] Özel, T., and Altan, T., 2000, "Process Simulation using Finite Element Method — Prediction of Cutting Forces, Tool Stresses and Temperatures in High-Speed Flat End Milling," International Journal of Machine Tools and Manufacture, **40**(5) pp. 713 - 738.

[46] Rai, J. K., and Xirouchakis, P., 2008, "Finite Element Method Based Machining Simulation Environment for Analyzing Part Errors Induced during Milling of Thin-Walled Components," International Journal of Machine Tools and Manufacture, **48**(6) pp. 629 - 643.

[47] Uddin, M. S., Ibaraki, S., Matsubara, A., 2009, "Prediction and Compensation of Machining Geometric Errors of Five-Axis Machining Centers with Kinematic Errors," Precision Engineering, **33**(2) pp. 194 - 201.

[48] Cortsen, J., and Petersen, H. G., 2012, "2012 IEEE/ASME International Conference on Advanced Intelligent Mechatronics (AIM); Advanced off-line simulation framework with deformation compensation for high speed machining with robot manipulators," 2012 IEEE/ASME, pp. 934 - 939.

[49] Hanwu, H., and Yueming, W., 2009, "Web-Based Virtual Operating of CNC Milling Machine Tools," Computers in Industry, **60**(9) pp. 686 - 697.

[50] Vichare, P., Nassehi, A., Kumar, S., 2009, "A Unified Manufacturing Resource Model for Representing CNC Machining Systems," Robotics and Computer-Integrated Manufacturing, **25**(6) pp. 999 - 1007.

[51] NVidia, "Parallel Programming and Computing Platform | CUDA | NVIDIA," **2012**(10/23/2012) .

[52] Microsoft, "Compute Shader Overview," **2012**(10/23/2012) .

[53] Khronos Group, "OpenCL - the Open Standard for Parallel Programming of Heterogeneous Systems," **2012**(10/23/2012) .

[54] Aaftab, M., 2011, "The OpenCL Specification," Khronos OpenCL Working Group .

[55] Zuperl, U., Cus, F., and Reibenschuh, M., 2011, "Neural Control Strategy of Constant Cutting Force System in End Milling," Robotics and Computer-Integrated Manufacturing, **27**(3) pp. 485 - 493.

[56] Yazar, Z., Koch, K., Merrick, T., 1994, "Feed Rate Optimization Based on Cutting Force Calculations in 3-Axis Milling of Dies and Molds with Sculptured Surfaces," International Journal of Machine Tools and Manufacture, **34**(3) pp. 365 - 377.

[57] Ghani, J. A., Choudhury, I. A., and Hassan, H. H., 2004, "Application of Taguchi Method in the Optimization of End Milling Parameters," Journal of Materials Processing Technology, **145**(1) pp. 84 - 92.

[58] Ridwan, F., and Xu, X., 2013, "Advanced CNC System with in-Process Feed-Rate Optimisation," Robotics and Computer-Integrated Manufacturing, **29**(3) pp. 12 - 20.

[59] Kanopoulos, N., Vasanthavada, N., and Baker, R. L., 1988, "Design of an Image Edge Detection Filter using the Sobel Operator," IEEE Journal of Solid-State Circuits, **23**(2) pp. 358 - 367.

[60] Lin, S., and Kernighan, B. W., 1973, "An Effective Heuristic Algorithm for the Traveling-Salesman Problem," Operations Research, **21**(2) pp. 498 - 516.

[61] Cerný, V., 1985, "Thermodynamical Approach to the Traveling Salesman Problem: An Efficient Simulation Algorithm," Journal of Optimization Theory and Applications, **45**(1) pp. 41 - 51.

[62] Chiou, C. -., and Lee, Y. -., 2002, "Swept Surface Determination for Five-Axis Numerical Control Machining," International Journal of Machine Tools and Manufacture, **42**(14) pp. 1497-1507.

[63] "ANSI/ASME B4.1-1967 (R1999) Preferred Limits and Fits for Cylindrical Parts," **2013**(3/3/2013) from: http://webstore.ansi.org/RecordDetail.aspx?sku=ANSI/ASME+B4.1-1967+(R1999)#.UTPwymdn15N

[64] "Machine Processing and Tolerance Grades," **2013**(3/3/2013) from: http://www.engineeringtoolbox.com/machine-processes-tolerance-grades-d_1367.html

[65] "Getting Started," **2013**(2/19/2013) from: http://www.ironcad.com/products/IronCADV9/getting_started.htm.

[66] Seong, J., Elber, G., and Kim, M., 2006, "Trimming Local and Global Self-Intersections in Offset Curves/Surfaces using Distance Maps," Computer-Aided Design, **38**(3) pp. 183 - 193.

[67] Fredman, M. L., and Tarjan, R. E., 1987, "Fibonacci Heaps and their Uses in Improved Network Optimization Algorithms," Journal of the ACM, **34**(3) pp. 596 - 615.

[68] Borgefors, G., 1986, "Distance Transformations in Digital Images," Computer Vision, Graphics, and Image Processing, **34**(3) pp. 344 - 371.

[69] Zhiwei, L., Hongyao, S., Wenfeng, G., 2011, "Approximate Tool Posture Collision-Free Area Generation for Five-Axis CNC Finishing Process using Admissible Area Interpolation," The International Journal of Advanced Manufacturing Technology, .

[70] Uddin, M. S., Ibaraki, S., Matsubara, A., 2009, "Prediction and Compensation of Machining Geometric Errors of Five-Axis Machining Centers with Kinematic Errors," Precision Engineering, **33**(2) pp. 194 - 201.

[71] Yang, W., Ding, H., and Xiong, Y., 1999, "Manufacturability Analysis for a Sculptured Surface using Visibility Cone Computation," The International Journal of Advanced Manufacturing Technology, **15**(5) pp. 317 - 321.